A NOVEL ANTIVIRAL THERAPEUTIC PLATFORM: ANCHORING IFN-β TO THE SURFACE OF INFECTIOUS VIRIONS EQUIPS INTERFERON-EVASIVE VIRIONS WITH POTENT ANTIVIRAL ACTIVITY

By

Hoda H. Jabbour

July 2025

Director of Dissertation: Mark D. Mannie, Ph.D.

Department of Microbiology and Immunology at East Carolina University Brody School of Medicine

ABSTRACT

Emerging viruses with the potential to cause epidemics and pandemics pose a severe threat to human health. Herein, we introduce a novel fusion protein platform that enables therapeutic targeting of distinct viral species based on host receptor specificity. Proof-of-concept studies focused on the human coronavirus NL63, which shares specificity for the ACE2 host receptor with the pandemic SARS-CoV and SARS-CoV-2 species. This antiviral fusion protein combines IFN-β with the soluble extracellular domain of ACE2 (IFNβ-ACE2). The physical linkage allows ACE2 to target IFN-β to the surface of NL63. The fusion protein is thereby designed to decorate virions with a surface array of IFN-β such that robust IFN-β signaling and upregulation of antiviral innate defenses invariably precede subsequent cellular infection. Both domains retained the predicted bioactivities in that the IFN-β domain exhibited potent anti-

proliferative activity and the ACE2 domain exhibited full binding to the transmembrane SARS-CoV-2 spike protein. In virus-washed (virus-targeted) and non-washed *in vitro* infection systems, we showed that the pool of IFNβ-ACE2 targeted to the virion surface had potent and superior antiviral activity against NL63 infection compared to soluble ACE2, IFN-β, or the unlinked combination of ACE2 and IFN-β. The pool of IFNβ-ACE2 on the virion surface exhibited robust antiviral efficacy based on the preemptive targeting of antiviral IFN-β activity to the proximal site of viral infection. In conclusion, virus-targeted IFN-β places interferon optimally and antecedent to viral infection to constitute a new antiviral therapeutic strategy.

The COVID-19 pandemic highlighted the need for new antiviral strategies to counter emerging pathogenic viruses. According to a recent study, there is a 38% probability of experiencing a similar pandemic in an individual's lifetime, and this number may double in the next few decades (1). Our best chance of combating new outbreaks and pandemics is by being proactive rather than reactive. With continuous antiviral development, we can quickly eliminate and potentially obviate emerging problematic viruses. This platform can be re-engineered to target various viral species by altering the receptor domain. Additionally, the IFN-β domain can be modified to a different effector protein (e.g. IFN-α) with superior activity against the targeted virus.

A NOVEL ANTIVIRAL THERAPEUTIC PLATFORM: ANCHORING IFN-β TO THE SURFACE OF INFECTIOUS VIRIONS EQUIPS INTERFERON-EVASIVE VIRIONS WITH POTENT ANTIVIRAL ACTIVITY

A Dissertation

Presented to the Faculty of the Department of Microbiology and Immunology

Brody School of Medicine at East Carolina University

In Partial Fulfillment of the Requirements for the Degree

Doctor of Philosophy in Biomedical Sciences with a concentration in Microbiology and Immunology

By

Hoda H. Jabbour

July 2025

Director of Dissertation: Mark D. Mannie, Ph.D.
Dissertation Committee Members:
Akshaya K. Meher, Ph.D.
Isabelle M. Lemasson, Ph.D.
Brandon L. Garcia, Ph.D.
Ruth A. Schwalbe, Ph.D.

ACKNOWLEDGMENTS

First and foremost, I would like to thank my family for their unwavering love and support throughout this journey. To my mother, whose memory continues to guide and inspire me every day – I carry your strength and love in all that I do. To my father, thank you for your endless encouragement and belief in me. You have been my rock through every challenge, and I am so grateful for your steady presence and unconditional support. To my brothers, Nadim and Shadi, your constant support, humor, and faith in me have meant the world, and I am forever grateful for your presence in my life. I also want to thank my new family for welcoming me so warmly and wholeheartedly. Don, Marcia, Eleana, Gary, baby Nora, and the little one on the way, your kindness and support have meant so much to me.

I am deeply thankful to my dissertation committee for their guidance and mentorship. I owe special thanks to Dr. Mark Mannie for his mentorship, thoughtful insight, and belief in my potential. Our long conversations challenged me to think critically, ask better questions, and continually push myself as a scientist. I am also grateful to Dr. Brandon Garcia, Dr. Isabelle Lemasson, Dr. Akshaya Meher, and Dr. Ruth Schwalbe for their valuable input, time, and encouragement throughout this process.

I extend my heartfelt thanks to both current and former members of the Mannie lab, who made this experience so meaningful. To Sunny and Chandler, thank you for your camaraderie and support in the final stretch of this journey. To Dr. Alexander Bastian and Dr. Kayla DeOca, thank you for your early mentorship and for helping lay the foundation for my project and my growth as a scientist.

To my friends, thank you for the laughter, advice, encouragement, and love you've shown me over the years. I want to thank my work bestie, Dr. Melissa Lempicki, for all the support and laughs. I'm going to miss our long lunches, inside jokes, and being able to barge into your office whenever something mildly interesting (or completely chaotic) happened – you made the hardest days lighter. Sylvia Issa, my childhood best friend, thank you for always being a constant voice of support, no matter the distance between us or how busy life got. Maya Jabbour, thank you for the many phone calls, your listening ear, and your endless encouragement throughout this journey. Cynthia Ishak, thank you for your constant phone calls that kept me company during long days in the lab – your friendship helped carry me through. And to Dr. Ryan Garrigues and Dr. Ian Barton, our midday coffee runs were often the highlight of my day. Thank you for the laughs, the caffeine, and the much-needed breaks.

Finally, to my fiancé, Dr. Alexander Bastian – thank you for everything. From the moment we met in the lab, you've been a mentor, my teammate, and my greatest support. You celebrated my every success and were a shoulder to cry on after rough days. I will be forever grateful for the Mannie lab for bringing me close to you. Your guidance helped me grow, your love helped me persevere, and I can't wait to marry you in just a few short weeks. I am so proud to be walking into the next chapter of life with you by my side.

TABLE OF CONTENTS

LIST OF TABLES

LIST OF FIGURES

LIST OF ABBREVIATIONS

229E	human coronavirus 229E
ACE	angiotensin-converting enzyme
ACE2	angiotensin-converting enzyme 2
AKI	acute kidney injury
ALI	acute lung injury
APN	aminopeptidase N
ARDS	acute respiratory distress syndrome
COVID-19	coronavirus disease 2019
CVD	cardiovascular disease
CYP3A	Cytochrome P450, family 3, subfamily A
dsRNA	double stranded ribonucleic acid
EUA	Emergency Use Authorization
ExoN	exoribonuclease
FBS	fetal bovine serum
FDA	U.S. Food and Drug Administration
GM-CSF	granulocyte-macrophage colony-stimulating factor
hACE2	human angiotensin converting enzyme 2
HCoV	human coronavirus
ICU	intensive care unit
IFN	interferon
IFN-I	type I interferon
IFN-α	interferon-alpha

IFN-β	interferon-beta
IFN-γ	interferon-gamma
IFN-λ	interferon-lambda
IFN-ω	interferon-omega
IFNAR	interferon-alpha/beta receptor
IL-1	interleukin-1
IL-6	interleukin-6
IPS-1	interferon-beta promoter stimulator 1
IRF-1	interferon regulatory factor 1
IRF-3	interferon regulatory factor 3
IRF-7	interferon regulatory factor 7
IV	intravenous
JAK	Janus kinase
K18	human keratin 18
mAb	monoclonal antibody
MAVS	mitochondrial antiviral-signaling protein
MERS-CoV	Middle East respiratory syndrome coronavirus
MOI	multiplicity of infection
MWCO	molecular weight cut-off
NL63	human coronavirus NL63
Nsp5	nonstructural protein 5
Nsp14	nonstructural protein 14
PACS	post-acute COVID-19 syndrome

PAH	pulmonary arterial hypertension
PHEIC	Public Health Emergency of International Concern
PPE	personal protective equipment
PRR	pattern recognition receptor
qRT-PCR	quantitative reverse transcription polymerase chain reaction
RAS	renin-angiotensin system
RdRp	RNA-dependent, RNA polymerase
rhACE2	recombinant human angiotensin-converting enzyme 2
RIG-I	retinoic acid-inducible gene I
RNA	ribonucleic acid
SARS	severe acute respiratory syndrome
SARS-CoV	severe acute respiratory syndrome coronavirus
SARS-CoV-2	severe acute respiratory syndrome coronavirus 2
SDS-PAGE	Sodium Dodecyl Sulfate-Polyacrylamide Gel Electrophoresis
SoC	standard of care
STAT	signal transducers and activators of transcription
suPAR	soluble urokinase plasminogen activator receptor
TF-1	human bone marrow Erythroleukemia
TMPRSS2	transmembrane protease, serine 2
TNF-α	tumor necrosis factor-alpha
VOC	variants of concern
WHO	World Health Organization

CHAPTER 1: INTRODUCTION

1.1 CORONAVIRUS DISEASE 2019 PANDEMIC

The first cases of severe acute respiratory syndrome coronavirus 2 (SARS-CoV-2) were reported in Wuhan, China in December 2019. The World Health Organization (WHO) received reports of a cluster of patients with pneumonia-like symptoms of unknown etiology. By January 2020, the genome of SARS-CoV-2 was sequenced and released, the first cases of SARS-CoV-2 infection were detected in at least 25 other countries, including the United States, and the WHO declared the coronavirus outbreak a Public Health Emergency of International Concern (PHEIC) (2). As of May 2025, over 777 million coronavirus disease 2019 (COVID-19) cases have been reported to the WHO, resulting in over 7 million deaths worldwide (3). In the United States alone, the cumulative case count has surpassed 103 million, with total deaths exceeding 1.2 million (3).

The COVID-19 pandemic highlighted weaknesses in our ability to respond quickly to emerging viruses. Despite advancements in medical research and technology, healthcare systems were unprepared for the scale and rapid spread of SARS-CoV-2. Hospital staff saw shortages in necessary medical equipment such as personal protective equipment (PPE) and ventilators. Governments were delayed in implementing crucial measures such as contact tracing, routine testing, and proper quarantining to prevent the rapid spreading of the virus. The lack of early communication and coordination among countries also added to the difficulty in containing and properly responding to the virus.

We can learn several lessons from the COVID-19 pandemic. With global travel at an all-time high, diseases can easily transfer between countries and continents, and the need for global

coordination on disease containment is more important than ever. Early communication and coordination among countries and international organizations is key to preventing rapid and widespread disease. Prompt detection and surveillance of the spread of the virus by improving data-sharing among countries can help identify potential risks sooner and allow for quicker response times. The pandemic also highlighted the need for clear and consistent communication to the public to help guide behavior and educate on proper safety measures. Finally, the pandemic highlighted the need for continuous development of new classes of antiviral drugs that can be tested and repurposed during viral outbreaks. By ensuring a diverse stock of antiviral drugs for testing against emerging viruses, we can enhance our ability to efficiently and effectively contain outbreaks before they escalate into pandemics.

Given the ongoing challenges of containing diseases due to global travel and the rise of new infectious diseases, the possibility of experiencing a pandemic similar to COVID-19 remains an active concern for researchers and healthcare personnel. According to a recent study, there is a 38% probability of experiencing a pandemic similar to COVID-19 in an individual's lifetime, and this number may double in the next few decades (1). Additionally, on average, the last four pandemics occurred every 15 years (4). Our best chance of combating new outbreaks and pandemics is by being proactive rather than reactive. With continuous development of antiviral drugs, we can more quickly eliminate and potentially obviate emerging problematic viruses.

1.2 SEVERE ACUTE RESPIRATORY SYNDROME CORONAVIRUS 2

SARS-CoV-2 is the etiological agent responsible for the COVID-19 pandemic. SARS-CoV-2 belongs to the Coronaviridae family of the order Nidovirales (Figure 1). Coronaviruses

are a family of respiratory and enteric viruses that can infect humans and animals. Additional coronaviruses that have caused outbreaks are severe acute respiratory syndrome coronavirus (SARS-CoV) in 2002 and Middle East respiratory syndrome coronavirus (MERS-CoV) in 2012.

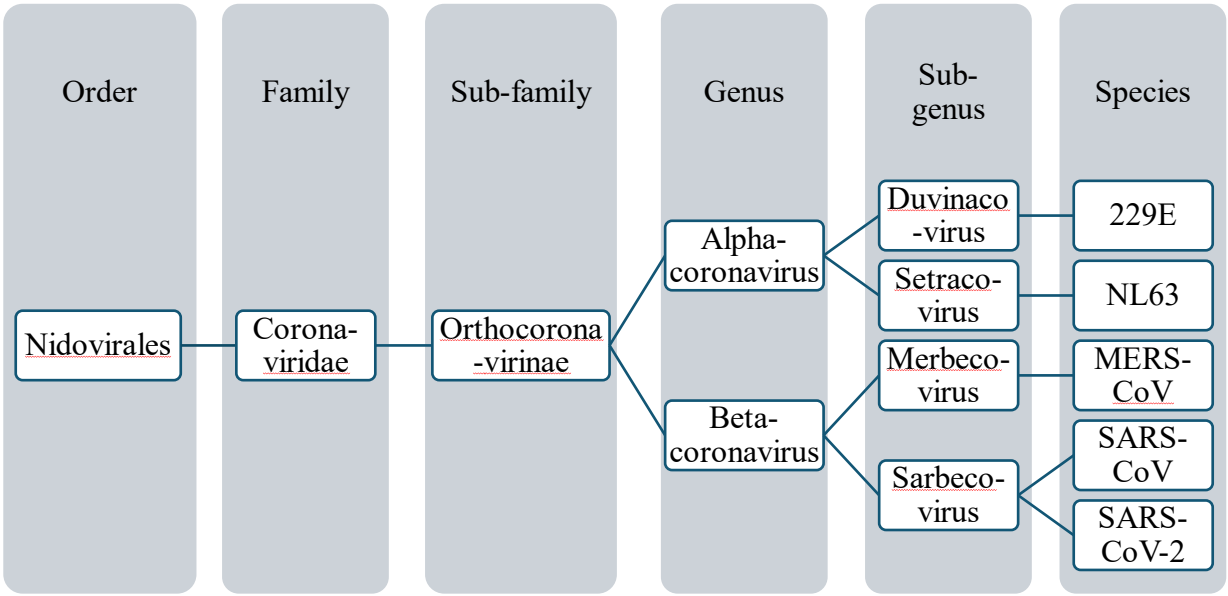

FIGURE 1.1. Coronavirus Taxonomy

SARS-CoV-2 is a positive-sense, single-stranded enveloped ribonucleic acid (RNA) virus. The main structural proteins that make up the virus are the nucleocapsid, membrane, envelope, and spike protein. The spike proteins are glycoproteins that give the virus its characteristic crown-like appearance under an electron microscope. The spike proteins on the surface of SARS-CoV-2 allow the virus to bind to and infect host cells that express angiotensin-converting enzyme 2 (ACE2).

During SARS-CoV-2 synthesis in an infected cell, the spike protein is cleaved by proprotein convertases such as furin (5). The mature virions released have two non-covalently associated subunits, S1 and S2. The S1 subunit is responsible for binding to ACE2, while the S2 subunit is responsible for virus-cell anchoring and membrane fusion. ACE2 binding to the S1 subunit induces conformational changes in the spike protein, exposing the S2' cleavage site

within the S2 subunit. Transmembrane protease, serine 2 (TMPRSS2) at the cell surface or cathepsin L in the endosomal compartment after ACE2-mediated endocytosis cleave the S2 subunit at the S2' cleavage site, releasing the fusion peptide and initiating fusion pore formation (5). Once the fusion pore at the virus-cell complex is formed, the virus genome is released into the host cell's cytoplasm where the genome is translated into additional viral proteins or replicated to produce new viral genome. New virions are assembled in the endoplasmic reticulum-Golgi intermediate compartment (ERGIC) and are transported to the cell membrane in Golgi vesicles. These vesicles then fuse with the cell membrane and mature virions are released by exocytosis, also known as cell budding (6, 7).

RNA viruses are notorious for high error rates, or low viral fidelity, in genome replication. The errors in genome replication allow RNA viruses to mutate at a high rate and adapt to replication in various environments and under selective stress (8). SARS-CoV-2, along with other coronaviruses, have some proofreading capabilities. For example, nonstructural protein 14 (Nsp14) is a highly conserved protein encoded by coronaviruses. Nsp14 contains an N-terminal exoribonuclease (ExoN) that provides proofreading capabilities and replication fidelity (8-10). Despite the proofreading machinery, many SARS-CoV-2 variants have emerged throughout the COVID-19 pandemic.

Since the beginning of the pandemic, the WHO identified many SARS-CoV-2 variants of concern (VOC) and variants of interest (VOI). These variants have shown different levels of transmissibility, antigenicity, and immune evasion and drug-resistance tactics. In 2020, the Alpha (B.1.1.7), Beta (B.1.351), Gamma (P.1), and Delta (B.1.617.2) variants of SARS-CoV-2 were first identified (11-13). The Alpha variant was characterized with increased transmissibility and virulence due to mutations in the spike protein in comparison to the original Wuhan strain (14).

The Beta variant showed high immune evasion, raising vaccine efficacy concerns (15-18). The Gamma variant showed about 2-fold increase in transmissibility and higher viral load than previous variants (16, 19). The Delta variant also showed higher transmissibility and infection severity than previous variants and was responsible for the deadly third wave of COVID-19, due to increased severity of disease (15, 20, 21). The Omicron variant (B.1.1.529) was first identified in 2021. This variant had 3- to 4-fold more mutations than previous variants. With over 18,000 mutations, this variant showed higher rates of transmissibility and immune evasion, with lower susceptibility to neutralization by vaccine- and naturally-induced antibodies (11-13). This led to the development of new COVID-19 vaccine formulations to address breakthrough infection concerns. The Alpha, Beta, Delta, Gamma, and Omicron variants were identified by the WHO as VOCs due to high transmissibility and immune evasion. The WHO also identified eight VOIs: Epsilon (B.1.427 and B.1.429), Eta (B.1.525), Kappa (B.1.617.1), Mu (B.1.621), Lambda (C.37), Theta (P.3), Zeta (P.2), and Lota (B.1.526) (11, 12).

1.3 PATHOGENESIS AND DISEASE PROGRESSION

SARS-CoV-2 is predominantly transmitted through respiratory droplets or aerosolized particles when an infected individual coughs, sneezes, or speaks. After transmission, SARS-CoV-2 enters host cells through the ACE2 receptor that is present on the surface of many different cell types. SARS-CoV-2 primarily infects the respiratory system, leading to diseases ranging from mild flu-like symptoms to severe illnesses such as pneumonia, acute respiratory distress syndrome (ARDS), and acute lung injury (ALI) (22). Common symptoms associated with SARS-CoV-2 infection include cough, fever, myalgia, fatigue, dyspnea, loss of taste and smell, runny nose, and congestion.

ACE2 is the main host receptor for SARS-CoV-2 and is expressed on many different cell types throughout the body, allowing SARS-CoV-2 to infect a wide range of tissues. ACE2 is expressed on cells in the respiratory system, cardiovascular system, gastrointestinal tract, and other organs and immune cells. Type 2 alveolar cells in the lungs express high levels of ACE2, making the lower respiratory tract particularly vulnerable to infection by SARS-CoV-2 (23, 24). SARS-CoV-2 infection of these cells can cause inflammation and pulmonary fibrosis, leading to potentially permanent lung damage.

Symptoms of COVID-19 can persist in some patients for months, a phenomenon known as long COVID, or post-acute COVID-19 syndrome (PACS) (25, 26). Long COVID is a condition that can affect one or multiple systems in the body, such as the gastrointestinal tract, respiratory system, cardiovascular system, etc. (27-29). Other symptoms may include memory loss, difficulty concentrating, and fatigue. The cause of long COVID is still under debate, and multiple mechanisms have been proposed. Among the hypothesized mechanisms are viral antigen persistence, tissue-specific or systemic inflammation, SARS-CoV-2-specific or autoreactive immune responses, gut microbiome dysbiosis, and reactivation of herpesviruses including Epstein-Barr virus (30-35). Therapeutics used for treatment of long COVID are dependent on the system affected and the potential underlying cause.

1.4 FDA-APPROVED AND AUTHORIZED UNDER EUA THERAPEUTICS FOR COVID-19

During the early days of the COVID-19 pandemic, researchers and medical professionals were forced into a race against time to understand the novel SARS-CoV-2 virus and identify potential therapeutics. With the unprecedented public health crisis claiming the lives of

thousands of patients and straining the healthcare system, the search for and development of effective treatments and vaccines became a top priority. As developing new therapeutics would take too long, the urgent need for interventions led to an intense effort to repurpose existing therapeutics that had already been clinically tested and approved by the U.S. Food and Drug Administration (FDA) for other diseases. Medications like remdesivir and dexamethasone were quickly evaluated for effectiveness against COVID-19, as researchers sought to determine whether these drugs could inhibit SARS-CoV-2's ability to replicate or reduce the severity of symptoms.

As the pandemic progressed, the scientific community leaned heavily on knowledge from previous viral pandemics, including the severe acute respiratory syndrome (SARS) pandemic. Researchers explored various treatment options, including antiviral drugs, immune modulators, and corticosteroids, individually and in combination with other treatments. Many drugs were tested for the ability to inhibit viral infection and replication, modulate the immune response, or alleviate symptoms.

There are currently two FDA-approved antiviral drugs to reduce the risk of hospitalization or death in high-risk patients with mild to moderate COVID-19: Paxlovid and Veklury. Paxlovid is an FDA-approved antiviral drug for adults who are at high risk for progression to severe COVID-19 and is authorized under Emergency Use Authorization (EUA) for adolescents. Paxlovid consists of two drugs co-packaged for oral use: a nirmatrelvir tablet and a ritonavir tablet. Nirmatrelvir inhibits nonstructural protein 5 (Nsp5), SARS-CoV-2's main protease that plays a vital role in viral replication and immune evasion. Specifically, Nsp5 is responsible for cleaving SARS-CoV-2 polyproteins into functional viral proteins to allow for assembly of new virions (36). Nsp5 also cleaves retinoic acid-inducible gene I (RIG-I), a pattern

recognition receptor (PRR) that detects cytosolic double-stranded RNA (dsRNA) (37). Ritonavir is a Cytochrome P450, family 3, subfamily A (CYP3A) inhibitor, used to enhance the bioavailability of nirmatrelvir. Together, nirmatrelvir and ritonavir work synergistically to inhibit SARS-CoV-2 replication by blocking key steps in the viral life cycle. In a phase 2-3 clinical trial, patients with symptomatic COVID-19 receiving nirmatrelvir and ritonavir had lower hospitalization rates (0.7% versus 7.1%, respectively) and deaths (0 versus 7, respectively) in comparison to patients receiving the placebo (ClinicalTrials.gov ID NCT04960202) (38, 39). Additionally, the viral titer was lower by day 5 in patients receiving nirmatrelvir and ritonavir compared to patients receiving the placebo (ClinicalTrials.gov ID NCT04960202) (38).

Veklury (also known as remdesivir) is an FDA-approved antiviral drug for adults and children who are either hospitalized with COVID-19 or have mild to moderate COVID-19 and are at high risk for progression to severe COVID-19. Remdesivir is a broad-spectrum antiviral medication administered via intravenous (IV) injection. Remdesivir is a nucleoside analog that inhibits RNA-dependent, RNA polymerase (RdRp). By interfering with viral RNA synthesis, remdesivir prevents viral replication and the progression of infection. In clinical trials, patients who received remdesivir had a decreased time to recovery compared to those who received the placebo (10 versus 15 days, respectively) (ClinicalTrials.gov ID NCT04280705) (40). Patients who received remdesivir were more likely to show clinical improvement at day 15 in comparison to patients who received the placebo (40). Additionally, remdesivir showed significantly greater recovery and reduced risk of death in comparison to the standard care of treatment by day 14 in patients with severe COVID-19 (ClinicalTrials.gov ID NCT04292899) (41).

Lagevrio (also known as molnupiravir) is an antiviral drug authorized under EUA for treatment of mild to moderate COVID-19 in adults who are at high risk for progression to severe

COVID-19. Molnupiravir is a nucleoside analog which serves as a competitive substrate for RdRp, resulting in accumulation of mutations in the genome of the virus (42). In a phase 3 clinical trial of at-risk or unvaccinated patients with mild to moderate COVID-19, patients who received molnupiravir capsules had a reduced risk of hospitalization or death in comparison to patients who received the placebo (ClinicalTrials.gov ID NCT04575597) (43).

In addition to the two FDA-approved antiviral drugs, there are currently two FDA-approved immune modulator drugs for COVID-19: Actemra and Olumiant. Actemra (also known as tocilizumab) is FDA-approved for IV or subcutaneous injection in hospitalized adult patients with COVID-19 who are receiving systemic corticosteroids and require supplemental oxygen, mechanical ventilation, or extracorporeal membrane oxygenation. Tocilizumab is a recombinant interleukin-6 (IL-6) receptor monoclonal antibody that inhibits IL-6 signaling, reducing inflammation. Due to its anti-inflammatory effect, tocilizumab is indicated for treatment of rheumatoid arthritis, giant cell arteritis, systemic sclerosis-associated interstitial lung disease, polyarticular juvenile idiopathic arthritis, systemic juvenile idiopathic arthritis, cytokine release syndrome, and COVID-19. A clinical trial in hospitalized patients with COVID-19-related hypoxia or systemic inflammation showed that tocilizumab improved survival and hospital discharge rates compared to standard care alone (ClinicalTrials.gov ID NCT04381936) (44). These results were supported by a separate phase 3 clinical trial showing that tocilizumab reduced the risk of progression to mechanical ventilation or death (ClinicalTrials.gov ID NCT04372186) (45).

Olumiant (also known as baricitinib) is a Janus kinase (JAK) inhibitor which prevents the phosphorylation and activation of signal transducers and activators of transcription (STAT) responsible for the inflammatory response in COVID-19. Baricitinib tablets are indicated for

patients with rheumatoid arthritis and alopecia areata. Olumiant is FDA-approved for adults or authorized under EUA for pediatric (above 2 years of age) patients hospitalized with COVID-19 and requiring supplemental oxygen, mechanical ventilation, or extracorporeal membrane oxygenation. A phase 3 clinical trial comparing baricitinib and remdesivir (combination treatment) to placebo and remdesivir (control treatment) showed that patients receiving the combination treatment had greater odds of improvement in clinical status (ClinicalTrials.gov ID NCT04401579) (46). Additionally, patients receiving the combination treatment had quicker recovery and lower mortality rates in comparison to the control treatment group (ClinicalTrials.gov ID NCT04401579) (46).

Kineret (also known as anakinra) is an immune modulator drug authorized under EUA for treatment of COVID-19 pneumonia in hospitalized adults requiring supplemental oxygen who are at risk of progressing to severe respiratory failure and likely to have an elevated plasma soluble urokinase plasminogen activator receptor (suPAR). Kineret is FDA-approved for rheumatoid arthritis, neonatal-onset multisystem inflammatory disease, and deficiency of IL-1 receptor antagonist. Kineret is an interleukin-1 (IL-1) receptor antagonist that is administered via subcutaneous injection. A phase 3 trial of anakinra in COVID-19 patients at risk of progressing to respiratory failure as identified by plasma suPAR showed decreased mortality and hospital stay in comparison to the placebo (ClinicalTrials.gov ID NCT04680949) (47, 48).

Gohibic (also known as vilobelimab) is an immune modulator drug authorized under EUA for treatment of COVID-19 in hospitalized adults when initiated within 48 hours of receiving invasive mechanical ventilation or extracorporeal membrane oxygenation. Vilobelimab is a recombinant anti-C5a antibody that blocks the interaction of C5a with its receptor. In a phase 3 clinical trial, patients receiving vilobelimab showed a decreased mortality rate and increased

likelihood of improvement on the WHO COVID-19 ordinal scale in comparison to patients receiving the placebo (ClinicalTrials.gov ID NCT04333420) (49). Vilobelimab also protected against renal replacement therapy (ClinicalTrials.gov ID NCT04333420) (49).

1.5 ACE2 IN CLINICAL TRIALS

ACE2 is an enzyme found on the surface of many different cell types in the human body, including the lungs, heart, and kidneys. ACE2 plays a crucial role in regulating the renin-angiotensin system (RAS), which controls blood pressure, fluid balance, and other important cardiovascular functions. ACE2 counterbalances the actions of angiotensin-converting enzyme (ACE), which increases blood pressure by converting angiotensin I to angiotensin II. Specifically, ACE2 converts angiotensin II into angiotensin 1-7. Angiotensin 1-7 signaling through Mas1 exerts vasodilatory, anti-inflammatory, and anti-fibrotic effects (50). Thus, ACE2's enzymatic activity helps maintain cardiovascular homeostasis.

Due to its anti-inflammatory effects, recombinant soluble ACE2 (sACE2) has shown promise as a therapeutic agent in various diseases. For example, sACE2 has been tested in clinical trials to treat ARDS and pulmonary arterial hypertension (PAH). In a phase 2 clinical trial, researchers found that sACE2 was well-tolerated in patients diagnosed with ARDS that had been mechanically ventilated for less than 72 hours (ClinicalTrials.gov ID NCT01597635) (51). Angiotensin II and IL-6 levels decreased, while angiotensin 1-7 and surfactant protein D levels increased in patients receiving sACE2 twice daily for 3 days (ClinicalTrials.gov ID NCT01597635) (51). In a phase 2a trial, a single IV infusion of sACE2 in patients with PAH led to significant improvement in cardiac output and pulmonary vascular resistance and a reduction in inflammation markers (ClinicalTrials.gov ID NCT01884051) (52).

ACE2 has gained significant attention due to its role as the primary receptor for SARS-CoV-2, as well as being the main host receptor for NL63 and SARS-CoV (5, 53-56). Upon binding of the spike protein of these viruses to ACE2 on the surface of cells, these viruses are internalized via receptor-mediated endocytosis. Acidification of the endosome allows for the fusion of the viral membrane with the endosomal membrane and the release of viral genome into the cytoplasm (5, 57, 58). ACE2 is widely expressed in tissues of the lungs, heart, and kidneys, contributing to the multi-organ complications observed in COVID-19. While ACE2 plays a protective role within the RAS, its interaction with SARS-CoV-2 disrupts normal cellular functions. Namely, SARS-CoV-2 infection leads to ACE2 downregulation by the infected cells, contributing to an imbalance in the RAS and promoting the harmful effects of angiotensin II on inflammation and tissue damage.

Researchers have extensively tested sACE2's ability to blunt infection of NL63, SARS-CoV, and SARS-CoV-2 by neutralization (54, 56, 59). *In vitro* assays showed that sACE2 neutralized pseudovirions expressing SARS-CoV spike and NL63 spike proteins but not 229E spike protein (54). Additionally, sACE2 inhibited SARS-CoV-2 infection of engineered human blood vessel organoids and human kidney organoids (59). *In vivo* preclinical studies showed that sACE2 increased survival, improved lung histopathology, and decreased viral titers in a k18-hACE2 mouse SARS-CoV-2 infection model (60). Therefore, by acting as a decoy receptor, sACE2 can bind to the spike protein on NL63, SARS-CoV, and SARS-CoV-2, preventing infection and reducing viral load.

Due to its anti-inflammatory and neutralizing effects, sACE2 has also been explored as a potential therapeutic intervention for COVID-19 (Table 1.1) (61). A double-blinded, randomized, placebo-controlled, phase 2 trial for COVID-19 showed that intravenous sACE2 significantly

improved mechanical ventilator-free days and reduced viral RNA load compared to placebo (ClinicalTrials.gov ID NCT04335136). Additionally, intravenous sACE2 led to a decrease in pro-inflammatory angiotensin II and an increase in anti-inflammatory angiotensin 1-7 and angiotensin 1-5 (ClinicalTrials.gov ID NCT04335136). In a phase I, double-blind, placebo-controlled, dose-escalation study, aerosolized sACE2 was found to be safe and well-tolerated, with no dose-limiting toxicities and no detection of anti-ACE2 antibodies (ClinicalTrials.gov ID NCT05065645) (62).

Overall, sACE2 has various functions that make sACE2 a promising therapy for multiple diseases, including ARDS, PAH, and COVID-19. First, sACE2's anti-inflammatory and anti-fibrotic effects protect against tissue damage seen in these diseases. Second, sACE2's neutralizing activity against NL63, SARS-CoV, and SARS-CoV-2 protects against infection, reducing damage to tissue and exacerbation of disease. Finally, all emergent pathogenic variants of NL63, SARS-CoV, and SARS-CoV-2 continue to share specificity for the ACE2 host receptor. Therefore, sACE2 may serve as a promising decoy receptor for any variant of these viruses.

TABLE 1.1. Soluble ACE2 in COVID-19 Clinical Trials and Case Studies

Title	Completion or Publication Date	Intervention	Outcomes
Human recombinant soluble ACE2 in severe COVID-19 **(61)**	September 24, 2020	Hospitalized patient with severe COVID-19: Drug: IV rhACE2	IV rhACE2 decreased angiotensin II; increased angiotensin 1-7, angiotensin 1-9, and angiotensin 1-5; decreased IL-6 and interleukin-8 (IL-8); and decreased viral load.

Recombinant Human Angiotensin-converting Enzyme 2 (rhACE2) as a Treatment for Patients With COVID-19 (APN01-COVID-19) **(ClinicalTrials.gov ID NCT04335136)**	December 26, 2020	Hospitalized COVID-19 patients: Drug: IV rhACE2 Placebo: IV physiological saline solution	IV rhACE2 improved mechanical ventilator-free days, reduced viral RNA load, decreased pro-inflammatory angiotensin II, and increased anti-inflammatory angiotensin 1-7 and angiotensin 1-5.
Study to Assess the Safety, Tolerability, Pharmacokinetics and Pharmacodynamics of Inhaled APN01 Developed as Treatment for COVID-19 **(ClinicalTrials.gov ID NCT05065645)**	May 27, 2022	Healthy volunteers: Drug: nebulized rhACE2 Placebo: nebulized 0.9% sodium chloride	Nebulized rhACE2 was safe and well tolerated and did not trigger an immune response. Nebulized rhACE2 increased angiotensin 1-5 levels.

1.6 TYPE I INTERFERONS

Interferons (IFNs) are a group of cytokines that play a crucial role in the induction of an antiviral state in cells following viral infection, the enhancement of innate immune responses, and the facilitation of adaptive immune responses. IFNs inhibit viral replication and help initiate the adaptive immune response against the infective virus. The antiviral state induced in cells by interferon signaling is the first line of defense following viral infection. The antiviral state inhibits viral replication and viral spread to nearby cells by inhibiting viral protein synthesis, degrading viral RNA, and trapping newly formed virions, preventing viral release from the infected cell to infect other nearby cells (63).

SARS-CoV-2, among other viruses, inhibits IFN production and signaling. Multiple proteins encoded by SARS-CoV-2 have been shown to act as IFN antagonists by inhibiting different key pathways in the IFN induction and signaling pathways (64-67). For example, Nsp5 is a protease encoded by the SARS-CoV-2 genome. Once expressed in the host cell after infection, Nsp5 cleaves RIG-I, a PRR that detects cytosolic dsRNA (37). The cleavage of RIG-I inhibits its activation of mitochondrial antiviral-signaling protein (MAVS), also known as the IFN-β promoter stimulator 1 (IPS-1) (37). MAVS activation is one pathway responsible for IFN production by activating interferon regulatory factors 1 and 3 (IRF1 and IRF3, respectively). Additionally, Nsp5 promotes the ubiquitination and proteasome-mediated degradation of MAVS (37). Thus, Nsp5 inhibits antiviral IFN production by at least two different methods.

The inhibition of antiviral IFN production by various SARS-CoV-2 proteins allows the virus to replicate unchecked, leading to a high viral load and increased tissue damage. The lack of an adequate IFN response could also contribute to a dysregulated immune response against SARS-CoV-2, resulting in an exaggerated inflammatory response known as a "cytokine storm." The cytokine storm can lead to widespread tissue damage, organ failure, and death (68, 69). A cytokine storm is characterized by the overproduction of pro-inflammatory cytokines such as tumor necrosis factor-alpha (TNF-α), IL-1, and IL-6 (70). Typically, these cytokines play a crucial role in inhibiting viral infection. However, the overproduction of these cytokines may have a detrimental effect on the human body, including systemic inflammation, damage to blood vessels, and increased vascular permeability, leading to fluid leakage into tissues, including the lungs. As a result, patients with unmanaged severe COVID-19 may develop ARDS, ALI, acute kidney injury (AKI), and cardiovascular disease (CVD) (70).

Severe COVID-19 has been linked to inborn errors as well as neutralizing autoantibodies against IFN-I. Inborn errors of essential IFN-I mediators underlie about 5% of severe COVID-19 cases (71). These inborn errors include mutations to IRF-3 (68), interferon regulatory factor 7 (IRF-7) (72), interferon alpha and beta receptor subunit 1 and 2 (IFNAR1 and IFNAR2, respectively) (68, 73, 74), toll-like receptor 3 and 7 (TLR3 and TLR7, respectively) (68, 75, 76), and many others (71). Neutralizing autoantibodies against IFN-α and interferon-omega (IFN-ω) have been detected in 20% of patients with fatal COVID-19 and 20% of patients above the age of 70 with severe COVID-19 (71, 77-79). The presence of autoantibodies against IFN-I correlates with the fatality rate of COVID-19 patients.

Given the critical role of IFNs in viral clearance – and the impaired production and function of IFNs in SARS-CoV-2-infected patients – researchers have evaluated IFNs alone or in combination with antiviral drugs in COVID-19 clinical trials (Table 1.1). In these clinical trials, IFNs showed different efficacies depending on the route of administration, the severity of the disease during administration, and the antiviral drugs used in combination with IFN (80-82). Early in the pandemic, the WHO tested four repurposed antiviral drugs for COVID-19 independently – remdesivir, hydroxychloroquine, lopinavir, and interferon-beta (IFN-β). In this trial, IFN-β was administered either intravenously (10 μg daily for 6 days) or subcutaneously (44 μg on days 1, 3, and 6), depending on availability (83). No effect in mortality rate, hospital duration, or initiation of ventilation was seen in patients who received IFN-β treatments (83).

Synairgen developed a nebulized formula of IFN-β for treatment of COVID-19. In a randomized, double-blind, placebo-controlled, phase 2 trial of IFN-β delivered via nebulization once daily for 14 days, patients who received the treatment had accelerated recovery and a 79% decrease in progression to severe disease or death compared to patients who received the placebo

(ClinicalTrials.gov ID NCT04385095) (84). A randomized, double-blind, placebo-controlled, phase 3 trial showed that nebulized IFN-β trended towards reducing relative risk of progression to severe disease or death within 35 days compared to patients who received placebo, especially in high-risk patient subgroups (ClinicalTrials.gov ID NCT04732949) (85). However, this trial did not meet its primary objective, as patients who received nebulized IFN-β were not discharged any sooner and did not recover more rapidly than patients who received the placebo (ClinicalTrials.gov ID NCT04732949) (85).

Two key variables to note from the WHO and Synairgen trials were severity of disease at time of IFN-β administration and route of administration. In both trials, recipients were hospitalized COVID-19 patients, with those in the Synairgen trial also requiring oxygen via nasal prongs or a mask. IFN treatment has been shown to be most effective early in disease, while late administration of IFN can be contraindicated (81, 86). Administration of IFN during early stages of disease is beneficial, since SARS-CoV-2 typically inhibits production of IFN-I in the early stages of infection. However, IFN administration during the later stages of SARS-CoV-2 infection and in severe COVID-19 can enhance immunopathology and damage to the lungs. During severe COVID-19, the cytokine storm causes overstimulation of the immune system, leading to ALI. IFN administration during this stage can worsen this condition and lead to permanent damage to the lungs (81, 86, 87). Therefore, early administration of IFN-β to patients not yet hospitalized but with comorbidities making them at high risk for severe COVID-19 could have proven to be more protective than IFN-β administration to hospitalized patients.

Route of administration is also critical in targeting IFN-β to the site of infection and reducing systemic side effects. Administering IFN-β via subcutaneous or intravenous injection results in systemic distribution of IFN-β coupled with highly diffuse antiviral function and a

primary impact on non-target cell types irrelevant to the viral infection. IFN-β targeted directly to the lungs via nebulization was a key difference between the WHO trial and Synairgen trials and potentially a reason why the Synairgen trials were more successful at treating patients with COVID-19.

TABLE 1.2 IFN-β in COVID-19 Clinical Trials

Title	Publication Date	Intervention	Outcomes
Triple combination of interferon beta-1b, lopinavir-ritonavir, and ribavirin in the treatment of patients admitted to hospital with COVID-19: an open-label, randomized, phase 2 trial (88)	May 8, 2020	Hospitalized patients with mild to moderate COVID-19: Combination group: lopinavir, ritonavir, ribavirin and IFN-β1b Control group: lopinavir and ritonavir	Combination therapy significantly reduced the duration of viral shedding and hospital stay.
Clinical evaluation of IFN beta1b in COVID-19 pneumonia: a retrospective study (89)	May 21, 2020	Hospitalized patients with moderate to severe COVID-19 pneumonia: Interferon group: subcutaneous IFN-β1b (Betaferon) and antivirals (lopinavir/ritonavir, and/or hydroxychloroquine or chloroquine), and/or anti-inflammatory drugs (steroids and/or tocilizumab) Control group: antivirals (lopinavir/ritonavir, and/or hydroxychloroquine or chloroquine), and/or anti-inflammatory drugs (steroids and/or tocilizumab)	IFN-β1b did not significantly decrease in-hospital mortality. The treatment's effectiveness was difficult to evaluate since most patients were also receiving other forms of treatment.
A randomized clinical trial of the efficacy and safety of interferon β-1a in treatment of severe COVID-19 (90)	August 20, 2020	Hospitalized patients with severe COVID-19: Interferon group: IFN-β1a and hydroxychloroquine plus lopinavir-ritonavir or atazanavir-ritonavir	IFN-β1a significantly increased discharge rate on day 14 and reduced 28-day mortality.

		Control group: hydroxychloroquine plus lopinavir-ritonavir or atazanavir-ritonavir	
Interferon β−1b in treatment of severe COVID-19: A randomized clinical trial (91)	August 24, 2020	Hospitalized patients with severe COVID-19: Interferon group: IFN-β1b subcutaneously plus lopinavir/ritonavir or atazanavir/ritonavir plus hydroxychloroquine Control group: lopinavir/ritonavir or atazanavir/ritonavir plus hydroxychloroquine	IFN-β1b significantly decreased time to clinical improvement, decreased ICU admission rate, and increased 14-day discharge rate.
Randomized controlled open label trial on the use of favipiravir combined with inhaled interferon beta-1b in hospitalized patients with moderate to severe COVID-19 pneumonia (92)	November 9, 2020	Hospitalized patients with moderate to severe COVID-19 pneumonia: Interferon group: favipiravir with IFN-β1b by inhalation aerosol Control group: hydroxychloroquine	IFN-β1b did not significantly change clinical outcomes or inflammatory markers.
Safety and efficacy of inhaled nebulized interferon beta-1a (SNG001) for treatment of SARS-CoV-2 infection: a randomized, double-blind, placebo-controlled, phase 2 trial (84)	November 12, 2020	Hospitalized COVID-19 patients: Interferon group: nebulized IFN-β1a Control group: placebo	IFN-β1a significantly increased odds of improvement and speed of recovery.
Repurposed antiviral drugs for COVID-19 – interim WHO Solidarity trial results (83)	December 2, 2020	Hospitalized COVID-19 patients: Interferon group: subcutaneous or intravenous IFN-β1a Control group: local standard of care	IFN-β1a did not decrease mortality, initiation of ventilation, or hospitalization duration.
Combination therapy of IFNβ1 with lopinavir–ritonavir, increases	December 26, 2020	Hospitalized COVID-19 patients: Interferon group: subcutaneous IFN-β1a, lopinavir and ritonavir	IFN-β1a significantly reduced mortality rate.

oxygenation, survival and discharging of sever COVID-19 infected inpatients (93)		Control group: lopinavir and ritonavir	
Clinical outcomes of different therapeutic options for COVID-19 in two Chinese case cohorts: a propensity-score analysis (94)	February 13, 2021	Symptomatic hospitalized COVID-19 patients: IFN-β1b monotherapy IFN-β1b and ribavirin IFN-β1b and lopinavir-ritonavir IFN-β1b and ribavirin and lopinavir-ritonavir	IFN-β1b monotherapy and IFN-β1b plus ribavirin improved clinical outcomes and decreased hospitalization time.
Role of interferon therapy in severe COVID-19: The COVIFERON randomized controlled trial (95)	April 13, 2021	Hospitalized patients with severe COVID-19: Interferon group 1: subcutaneous IFN-β1a + lopinavir/ritonavir and hydroxychloroquine Interferon group 2: subcutaneous IFN-β1b + lopinavir/ritonavir and hydroxychloroquine Control group: lopinavir/ritonavir and hydroxychloroquine	IFN-β1a significantly decreased time to clinical improvement compared to the control group.
An open-label randomized controlled trial of the effect of lopinavir/ritonavir, lopinavir/ritonavir plus IFN-β1a and hydroxychloroquine in hospitalized patients with COVID-19 (96)	May 26, 2021	Hospitalized COVID-19 patients: Interferon group: subcutaneous INF-β1a + lopinavir/ritonavir + SoC Control group: SoC	IFN-β1a did not significantly impact clinical status or SARS-CoV-2 clearance.
Efficacy of interferon beta-1a plus remdesivir compared with remdesivir alone in hospitalized adults with COVID-19: a double-blind, randomized, placebo-	October 18, 2021	Hospitalized COVID-19 patients + presence of radiographic infiltrates on imaging, a peripheral oxygen saturation on room air of 94% or less, or requiring supplemental oxygen: Interferon group: subcutaneous IFN-β1a plus remdesivir	IFN-β1a did not improve time to recovery. IFN-β1a caused worse outcomes in patients who required high-flow oxygen at baseline compared

controlled, phase 3 trial (97)		Control group: placebo plus remdesivir	with those given the placebo.

1.7 SUMMARY AND RATIONALE FOR THIS STUDY

The COVID-19 pandemic is driven by the repeated emergence of new pathogenic variants that continually diversify under evolutionary pressure from the global pool of anti-SARS-CoV-2 immunity (98-106). The evolutionary drive on pathogenic variants is shaped by the lack of sterilizing immunity in infected and/or vaccinated individuals and particularly in immunocompromised individuals who harbor replicating virus for prolonged periods. Rapid evolution of SARS-CoV-2 is compounded by the inherent mutability of the viral genome, which is driven via the accumulation of point mutations and genetic recombination with other circulating variants (107-109). Both types of mutations compromise the affinity and neutralization capacity of pre-existing anti-Spike antibodies in the human population, thereby generating immune escape variants. Notably, however, all emergent pathogenic variants continue to share specificity for the ACE2 host receptor, thereby providing a means to target all SARS-CoV-2 variants and all other viral species sharing the ACE2 host receptor specificity.

To exploit the common ACE2 host receptor specificity, we developed a novel anti-viral platform comprised of the antiviral effector cytokine IFN-β fused to sACE2. This IFNβ-ACE2 fusion protein is predicted to bind human coronaviruses (HCoV) NL63, SARS-CoV, and SARS-CoV-2 via the virion surface spike glycoprotein (53, 54, 110-113). The rationale is that the physical coupling of the IFN-β and sACE2 domains will confer synergistic activities not realized by either domain acting alone, based on the following postulates. (a) The sACE2 domain is

predicted to anchor IFN-β to the virion surface and thereby coat the virion with a surface array of IFN-β. (b) Upon interaction of a partially neutralized virion with a host target cell, the IFN-β domain anchored to the surface of the virion is predicted to trigger IFNAR signaling before host cell infection, such that the virion will only infect host cells with previously upregulated IFN-I antiviral defenses. (c) Induction of IFN-I defenses prior to infection is predicted to abrogate subsequent viral replication, thereby blocking amplification of viral cytopathic effects and cytokine-storm immunopathogenesis. Given that HCoV NL63, SARS-CoV, and SARS-CoV-2 robustly block IFN-β production (65, 114-121), delivery of exogenous IFN-β via an IFNβ-ACE2 targeting mechanism is predicted to obviate a primary immune evasion tactic of coronaviruses, thereby blocking viral infection and systemic dissemination. Clinical application of IFNβ-ACE2 via nebulized aerosols directly to the pulmonary system would be of potential benefit during infection with ACE2-targeting viruses in patients who are asymptomatic, pre-symptomatic, or presenting with mild to severe disease including ARDS or cytokine-release/vascular-leak immunopathology.

Although engineering a virion surface-targeted IFN-β array is an attractive antiviral strategy, the concept requires experimental validation. Potential pitfalls include: (a) The IFN-β domain arrayed on the virion surface may not have the appropriate molecular orientation to efficiently engage IFNAR on the host cell to initiate antiviral signaling. (b) The concentration of IFN-β array at the virion surface may be insufficient to trigger a protective antiviral response. (c) The virion-surface IFN-β array may not provide an adequate lead-time to establish antiviral innate immunity before viral infection. (d) The IFN-β domain may augment viral infectivity by bridging virus and host cell membranes. To address these potential concerns, *in vitro* infection studies were used to test the conceptual basis of the IFNβ-ACE2 modality. These experiments

revealed that IFNβ-ACE2 had enhanced antiviral activity against NL63 compared to sACE2, IFN-β, and the unlinked combination of ACE2 and IFN-β. Additionally, *in vitro* targeting studies were performed in which NL63 virions were incubated with IFNβ-ACE2 and then washed to remove unbound proteins to test the antiviral activity of IFNβ-ACE2 physically linked to the viral surface. These 'virus-washed' experiments revealed that virion surface-bound IFNβ-ACE2 had potent antiviral activities that were superior compared to either or both sACE2 and/or IFN-β. Additionally, there was no evidence that IFNβ-ACE2 enhanced infection by bridging the virus and host cell membranes. The main conclusion is that the IFNβ-ACE2 array on the virion surface has potent antiviral activity due to the preemptive targeting of antiviral IFN-β activity to the exact site and time of imminent viral infection. Thus, virus surface-targeted IFN-β provides a conceptual basis for a new platform technology and a new category of antiviral therapy.

CHAPTER 2: MATERIALS AND METHODS

This chapter is modified from Jabbour et al., A novel antiviral therapeutic platform: anchoring IFN-β to the surface of infectious virions equips interferon-evasive virions with potent antiviral activity. Viruses 2025, 17, 697. https://doi.org/10.3390/v17050697

2.1. PROTEIN, VIRUS, AND CELLS

Human IFN-β (300-02BC) was purchased from Peprotech and is referenced as 'IFN-β (Peprotech)'. Cercopithecus aethiops kidney epithelial cells expressing trans-membrane protease, serine 2 and human angiotensin-converting enzyme 2 (Vero E6-TMPRSS2-T2A-ACE2 cells) (NR-54970), Homo sapiens lung carcinoma (A549) cells (NR-52268), human coronavirus NL63 (NR-470), and human coronavirus 229E (NR-52726) were obtained from BEI Resources. LLC-MK2 cells (CCL-7) were purchased from ATCC. Vero E6-TMPRSS2-T2A-ACE2, A549, and LLC-MK2 cells were cultured in Dulbecco's modified Eagle's medium (DMEM) supplemented with 10% fetal bovine serum (FBS). Human embryonic kidney 293-F (HEK) cells (R79007, Gibco) were cultured in FreeStyle 293 Expression Medium (12338018, Gibco). Genes encoding full-length SARS-CoV-2 spike (D614G) (VG40589-UT, Sino-Biological) and full-length CD25 (122) were cloned into pIRES AcGFP1 expression vector (632435, Clontech), and these vectors were used to transfect HEK cells to derive stable lines (HEK-Spike and HEK-control, respectively) that expressed the respective transmembrane proteins. Because stably transfected cells expressed GFP, flow cytometric analyses focused on HEK cells in the viable GFP+ gate. Human bone marrow Erythroleukemia (TF-1) cells (CRL-2003, ATCC) were cultured in RPMI

supplemented with 5% FBS and 1 nM granulocyte-macrophage colony-stimulating factor (GM-CSF). The NL63 and 229E viruses were propagated on LLC-MK2 and A549 cells, respectively, and were concentrated at 4 °C by either ultracentrifugation at 48,000 g for 5 hours or ultrafiltration on YM100 membranes. Viruses were then aliquoted and frozen at -80 °C.

2.2. TISSUE CULTURE INFECTION DOSE 50 ($TCID_{50}$)

Infectious titers of NL63 and 229E were quantified in 96-well plate plaque assays in Vero E6-TMPRSS2-T2A-ACE2 cells and MRC-5 cultures, respectively. Cells were seeded at 30,000 cells/well and incubated at 33 °C. After 24 hours, the cells were inoculated with a half-log serial dilution of the virus stock (8 replicates per dilution) and incubated at 33 °C. At 5 days post-infection, the supernatant was discarded, and the cell monolayer was washed with PBS and stained with crystal violet. After 15 minutes of staining, the crystal violet was discarded, the number of wells with plaques was counted for each dilution, and the $TCID_{50}$ was calculated according to the Reed-Münch method (123).

2.3. GENERATION AND PURIFICATION OF RECOMBINANT PROTEINS

We used stable mammalian expression systems for recombinant proteins. In addition to IFN-β (Peprotech), we expressed a recombinant IFN-β control protein (referenced as recombinant IFN-β) that was comprised of the human IFN-β sequence (P01574), except that a non-native alanine residue was added as the second N-terminal amino acid to encode an optimal Kozak translation-initiation site (GCCGCCACC-ATG-GCC-). To control for the enterokinase

linker and poly-histidine sequence in IFNβ-ACE2, the C-terminus of recombinant IFN-β included an enterokinase linker cleavage site (GDDDDKG) and a C-terminal histidine purification tag (TRTSTHHHHHHHH). Thus, IFNβ-ACE2 and recombinant IFN-β represented a controlled comparison because both shared similar linker sequences. The IFNβ-ACE2 (P01574 and Q9BYF1, respectively) included an N-terminal Rat Albumin Signal Sequence (MAKWVTFLLLLFISGSAFS), the secreted human N-terminal IFN-β sequence (MSYN….GYLRN), an enterokinase cleavage site (GDDDDKG), a 9-histidine purification tag, and the human C-terminal sACE2 metallopeptidase domain (18-611) (GSTIE….STDWS). The sACE2(18-611) and sACE2(18-740) control proteins were comprised of the human ACE2 sequence (Q9BYF1). These sequences included an N-terminal Rat Albumin Signal Sequence (MAKWVTFLLLLFISGSAFS), a 9-histidine purification tag, the respective sACE2 18-611 or 18-740 sequence, a linker (AKGGGSEGGGSEGGGSG), and a C-terminal GFP sequence (P42212). These constructs were cloned into pIRES AcGFP1 expression vector (632435, Clontech). HEK cells were stably transfected with these vectors and grown in FreeStyle 293 Expression Medium (Gibco). Expression supernatants were collected every 2-3 days and cells were reseeded under selection pressure by G418 (Biovision, Waltham, MA). Expression supernatants were concentrated and buffer exchanged into 50 mM NaH2PO4 (pH 8.0) on YM10 ultrafiltration membranes. The concentrated protein was then directly applied to Ni-NTA Agarose columns (Qiagen, Chatsworth, CA), and the resin was extensively washed with increasing amounts of imidazole (50 mM NaH2PO4 with 0-, 20-, 40-, or 60-mM imidazole, pH 8.0). IFN-β, sACE2(18-611), sACE2(18-740) and IFNβ-ACE2 were eluted with 50 mM NaH_2PO_4 with 250 mM imidazole (pH 8.0), concentrated in Amicon Ultra-15 centrifugal filter devices (EMD Millipore, Billerica, MA), and dialyzed in Slide-A-Lyzer dialysis cassettes G2

(87735, ThermoFisher Scientific). The protein was quantified by absorbance at 280 nm, and the purity was assessed by Sodium Dodecyl Sulfate-Polyacrylamide Gel Electrophoresis (SDS-PAGE).

2.4. VALIDATION OF IFN-β DOMAIN OF IFNβ-ACE2: IFN-β ANTI-PROLIFERATION ASSAY

The IFN-β bioactivities of recombinant proteins were measured *in vitro* by inhibition of GM-CSF-dependent proliferation of TF-1 cells. TF-1 cells were incubated with 1 nM GM-CSF and IFNβ-ACE2, IFN-β (Peprotech), recombinant IFN-β, or sACE2(18-611) in complete RPMI for 3 days at 37 °C. The culture was pulsed with 1 μCi [^{3}H]thymidine after 48 hours of the 72-hour culture. Cells were harvested onto filters by use of a Tomtec Mach III harvester (Hamden, CT, United States). Proliferation was measured via [^{3}H]thymidine incorporation into DNA using a Perkin Elmer MicroBeta2 liquid scintillation counter.

2.5. VALIDATION OF sACE2 DOMAIN OF IFNβ-ACE2: sACE2 BINDING TO HEK-SPIKE

The sACE2 domain was assessed by binding to HEK-Spike cells. HEK-Spike or HEK-control cells (100,000 cells/tube) were incubated with either sACE2(18-611) or IFNβ-ACE2 at 4 °C. After a 1-hour incubation, cells were washed twice with PBS with 2% FBS and blocked with Fc Receptor Binding Inhibitor Polyclonal Antibody (14-9161-73, Invitrogen) for 1 hour at 4 °C. Following the blocking step, cells were washed twice with PBS with 2% FBS and stained with

Alexa Fluor 647 (AF647)-conjugated rat anti-human ACE2 (375803, Biolegend) for 1 hour at 4 °C. Cells were then washed with PBS with 2% FBS and analyzed for surface-bound anti-ACE2 monoclonal antibodies (mAbs) on a Cytek Aurora Spectral Cytometer (Fremont, CA) with unmixing via unstained and single-stained control samples followed by analysis with De Novo Software FCS Express 7 (Glendale, CA). The percentage of ACE2 positive cells were gated as the number of viable, single, live, GFP^+ (stably transfected), and $ACE2^+$ cells divided by the total number of cells in the GFP^+ gate. The mean fluorescence intensity (MFI) of anti-ACE2 fluorescence was gated on all cells in the viable, single, live, GFP^+ gate.

2.6. INHIBITION ASSAYS OF HCOV NL63 AND 229E INFECTION *IN VITRO*

The antiviral activity of IFNβ-ACE2 was tested using HCoV NL63 and 229E infection assays on Vero E6-TMPRSS2-T2A-ACE2 and A549 cells, respectively. Cells were seeded into a 96-well plate at 30,000 cells/well and grown for 24 hours at 33 °C. NL63 and 229E were used at a multiplicity of infection (MOI) of 0.1. NL63 and 229E were incubated with either IFNβ-ACE2, sACE2(18-611), sACE2(18-740), IFN-β (Peprotech), recombinant IFN-β, or the unlinked combination of IFN-β and sACE2(18-611) for 1 hour at 4 °C. For the 'no wash' system, the virus and protein were then added directly to the cells in that both virus-bound and non-bound protein were carried into the infection culture. For the 'virus-washed' system, the virus and protein mixtures were subjected to five ultrafiltration washing steps (300 kDa MWCO Nanosep centrifugal filters, OD300C34, Cytiva) in PBS with 0.5% poloxamer (sheer protectant) (pH 7.5). This virus-washing protocol retained virus and virus-bound protein in the retentate but eliminated unbound protein in the filtrate. Five washes eliminated unbound protein while

maintaining viral infectivity, based on calculations as well as flow cytometry analyses of infectivity. The 'washed' virus preparations in the retentate were then added to the cells. For both non-washed and virus-washed protocols, virus and host cells were cultured for 2 days at 33 °C. After 2 days, cells were detached using TrypLE Express Enzyme (12563029, Gibco), transferred to a V-bottom 96-well plate, and blocked with Fc Receptor Binding Inhibitor Polyclonal Antibody (14-9161-73, Invitrogen) for 1 hour at 4 °C. Control (non-infected) cells and virally infected cells were stained with a 1:1000 dilution of LIVE/DEAD Fixable Blue Dead Cell Stain Kit (L23105, Invitrogen) for 1 hour at 4 °C. After washing with PBS with 5% FBS, Vero E6-TMPRSS2-T2A-ACE2 cells were surface-stained with 1:1600 dilution of PE-conjugated mouse anti-human TMPRSS2 (378403, Biolegend) and 1:100 dilution of FITC-conjugated mouse anti-human ACE2 (10108-MM36-F, Sino Biological) for 1 hour at 4 °C and then were washed twice with PBS with 5% FBS. For intracellular staining, Vero E6-TMPRSS2-T2A-ACE2 and A549 cells were fixed and permeabilized using eBioscience Foxp3/Transcription Factor Staining Buffer Set (00-5523-00, Invitrogen) by incubating cells in the Fixation/Permeabilization buffer for 30 minutes at room temperature. Cells were then washed twice with the Permeabilization buffer and blocked with 10% rabbit serum (16120-099, Gibco) for 1 hour at 4 °C. Antibodies for intracellular staining of nucleocapsid protein were previously prepared by conjugating rabbit anti-NL63 nucleocapsid antibody (40641-T62, Sino Biological) or rabbit anti-229E nucleocapsid antibody (40640-T62, Sino Biological) with AF647 by use of the AF647 Conjugation Kit (Fast) - Lightning-Link (ab269823, Abcam). Intracellular staining of cells infected with HCoV NL63 and 229E was performed by incubating cells with 1:1600 dilution of AF647-conjugated rabbit anti-NL63 nucleocapsid antibody or 1:1600 dilution of AF647-conjugated rabbit anti-229E nucleocapsid antibody, respectively, for 1 hour at 4 °C. After

washing once with permeabilization buffer and once with PBS with 2% FBS, cells were resuspended in PBS with 2% FBS and analyzed on a Cytek Aurora Spectral Cytometer (Fremont, CA) with unmixing via unstained and single-stained control samples followed by analysis with De Novo Software FCS Express 7 (Glendale, CA). Cells were gated on viable, single, and live cells before gating on $FITC^+$, PE^+, and $AF647^+$ gates. MFI of PE and FITC was gated on all viable, single, and live cells.

2.7. STATISTICAL ANALYSES, DATA PRESENTATION, AND EXPERIMENTAL REPRODUCIBILITY

Comparisons with one independent variable were assessed via one-way analysis of variance (ANOVA) with the Dunnett multiple comparisons test. Comparisons with two independent variables were assessed via two-way ANOVA with Tukey's multiple comparisons test. A p-value < 0.05 was considered significant. Significance was indicated as follows: (* or ° $p < 0.05$, ** or °° $p < 0.01$, *** or °°° $p < 0.001$, and **** or °°°° $p < 0.0001$). Each data point represents the mean value, and error bars represent the standard deviation (SD). Experiments shown in the figures are representative of three independent experiments.

CHAPTER 3: ACE2(18-611) AND IFN-β DOMAINS OF THE THERAPEUTIC FUSION PROTEIN MAINTAIN INDIVIDUAL ACTIVITIES

This chapter is modified from Jabbour et al., A novel antiviral therapeutic platform: anchoring IFN-β to the surface of infectious virions equips interferon-evasive virions with potent antiviral activity. Viruses 2025, 17, 697. https://doi.org/10.3390/v17050697

3.1 ABSTRACT

The COVID-19 pandemic highlighted the need for continuous development of new antiviral drug classes that can be modified or repurposed to target emerging problematic viruses in the early stages of viral outbreak. The quicker we can respond to emerging pathogenic viruses, the better we can prevent widespread viral transmission and mitigate potential public health crises. We have developed a new platform of antiviral therapeutics that consists of an immune modulator domain covalently linked to a viral host receptor. By covalently linking an immune modulator to a viral host receptor, we can localize the antiviral activity of the immune modulator to the surface of the infectious virus, targeting its antiviral activity to the exact site and time of viral infection.

IFN-β targeting to the surface of an infectious virion has inherent advantages over simply introducing IFN-β to the body via subcutaneous/intravenous injection or even nebulization. Targeting nebulized IFN-β directly to the surface of the virus can reduce or eliminate off-target binding of IFN-β. Additionally, lower doses of IFN-β may be administered to accomplish similar antiviral effects *in vivo* due to the precise targeting of IFN-β where needed within the body. This reduces potential negative side effects of IFN-β and enhances the antiviral activity where needed.

Additionally, this therapeutic is modular in nature as the ACE2 domain could be swapped for a different viral host receptor that targets IFN-β to the surface of emerging viruses of concern. By doing so, we have created a fusion protein therapeutic that can be easily repurposed during new outbreaks as long as we can identify the receptor of the new virus. Similarly, the IFN-β could be swapped for a different immune modulator or antiviral peptide that more efficiently blocks infection and replication.

The first step of testing a novel fusion protein is to validate whether the domains maintain individual, unhindered activities. We tested the sACE2 domain of the fusion protein in a flow-based binding assay and found that the fusion protein exhibited binding to the transmembrane SARS-CoV-2 spike protein similar to the sACE2(18-611) control protein. We tested the IFN-β domain of the fusion protein in an anti-proliferative assay using GM-CSF-dependent TF-1 cells. The IFN-β domain of the fusion protein had similar anti-proliferative activity on TF-1 cells as the control IFN-β proteins.

3.2 RESULTS

Mode of action and design of IFNβ-ACE2 (Figures 3.1, 3.2, 3.3).

Based on the standard mode of administration, IFN-β alone does not bind to the surface of virions, which leads to diffuse and non-targeted antiviral action (Figure 3.1, top). In contrast, IFNβ-ACE2 is designed to decorate infectious virions with a surface array of IFN-β to preemptively target and upregulate antiviral activity in host cells prior to viral infection (Figure 3.1, bottom). The fusion protein prototype consists of the antiviral cytokine IFN-β covalently linked to sACE2, the main host receptor for SARS-CoV, SARS-CoV-2, and NL63 (Figure 3.2A). We expressed IFNβ-ACE2, recombinant IFN-β, sACE2(18-611), and sACE2(18-740) in

stably transfected HEK cell lines (Figure 3.2A-D). Protein purification yielded 1.5 - 2 mg of protein per 500 mL of culture supernatant. Figures 3.3A-D show purity of each protein on SDS-Page gels. Lastly, we created an HEK cell line that expresses the full-length SARS-CoV-2 protein (D614G) (HEK-Spike) and a control HEK cell line that expresses the full-length CD25 (HEK-control) (Figure 3.2E,F).

The binding of soluble IFNβ-ACE2 to the virion-surface spike protein is dependent on affinity, the relative ligand concentrations, and the cooperative induction/ availability of the spike protein in the 'open' conformation. At low IFNβ-ACE2 concentrations, a hypothetical plot showing the distribution of virions based on the ranked percentage of spike occupancy per virion would predictably show a strong right/ positively-skewed distribution, where most virions exhibit low IFNβ-ACE2 occupancy of spike on a per virion basis. At intermediate IFNβ-ACE2 concentrations, this plot would show a symmetric bell-shaped distribution, where most virions exhibited approximately 50% occupancy of spike on a per virion basis. At high IFNβ-ACE2 concentrations, this plot would show a strong left/ negatively-skewed distribution, where most virions exhibited a high occupancy of spike on a per virion basis.

The low IFNβ-ACE2 concentration range represents the most feasible pharmacologic delivery scenario, wherein non-saturating IFNβ-ACE2 concentrations in the picomolar/ low nanomolar range can be achieved with high feasibility via standard delivery modalities including nebulized delivery of aerosols. These concentrations should provide effective therapeutic action based on the postulate that IFN-β directly anchored to the virion surface mediates the dominant anti-viral action of this platform independently of neutralization. Thus, in the most realistic scenarios, virions will be partly coated with IFNβ-ACE2, such that these virions may trigger IFN-β antiviral pathways concurrently with virus-host cell fusion and initial viral invasion. In

this scenario, the major question is whether the kinetics of the IFN-β antiviral response can outpace a concomitant infective process to afford aborted infection and protective innate immunity.

The IFN-β domain of IFNβ-ACE2 had anti-proliferative activity comparable to that of the IFN-β control proteins (Figure 3.4).

A central question was whether the individual domains of IFNβ-ACE2 exhibited predicted domain-specific activities. To assess the IFN-β domain, we used an anti-proliferative assay to compare IFNβ-ACE2 to control proteins including (a) human IFN-β (Peprotech), (b) human recombinant IFN-β protein, and (c) human recombinant sACE2(18-611) (Figure 3.4). The IFNβ-ACE2 and the control proteins were cultured at designated concentrations with GM-CSF-stimulated TF-1 cells for 3 days at 37 °C, and [^{3}H]thymidine incorporation was measured on the third day. As shown in Figure 3.4, IFNβ-ACE2 exhibited potent anti-proliferative activity that closely approximated the inhibitory activities of the two IFN-β control proteins. Conversely, sACE2 lacked anti-proliferative activity. These data showed that IFN-β domain of IFNβ-ACE2 retains potent interferon activity capable of inhibiting proliferative responses.

The sACE2 domain of IFNβ-ACE2 specifically bound the transmembrane SARS-CoV-2 spike protein (Figure 3.5).

To assess the sACE2 domain, ACE2 binding to HEK-Spike was compared to HEK-control cells. HEK-Spike or HEK-control cells (100,000 cells/tube) were incubated with

designated concentrations of either sACE2(18-611) or IFNβ-ACE2 for 1 hour at 4 °C. After washing, cells were stained with AF647-conjugated anti-human ACE2 antibody and were analyzed for ACE2 binding by flow cytometry. Figure 3.5A shows the gating scheme. Cells were gated on viable, single, live, and GFP^+ cells before gating on ACE2-bound cells. Figure 3.5B shows representative dot plots of ACE2-binding of 2 μM sACE2(18-611) or IFNβ-ACE2 to HEK-Spike and HEK-control cells. IFNβ-ACE2 had similar binding to HEK-Spike as sACE2(18-611), as indicated by percentages of cells in the $ACE2^+$ gate (Figure 3.5C) and by the MFI of anti-ACE2 (Figure 3.5D). As shown in Figure 3.5E, IFNβ-ACE2 and sACE2(18-611) exhibited robust binding to HEK-Spike cells but did not exhibit detectable binding to HEK-control cells. These data provide evidence that the sACE2 domain of IFNβ-ACE2 maintains robust binding to transmembrane SARS-CoV-2 spike protein.

3.3 DISCUSSION

As mentioned previously, IFN-β has been tested extensively in clinical trials. A comparison of the antiviral and anti-inflammatory benefits seen with different modes of IFN-β administration shows that the administration route plays a crucial role in targeting the effects of IFN-β to where needed. The antiviral and anti-inflammatory effects seen with subcutaneous and intravenous administration of IFN-β had lower efficacy in comparison to inhaled nebulized IFN-β. This result is likely due to off-target IFNAR on irrelevant cell types and the limited IFN-β biodistribution to the lungs during subcutaneous and intravenous administration. Off-target effects of IFN-β, as seen in subcutaneous administration, may also lead to negative side effects, as seen in multiple sclerosis patients receiving therapeutic IFN-β, including nausea, fatigue, and other flu-like symptoms. Nebulization of IFN-β is a more targeted approach of administering

IFN-β in comparison to subcutaneous and intravenous IFN-β because pulmonary administration directly delivers the therapeutic to the site of viral infection in COVID-19.

Although more targeted, inhaled IFN-β failed to show efficacy in a phase 3 clinical trial for COVID-19 (85). This clinical trial compared nebulized IFN-β to placebo and found that hospital discharge rates and time to recovery were similar between the two groups. However, their data showed that IFN-β may have prevented progression to severe disease, especially in high-risk patient subgroups. They attributed the difference in results between their phase 2 and phase 3 clinical trials to improvement in standard of care. Although nebulization is a more targeted approach than subcutaneous and intravenous administration, this administrative route confers considerable off-target binding of IFN-β to cell types irrelevant to the infection, leading to diffuse antiviral responses (Figure 3.1, top).

To minimize the off-target binding of IFN-β, we created an IFNβ-ACE2 fusion protein that is designed to target IFN-β to the surface of NL63, SARS-CoV, and SARS-CoV-2 through host receptor specificity. The ACE2 domain binds to the spike protein on the surface of the virions, coating them with a surface array of IFN-β. This places IFN-β at the exact site of imminent viral infection. By administering this fusion protein therapeutic via nebulization, the fusion protein is targeted to the site of infection (lungs) and further targeted to the surface of the virions through the ACE2 domain (Figure 3.1, bottom).

In addition to our therapeutic fusion protein (Figure 3.2A), we expressed monomeric sACE2(18-611) and dimeric sACE2(18-740) control proteins (Figure 3.2B and C, respectively) as well as an IFN-β control protein (Figure 3.2D) that we used in addition to the IFN-β control protein purchased from Peprotech. We also created HEK cells lines that express full-length SARS-CoV-2 spike protein or full-length CD25 (Figure 3.2E and F, respectively). These cell

lines were used in the binding assay shown in Figure 3.5. Following the expression and purification of IFNβ-ACE2, sACE2(18-740), sACE2(18-611), and IFN-β, we ran SDS-Page gels to test for purity of proteins (Figure 3.3A,B,C,D, respectively).

When designing a fusion protein, using a linker that provides the flexibility required to allow each domain to act independently is crucial. We tested the linker used in our fusion protein in previous fusion proteins designed and purified in our lab (124). The linker consists of an enterokinase cleavage site (GDDDDKG) and a 9-histidine purification tag (Figure 3.2A). After purifying IFNβ-ACE2, we compared the anti-proliferative activity of the IFN-β domain to recombinant IFN-β and IFN-β (Peprotech) in a [^{3}H]thymidine incorporation assay with TF-1 cells (Figure 3.4). We also compared the ACE2 domain to sACE2(18-611) in a spike-binding flow-based assay (Figure 3.5). Both domains of IFNβ-ACE2 exhibited predicted domain-specific activities, indicating that the linker used provided the flexibility required to allow the domains to function independently.

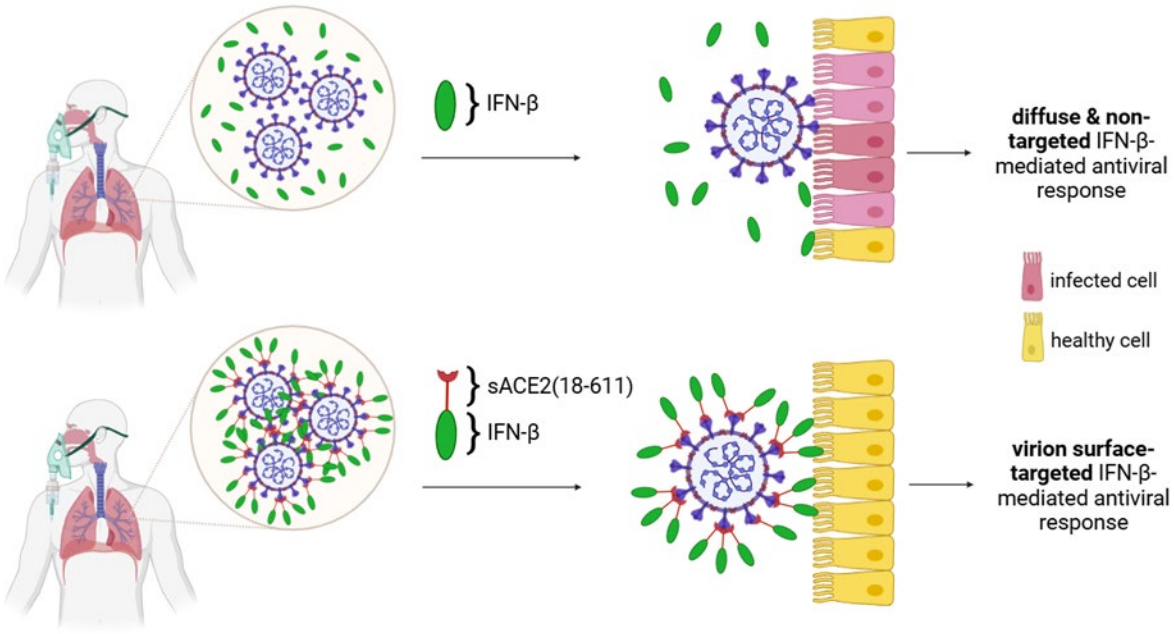

FIGURE 3.1. Postulated mechanism underlying the IFNβ-ACE2 fusion protein. A SARS-CoV-2 or NL63-infected individual is given IFNβ-ACE2 via nebulization to the lungs. The sACE2 domain is postulated to bind the spike protein and coat the virion with a surface array of IFN-β. Based on this strategy, the IFN-β domain will drive IFN-β signaling pathways and antiviral activity in the target cell before viral entry. IFNβ-ACE2 is postulated to provide a more concentrated and targeted approach to delivering IFN-β to the exact site and time of imminent viral infection (125).

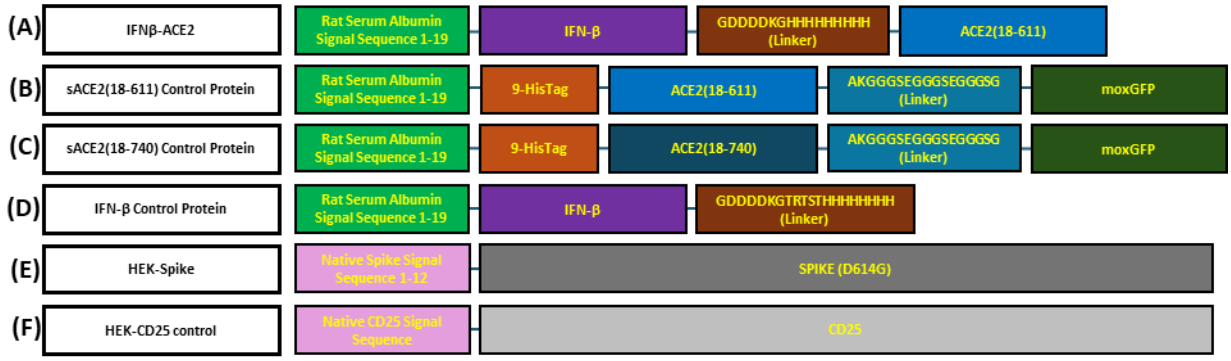

FIGURE 3.2. Schematic diagrams of expressed constructs and cell lines. (A) Schematic diagram of the soluble fusion protein constructs consisting of an IFN-β domain and a sACE2(18-611) domain. (B) Schematic diagram of the soluble control protein construct, sACE2(18-611). (C) Schematic diagram of the soluble control protein construct, sACE2(18-740). (D) Schematic diagram of the soluble control protein construct, IFN-β. (E) Schematic diagram of the transmembrane spike protein expressed in HEK cells for the ACE2-binding assay. (F) Schematic diagram of the transmembrane control CD25 protein expressed in HEK cells for the ACE2-binding assay.

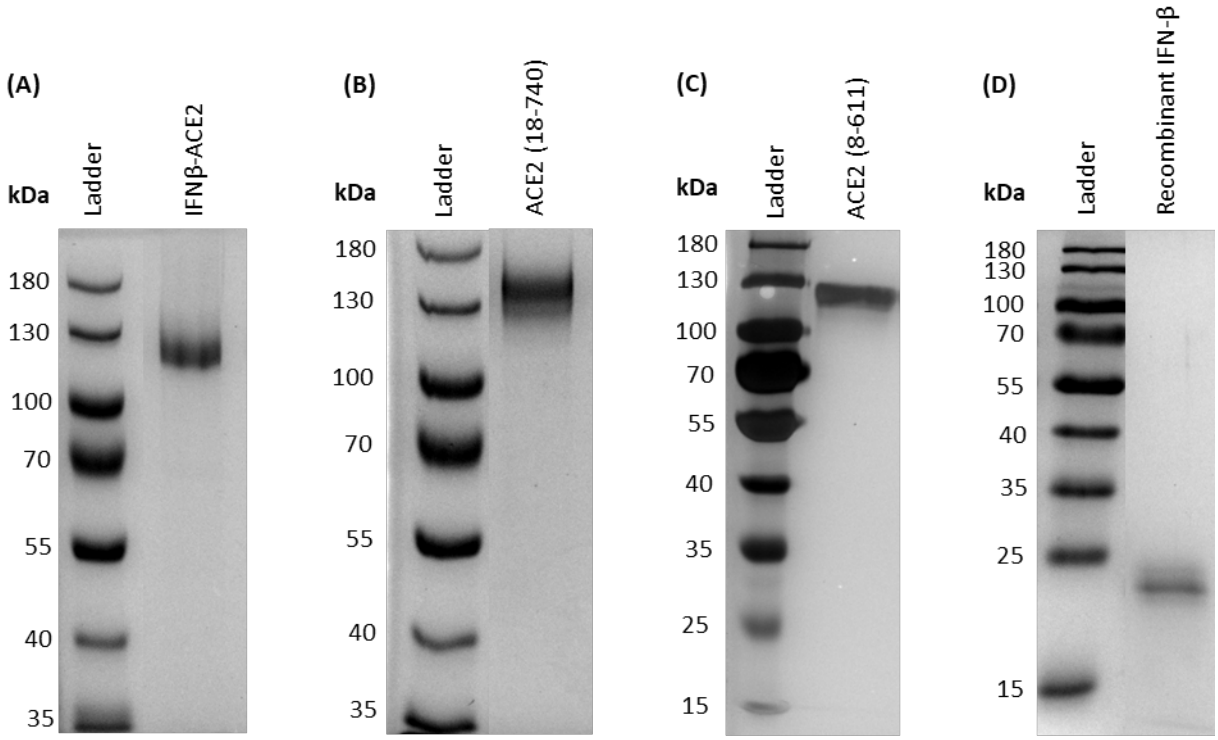

FIGURE 3.3. SDS-PAGE gels of purified proteins. (A) 8% SDS-Page gel showing purity of IFNβ-ACE2. (B) 8% SDS-Page gel showing purity of sACE2(18-740). (C) 8% SDS-Page gel showing purity of sACE2(18-611). (D) 12% SDS-Page gel showing purity of IFN-β.

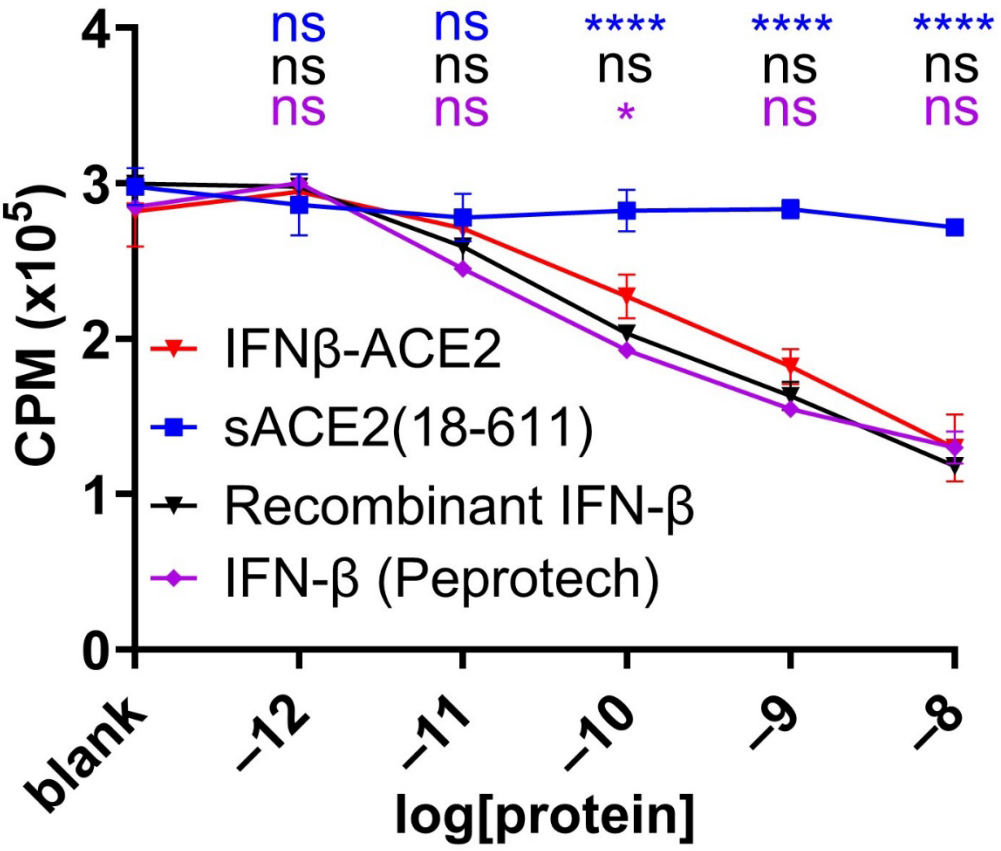

FIGURE 3.4. The IFN-β domain of IFNβ-ACE2 exhibited predicted bioactivity. To assay the IFN-β domain, TF-1 cells were incubated with GM-CSF and either IFN-β, sACE2(18-611), or IFNβ-ACE2 then pulsed with [^{3}H]thymidine during the last 24 hours of a 3-day culture. The y-axis represents counts per minute (CPM), and error bars represent the SD. Statistical significance was analyzed by use of two-way ANOVA with Tukey's multiple comparisons test comparing the three control groups to the IFNβ-ACE2 treatment group at each concentration (ns nonsignificant, * $p < 0.05$, **** $p < 0.0001$). Each data point represents the mean value (n=2), and error bars represent SD. These data are representative of three independent experiments.

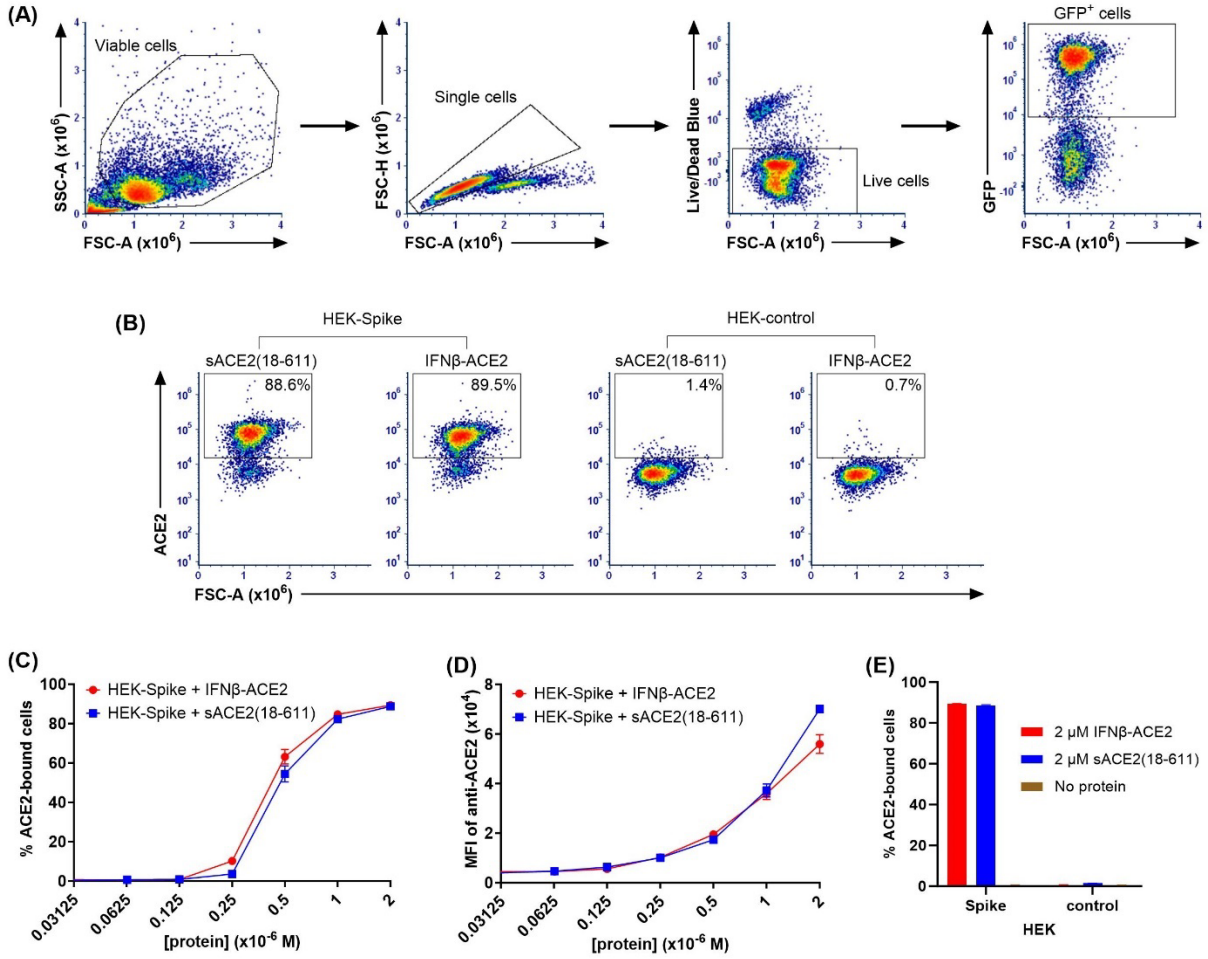

FIGURE 3.5. The sACE2 domain of IFNβ-ACE2 exhibited predicted bioactivity. To assay the ACE2 domain, HEK-Spike or HEK-control cells were incubated with designated concentrations of either sACE2(18-611) or IFNβ-ACE2 for 1 hour at 4 °C. After washing, cells were stained with AF647-conjugated anti-human ACE2 antibody for 1 hour at 4 °C. Cells were analyzed for ACE2 binding by flow cytometry. (A) Viable, single, live, and GFP^+ stably transfected cells (parental gate representing all cells in plot) were subgated to show the $ACE2^+$ subset. (B) Representative dot plots show binding of either sACE2(18-611) or IFNβ-ACE2 (2 μM each) to HEK-Spike or HEK-control cells. (C) Shown are percentages of $ACE2^+$ HEK-Spike cells ($ACE2^+$ gate/ parental gate). (D) The MFIs of anti-ACE2 fluorescence are shown for the

parental gate. (E) Bar graphs show mean percentages of HEK-Spike or HEK-control cells bound to ACE2 ($ACE2^+$ gate/ parental gate). Each data point represents the mean value (n=2), and error bars represent SD. These data are representative of three independent experiments.

CHAPTER 4: ACE2(18-611) DOMAIN OF THERAPEUTIC FUSION PROTEIN TARGETS IFN-β SPECIFICALLY TO THE SURFACE OF NL63 BUT NOT 229E

This chapter is modified from Jabbour et al., A novel antiviral therapeutic platform: anchoring IFN-β to the surface of infectious virions equips interferon-evasive virions with potent antiviral activity. Viruses 2025, 17, 697. https://doi.org/10.3390/v17050697

4.1 ABSTRACT

IFN-β is a potent antiviral modulator and an important first line of defense during viral infection. For this reason, IFN-β has been extensively tested in clinical trials as an antiviral therapeutic agent. However, as seen in IFN-β clinical trials for COVID-19, the antiviral and anti-inflammatory activity of IFN-β is equivocal, and IFN therapeutics have not generally advanced to phase 3 clinical trials. We believe that the mild activity of IFN-β in COVID-19 patients is due to the diffuse and off-target IFN-β signaling within the body. When given subcutaneously or intravenously, the majority of the IFN-β administered binds to cell types irrelevant to the infection, leading to adverse systemic side effects. Although inhalation is a more targeted approach to administering IFN-β to COVID-19 patients, this route of administration still fails to pinpoint IFN-β signaling to the exact cells of interest. We have designed a modular antiviral platform that targets IFN-β to the surface of a virion through host receptor specificity. Via this strategy, IFN-β signaling is directly targeted to the exact cells of interest and upregulates an antiviral state in target cells to preclude viral infection. For proof of concept, we have tested the ability of sACE2 to target IFN-β to the surface of NL63 through fusion protein technology.

Herein, we show that NL63-targeted IFN-β has potent antiviral activity against NL63 infection and that the covalent linkage of sACE2 to IFN-β is required for this targeting. We also show that this targeting is specific to NL63 and not the 229E control virus that does not bind ACE2. This platform is modular as the sACE2 domain of the fusion protein can be swapped with a different viral host receptor to target a different virus of interest.

4.2 RESULTS

The sACE2 domain of IFNβ-ACE2 targeted IFN-β to the surface of NL63 (Figure 4.1).

The primary question addressed by this study was whether the sACE2 domain of IFNβ-ACE2 targets IFN-β to the surface of NL63 to mediate preemptive antiviral activity. To assess this question, we ran flow cytometric assays to measure intracellular nucleocapsid expression as a measure of viral infection. NL63 (MOI of 0.1) was incubated for 1 hour with either IFNβ-ACE2, sACE2(18-611), IFN-β (Peprotech), or recombinant IFN-β. The virus plus protein preparations were then subjected to repeated centrifugal ultrafiltration through a 300 kDa MWCO filter to filter unbound protein into the filtrate, whereas stable virus-protein complexes were retained in the retentate. 'Virus-washed' NL63 and/or NL63-protein complexes in the retentate were subsequently seeded onto Vero E6-TMPRSS2-T2A-ACE2 cells. After a 48-hour incubation, cells were harvested, stained, and analyzed by flow cytometry to measure viral infection. Flow cytometric analysis showed that infected versus uninfected cells presented as qualitatively distinct populations, with virally infected cells presenting as a distinct nucleocapsid^{+} phenotype whereas uninfected cells were distinctly nucleocapsid^{-} (Figure 4.1A). IFNβ-ACE2 at an initial concentration range of 100 pM – 1 μM bound to NL63 and was retained as virion-bound IFNβ-ACE2 to cause inhibition of NL63 nucleocapsid production (Figure

4.1B,C). The mechanism of inhibition was attributed largely to the antiviral activity of the IFN-β domain rather than to ACE2-mediated neutralization, because sACE2(18-611) alone only exhibited inhibition at the highest concentration tested (1 μM) (Figure 4.1B). Rather, the sACE2 domain of IFNβ-ACE2 was needed to anchor IFN-β to the virion surface because neither IFN-β preparation alone had antiviral activity, presumably because IFN-β did not independently bind the virus and therefore was lost in the filtrate (Figure 4.1C). Distinction of nucleocapsid^{+} versus nucleocapsid^{-} subsets as infected versus uninfected subsets was validated in that nucleocapsid^{+} subset corresponded to an ACE2^{low} and TMPRSS2^{low} phenotype, and vice versa, which corresponds with the downregulation of the ACE2 host receptor and the TMPRSS2 coreceptor upon infection (Figure 4.1D-M). Based on ACE2 and TMPRSS2 expression, IFNβ-ACE2 robustly inhibited infection across a concentration range of 100 pM to 1 μM, whereas sACE2(18-611) alone inhibited infection only at the highest concentration tested (1 μM) (Figure 4.1E-F, J-K), and both IFN-β preparations alone lacked detectable antiviral activity (Figure 4.1G-H, L-M). Overall, these data reveal that IFNβ-ACE2 binds to virions to mediate robust antiviral interferon activity as evidenced by parallel concentration-response curves for the three infected nucleocapsid^{+}, ACE2^{low}, and TMPRSS2^{low} phenotypes. These data support the hypothesis that IFNβ-ACE2 provides specific targeting of interferon activity to the virion surface, which is the most proximal site of viral infectivity.

A remaining question was whether the covalent linkage between IFN-β and sACE2 in IFNβ-ACE2 was required for the enhanced antiviral efficacy. These experiments thereby addressed the formal possibility that unlinked sACE2 and IFN-β could act synergistically as independent molecules directly on the virus to inhibit viral infectivity, via unanticipated mechanisms. To address this question (Figure 4.2), we used the 'virus-washed' *in vitro* assay to

compare IFNβ-ACE2 to the unlinked combination of equimolar sACE2(18-611) and IFN-β, with nucleocapsid expression (Figure 4.2B,C) coupled with ACE2 and TMPRSS2 downregulation (Figure 4.2D-F and 4.2G-I, respectively) as measures of infection. Figure 4.2A shows the gating scheme. Cells were gated on viable, single, and live cells prior to gating on nucleocapsid^{+}, ACE2^{+}, and TMPRSS2^{+} cells (Figure 4.2A). As predicted, these data showed that the covalent linkage between IFN-β and sACE2 was critical for targeting. These data support the hypothesis that sACE2 binds the spike protein to anchor IFN-β on the virion surface to 'flip' the virus to a positive interferon-signaling entity.

ACE2 and TMPRSS2 expression negatively correlated with nucleocapsid expression (Figure 4.3).

To test whether ACE2 receptor and TMPRSS2 receptor expression could serve as markers for viral infection, we compared receptor expression to nucleocapsid expression under different treatment types and concentrations (various degrees of infection). Linear regression analyses revealed a significantly negative correlation between infection (MFI of anti-nucleocapsid) and receptor expression (MFI of anti-ACE2 and MFI of anti-TMPRSS2) (Figure 4.3A and Figure 4.3B, respectively). This indicates that higher infection levels are associated with increased receptor downregulation.

Additionally, we tested whether the downregulation of ACE2 expression was correlated with the downregulation of TMPRSS2 expression under various degrees of infection. Linear regression analysis revealed a significantly positive correlation between ACE2 expression and TMPRSS2 expression in infected cells (Figure 4.3C). This indicates that viral infection is

associated with coordinated downregulation of ACE2 (the main host receptor) and TMPRSS2 (a coreceptor).

The sACE2 domain of IFNβ-ACE2 did not target IFN-β to the surface of 229E (Figure 4.4 and 4.5).

A central question focused on the virus-targeting specificity of IFNβ-ACE2. An important question was whether the sACE2 domain of IFNβ-ACE2 also targeted IFN-β to the surface of HCoV 229E which binds human aminopeptidase N (APN) rather than ACE2 as the host receptor. To address this question, we performed 'virus-wash' experiments with HCoVs NL63 (MOI of 0.1) and 229E (MOI of 0.1) by incubating 1 nM IFNβ-ACE2 or the unlinked combination of 1 nM sACE2(18-611) and 1 nM IFN-β with NL63 or 229E. After 1 hour, the viruses were repeatedly washed via the 300 kDa MWCO Nanosep centrifugal filters. Ultrafiltration retentates containing NL63-protein complexes or 229E-protein complexes were then seeded onto Vero E6-TMPRSS2-T2A-ACE2 or A549 cells, respectively, with or without re-addition of protein (IFNβ-ACE2 or recombinant protein controls). After a 48-hour incubation, the cells were harvested, stained, and analyzed by flow cytometry. Figures 4.4A and 4.5A show the gating scheme. Cells were gated on viable, single, and live cells before gating on nucleocapsid^{+} cells (Figure 4.4A and 4.5A). Figure 4.5B shows representative dot plots of nucleocapsid gating under various treatment conditions. The central finding was that IFNβ-ACE2 exhibited antiviral activity against NL63 but had no antiviral effect against 229E (Figure 4.4B). The unlinked combination of sACE2(18-611) and IFN-β had no effect on either virus (Figure 4.4B) because sACE2(18-611) is sub-neutralizing at this concentration (1 nM) and the

IFN-β was presumably lost in the filtrate during the virus-wash procedure. The antiviral activity of IFN-β on 229E was confirmed in control groups wherein IFNβ-ACE2 or the IFN-β + sACE2(18-611) proteins were re-added to control host cell cultures after the virus-wash procedure (Figure 4.5C). These control groups validated the IFN-β-mediated antiviral susceptibility of 229E. These data show that the sACE2 domain specifically binds to NL63 but not 229E in accordance with spike host receptor specificity. Thus, sACE2 domain is a specific virus-targeting modality that reflects the host receptor specificity of the viral spike protein.

4.3 DISCUSSION

Two central questions are addressed in this chapter. First, can we target IFN-β to the surface of a virion by covalently linking IFN-β to the main host receptor of this virion? To address this, we performed "virus-washed" assays. In these assays, we incubated NL63 with either IFNβ-ACE2, sACE2(18-611), IFN-β, or the unlinked combination of sACE2(18-611) and IFN-β to allow for binding. After a 1-hour incubation, we repeatedly washed the virus using a 300 kDa centrifugal filter to eliminate any unbound protein. IFNβ-ACE2 and sACE2(18-611) inhibited viral infection despite the washing steps, whereas IFN-β was eliminated and did not have any effect on viral infection (Figures 4.1-4.3). This indicates that sACE2 successfully binds to and targets IFN-β to the surface of NL63. On the other hand, when 229E was incubated with IFNβ-ACE2, sACE2(18-611), IFN-β, or the linked combination of sACE2 and IFN-β for 1 hour then washed to eliminate any unbound protein, there was no inhibition of 229E infection (Figures 4.4 and 4.5). As a control, we re-added protein after the washing step to 229E to show that IFN-β does inhibit 229E infection (Figure 4.5). This indicates that the targeting of IFN-β through sACE2 is specific to NL63, due to host receptor specificity.

The second central question addressed in this chapter is: Does virion-targeted IFN-β maintain antiviral activity? In other words, do the two domains of the fusion protein maintain individual properties uninhibited by steric hindrance or other inhibitory factors? This question can also be answered with the viral wash assays. IFNβ-ACE2 bound to the surface of NL63 potently inhibited infection (Figures 4.1-4.3). This indicates that the ACE2 domain of the fusion protein maintained its ability to bind to spike protein on the surface of NL63, and virion-bound IFN-β maintains robust antiviral activity.

Soluble ACE2, rather than anti-Spike antibody, was chosen as the targeting domain in this fusion protein for various reasons. Soluble ACE2 plays dual roles in both dampening inflammation and combating NL63 or SARS-CoV-2 infection by viral neutralization. Within the renin-angiotensin system, ACE2 serves as a critical modulator by breaking down the pro-inflammatory molecule angiotensin II into angiotensin 1–7, promoting physiological balance. This anti-inflammatory function of ACE2 has been implicated in reducing the severity of conditions such as ARDS, ALI, and SARS. Infection with NL63 or SARS-CoV-2 leads to reduced expression of membrane-bound ACE2, a change that may worsen disease outcomes. For this reason, re-introduction of ACE2 in the form of sACE2 may reverse the inflammatory effects of the reduction of membrane-bound ACE2. In addition to these immunomodulatory effects, sACE2 also exhibits antiviral activity by directly binding to the spike proteins of HCoV-NL63, SARS-CoV, and SARS-CoV-2, thereby preventing these viruses from infecting host cells.

Additionally, unlike anti-spike antibodies, sACE2 binds all known variants of NL63, SARS-CoV, and SARS-CoV-2. Thus, although anti-Spike antibodies might bind more efficiently to the spike protein on certain virus strains in comparison to sACE2, sACE2 is impervious to

immune evasion by these viruses, thus providing a method to target IFN-β to the site of infection with any current or future pathogenic strain.

NL63 nucleocapsid expression in infected cells was negatively correlated with ACE2 and TMPRSS2 expression (Figures 4.3A,B). Additionally, ACE2 and TMPRSS2 downregulation in infected cells were positively correlated (Figure 4.3C). The coordinated downregulation of ACE2 and TMPRSS2 in infected cells could reflect multiple mechanisms potentially occurring at a per cell basis. (1) The decrease of ACE2 and TMPRSS2 on the surface of infected cells could be a result of receptor internalization after viral binding and internalization. (2) Host cell release of transmembrane ACE2 and TMPRSS2 or downregulation of ACE2 and TMPRSS2 could be a protective mechanism to limit further viral infection. (3) Viral proteins may cause the release of transmembrane ACE2 and TMPRSS2 or induce suppression of receptor expression as a mechanism to prevent superinfection. Altogether, these data indicate that ACE2 and TMPRSS2 downregulation may serve as a marker for viral infection.

This fusion protein serves as a proof-of-concept for our novel antiviral platform. We believe that, by switching out the host receptor domain to a different receptor, we can successfully target IFN-β to the surface of a specific virus of interest. This will allow us to quickly respond to future pathogens viruses.

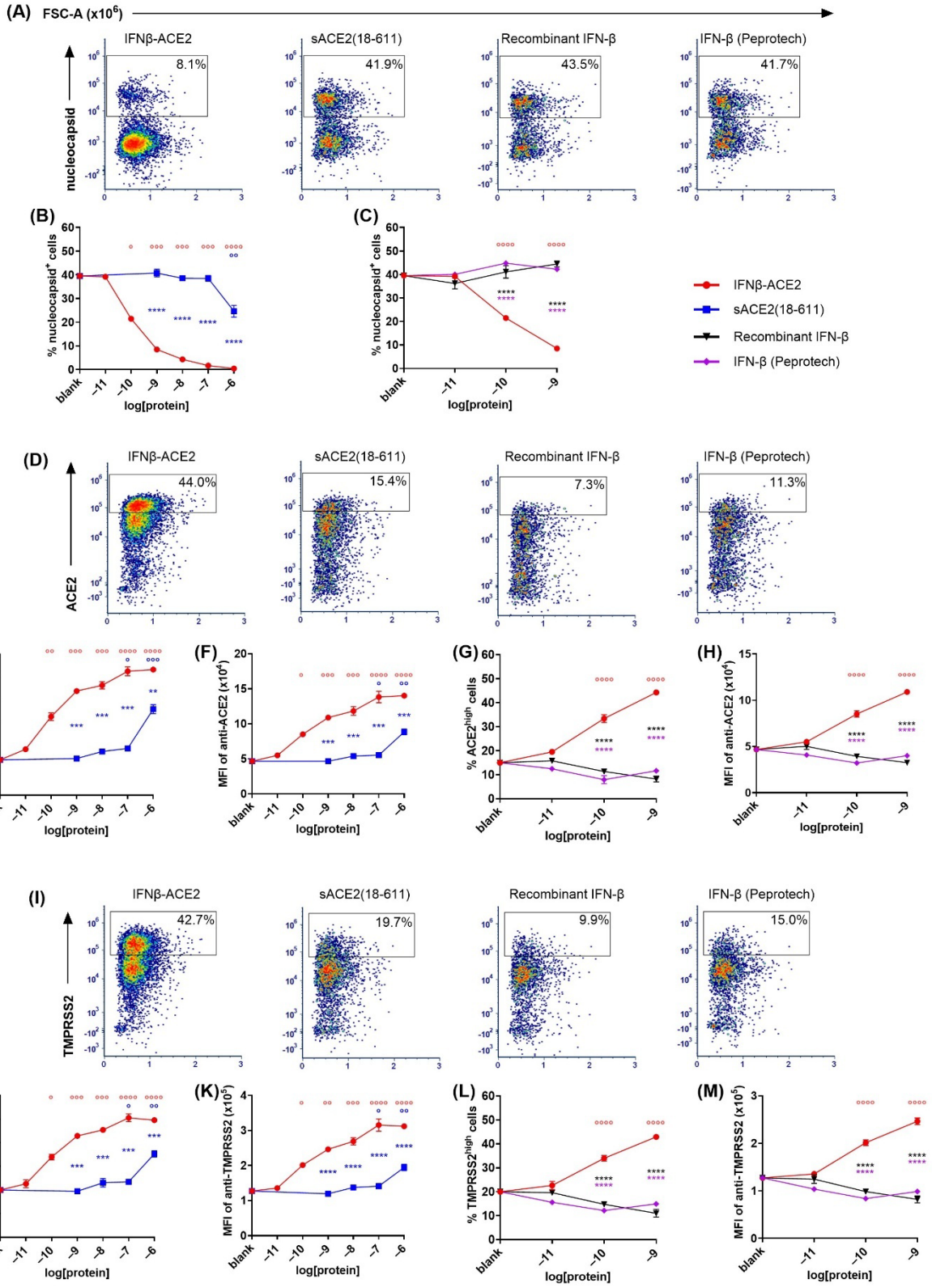
(A)
FSC-A (x10^6)
IFNβ-ACE2
sACE2(18-611)
Recombinant IFN-β
IFN-β (Peprotech)
nucleocapsid
8.1%
41.9%
43.5%
41.7%
(B)
% nucleocapsid+ cells
log[protein]
(C)
% nucleocapsid+ cells
log[protein]
IFNβ-ACE2
sACE2(18-611)
Recombinant IFN-β
IFN-β (Peprotech)
(D)
ACE2
44.0%
15.4%
7.3%
11.3%
(E)
% ACE2high cells
log[protein]
(F)
MFI of anti-ACE2 (x10^4)
log[protein]
(G)
% ACE2high cells
log[protein]
(H)
MFI of anti-ACE2 (x10^4)
log[protein]
(I)
TMPRSS2
42.7%
19.7%
9.9%
15.0%
(J)
% TMPRSS2high cells
log[protein]
(K)
MFI of anti-TMPRSS2 (x10^5)
log[protein]
(L)
% TMPRSS2high cells
log[protein]
(M)
MFI of anti-TMPRSS2 (x10^5)
log[protein]
blank
−11
−10
−9
−8
−7
−6

FIGURE 4.1. The sACE2 domain of IFNβ-ACE2 targeted IFN-β to the surface of NL63. NL63 was incubated at 4 °C with designated concentrations of IFNβ-ACE2, sACE2(18-611), recombinant IFN-β, or IFN-β (Peprotech). After a 1-hour incubation, NL63 was washed of any un-bound protein using 300 kDa centrifugal filters. NL63-protein complexes were then added to Vero E6-TMPRSS2-T2A-ACE2 cultures (100 µl) in a 96-well plate. The cells were harvested after a 2-day incubation at 33 °C, stained with LIVE/DEAD Fixable Blue Dead Cell Stain, and then surface labeled with FITC-conjugated anti-human ACE2 and PE-conjugated anti-human TMPRSS2. After fixation and permeabilization, cells were stained with AF647-conjugated rabbit anti-NL63 nucleocapsid antibody. Cells were then analyzed for viral infection by flow cytometry. Cells were gated on viable, single, and live cells (parental gate) before subgating on nucleocapsid^{+}, ACE2^{high}, or TMPRSS2^{high} cells. Shown are representative dot plots (A, D, and I, x-axis = FSC-A as in A) when NL63 was incubated with 1 nM IFNβ-ACE2 or controls. The IFNβ-ACE2 versus sACE2(18-611) groups were compared based on percentages of nucleocapsid^{+} cells (B), percentages of ACE2^{high} cells (E), MFI of anti-ACE2 staining (F), percentages of TMPRSS2^{high} cells (J), and MFI of anti-TMRSS2 staining (K). The IFNβ-ACE2 versus IFN-β groups were compared based on percentages of nucleocapsid cells (C), percentages of ACE2^{high} cells (G), MFI of anti-ACE2 staining (H), percentages of TMPRSS2^{high} cells (L), and MFI of anti-TMPRSS2 staining (M). Cell percentages were calculated by dividing events in the positive subgate by the parental gate, and MFI values represent all events in the parental gate. Each data point represents the mean value (n=2), and error bars represent SD. Statistical significance comparing IFN-β and ACE2 treatment groups to IFNβ-ACE2 treatment group at each concentration was analyzed by use of two-way ANOVA with Tukey's multiple comparisons test (* $p < 0.05$, ** $p < 0.01$, *** $p < 0.001$, **** $p < 0.0001$). Statistical

significance comparing each protein group at each concentration to blank was analyzed by use of two-way ANOVA with Tukey's multiple comparisons test (° $p < 0.05$, °° $p < 0.01$, °°° $p < 0.001$, °°°° $p < 0.0001$). These data are representative of three independent experiments.

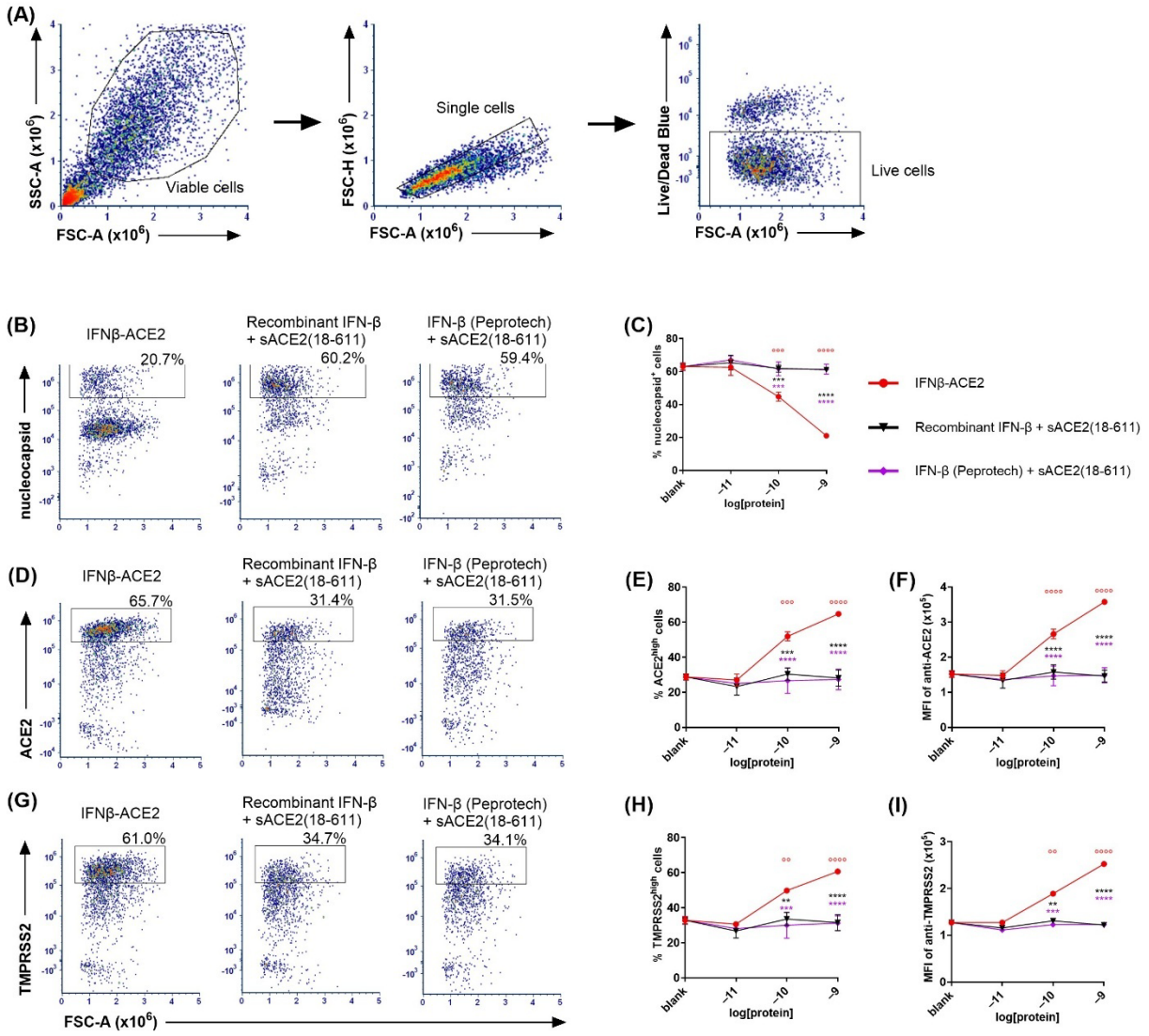

FIGURE 4.2. The covalent linkage of IFN-β and ACE2 was required for IFN-β targeting to NL63. NL63 was incubated at 4 °C with either IFNβ-ACE2 or the unlinked combination of sACE2(18-611) and IFN-β. After a 1-hour incubation, NL63 was repeatedly washed with 300 kDa centrifugal filters to remove proteins that lacked binding to virions. The retentates, which included virions and virion-bound proteins, were added to Vero E6-TMPRSS2-T2A-ACE2 cells in a 96-well plate. Cells were harvested after a 2-day incubation at 33 °C and stained with LIVE/DEAD Fixable Blue Dead Cell Stain. Cells were surface stained with PE-conjugated

mouse anti-human TMPRSS2 and FITC-conjugated mouse anti-human ACE2. After fixation and permeabilization, cells were stained with AF647-conjugated rabbit anti-NL63 nucleocapsid antibody. Cells were analyzed for viral infection by flow cytometry. Viable, single, live cells in the parental gate (A) were subgated as the nucleocapsid^{+} subset (B), the ACE2^{high} subset (D), and the TMPRSS2^{high} subset (G) as shown for the 1 nM concentration value. Shown are the percentages of nucleocapsid^{+}, ACE2^{high}, and TMPRSS2^{high} subsets together with the respective MFI values (C, E-F, and H-I, respectively). Cell percentages were calculated by dividing the events in the subset-positive/high subgate by those in the parental gate. MFI values were gated on all viable, single, and live cells (i.e., cells in the parental gate). Each data point represents the mean value (n=2), and error bars represent SD. Statistical significance of IFNβ-ACE2 versus 'IFN-β + sACE2' treatment group at each concentration was analyzed by use of two-way ANOVA with Tukey's multiple comparisons test (* $p < 0.05$, ** $p < 0.01$, *** $p < 0.001$, **** $p < 0.0001$). Statistical significance was also assessed for treatments groups at each concentration compared to the 'Blank' control via two-way ANOVA with Tukey's multiple comparisons test (° $p < 0.05$, °° $p < 0.01$, °°° $p < 0.001$, °°°° $p < 0.0001$). These data are representative of three independent experiments.

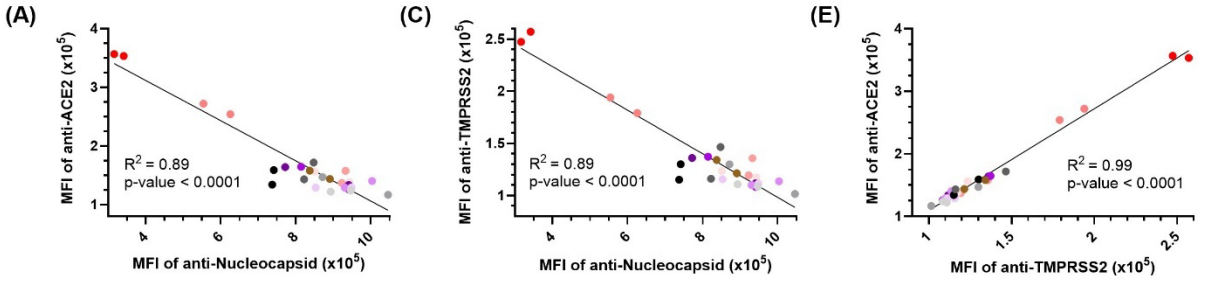

(B)

(nucleocapsid,ACE2)	IFNβ-ACE2	Recombinant IFN-β + sACE2(18-611)	IFN-β (Peprotech) + sACE2(18-611)
1 nM	(3.4,3.5)	(7.4,1.3)	(9.4,1.3)
	(3.2,3.6)	(7.4,1.6)	(7.7,1.6)
100 pM	(6.3,2.5)	(8.2,1.4)	(9.4,1.3)
	(5.5,2.7)	(8.5,1.7)	(8.1,1.6)
10 pM	(9.2,1.4)	(10.5,1.2)	(10.0,1.4)
	(9.3,1.6)	(8.7,1.5)	(9.3,1.3)
1 pM	(8.5,1.6)	(9.5,1.2)	(9.5,1.3)
	(9.4,1.4)	(8.9,1.2)	(8.5,1.3)
no protein	(8.4,1.6)		
	(8.9,1.4)		

(D)

(nucleocapsid,TMPRSS2)	IFNβ-ACE2	Recombinant IFN-β + sACE2(18-611)	IFN-β (Peprotech) + sACE2(18-611)
1 nM	(3.4,2.6)	(7.4,1.2)	(9.4,1.1)
	(3.2,2.5)	(7.4,1.3)	(7.7,1.4)
100 pM	(6.3,1.8)	(8.2,1.2)	(9.4,1.1)
	(5.5,1.9)	(8.5,1.5)	(8.1,1.4)
10 pM	(9.2,1.2)	(10.5,1.0)	(10.0,1.1)
	(9.3,1.4)	(8.7,1.3)	(9.3,1.1)
1 pM	(8.5,1.2)	(9.5,1.1)	(9.5,1.1)
	(9.4,1.2)	(8.9,1.1)	(8.5,1.2)
no protein	(8.4,1.3)		
	(8.9,1.2)		

(F)

(TMPRSS2,ACE2)	IFNβ-ACE2	Recombinant IFN-β + sACE2(18-611)	IFN-β (Peprotech) + sACE2(18-611)
1 nM	(2.6,3.5)	(1.2,1.3)	(1.1,1.3)
	(2.5,3.6)	(1.3,1.6)	(1.4,1.6)
100 pM	(1.8,2.5)	(1.2,1.4)	(1.1,1.3)
	(1.9,2.7)	(1.5,1.7)	(1.4,1.6)
10 pM	(1.2,1.4)	(1.0,1.2)	(1.1,1.4)
	(1.4,1.6)	(1.3,1.5)	(1.1,1.3)
1 pM	(1.2,1.6)	(1.1,1.2)	(1.1,1.3)
	(1.2,1.4)	(1.1,1.2)	(1.2,1.3)
no protein	(1.3,1.6)		
	(1.2,1.4)		

FIGURE 4.3. NL63 receptor expression negatively correlated with nucleocapsid expression.

(A) Simple linear regression of MFI of ACE2 and nucleocapsid expression, along with corresponding (x,y) MFI coordinates for each treatment group and concentration (B). (C) Simple linear regression of MFI of TMPRSS2 and nucleocapsid expression, along with corresponding (x,y) MFI coordinates for each treatment group and concentration (D). (E) Simple linear regression of MFI of ACE2 and TMPRSS2 expression (E), along with corresponding (x,y) MFI

coordinates for each treatment group and concentration (F). MFI values were gated on all viable, single, and live cells (i.e., cells in the parental gate). Each data point represents a distinct treatment group and concentration. Statistical significance was analyzed by use of a two-tailed t-test.

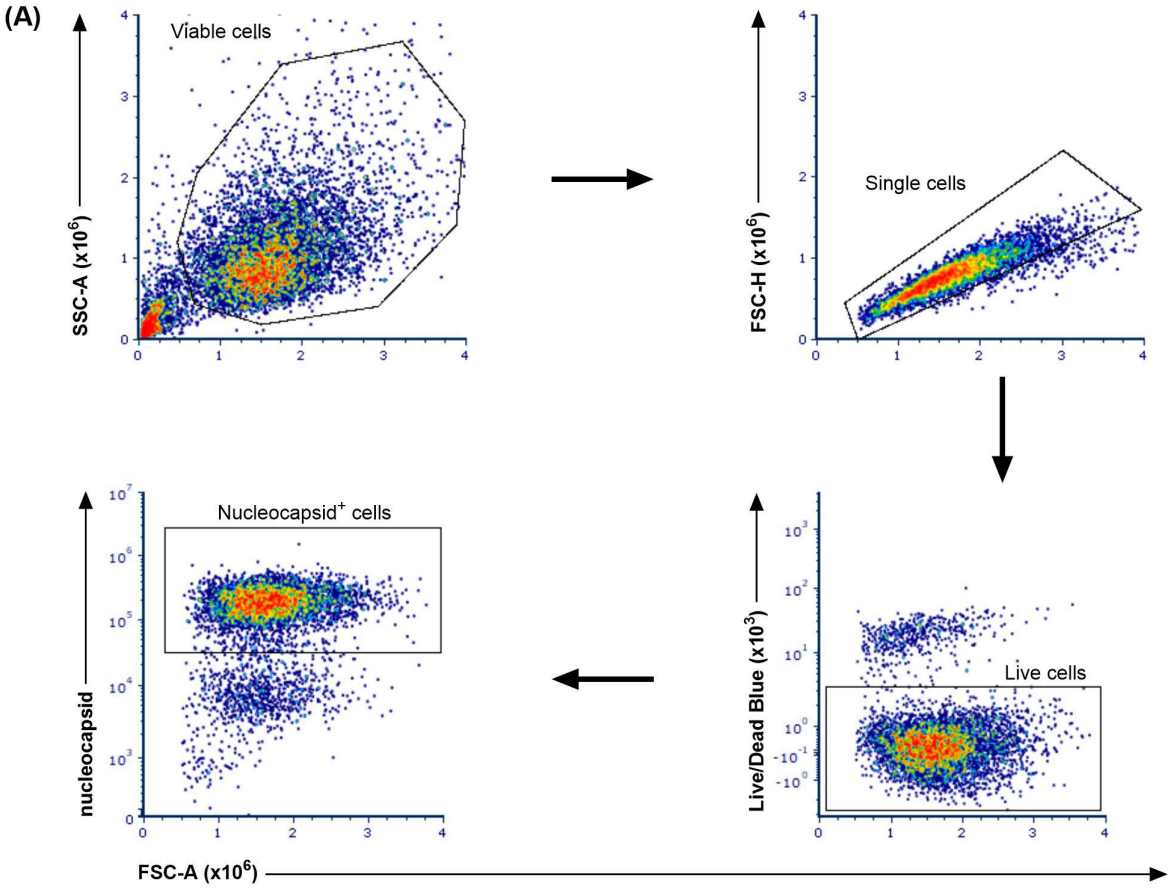
(A)
Viable cells
SSC-A (x10^6)
Single cells
FSC-H (x10^6)
Live cells
Live/Dead Blue (x10^3)
Nucleocapsid+ cells
nucleocapsid
FSC-A (x10^6)

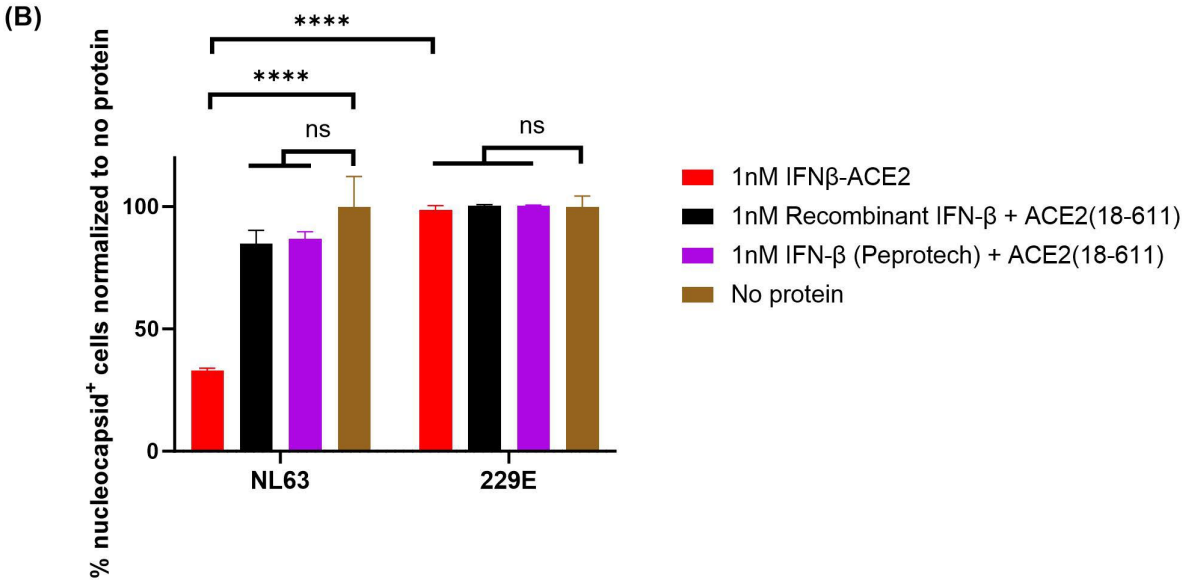
(B)
****
****
ns
ns
% nucleocapsid+ cells normalized to no protein
100
50
0
NL63
229E
1nM IFNβ-ACE2
1nM Recombinant IFN-β + ACE2(18-611)
1nM IFN-β (Peprotech) + ACE2(18-611)
No protein

FIGURE 4.4. IFNβ-ACE2 exhibited virus-specific targeting in accordance with viral host receptor specificity. The NL63 or 229E viruses were incubated at 4 °C with either IFNβ-ACE2 or the unlinked combination of IFN-β and sACE2(18-611). After a 1-hour incubation, the virus + protein mixtures were washed, and the retentate containing virion-protein complexes were used for infection of Vero E6-TMPRSS2-T2A-ACE2 or A549 cells, respectively, in a 96-well plate. The cells were harvested after a 2-day incubation and stained with LIVE/DEAD Fixable Blue Dead Cell Stain. After fixation and permeabilization, Vero E6-TMPRSS2-T2A-ACE2 cells were stained with AF647-conjugated rabbit anti-NL63 nucleocapsid antibody, and A549 cells were stained with AF647-conjugated rabbit anti-229E nucleocapsid antibody. Cells were then analyzed for viral infection by flow cytometry. (A) Cells were gated on viable, single, and live cells before subgating on nucleocapsid$^+$ cells. Shown (B) are the percentages of nucleocapsid$^+$ cells for each treatment group normalized to the 'no protein' control group (1 nM concentrations). Each data point represents the mean value (n=2), and error bars represent SD. Statistical significance was analyzed by use of two-way ANOVA with Tukey's multiple comparisons test (ns nonsignificant, **** $p < 0.0001$). Experiments shown are representative of three independent experiments.

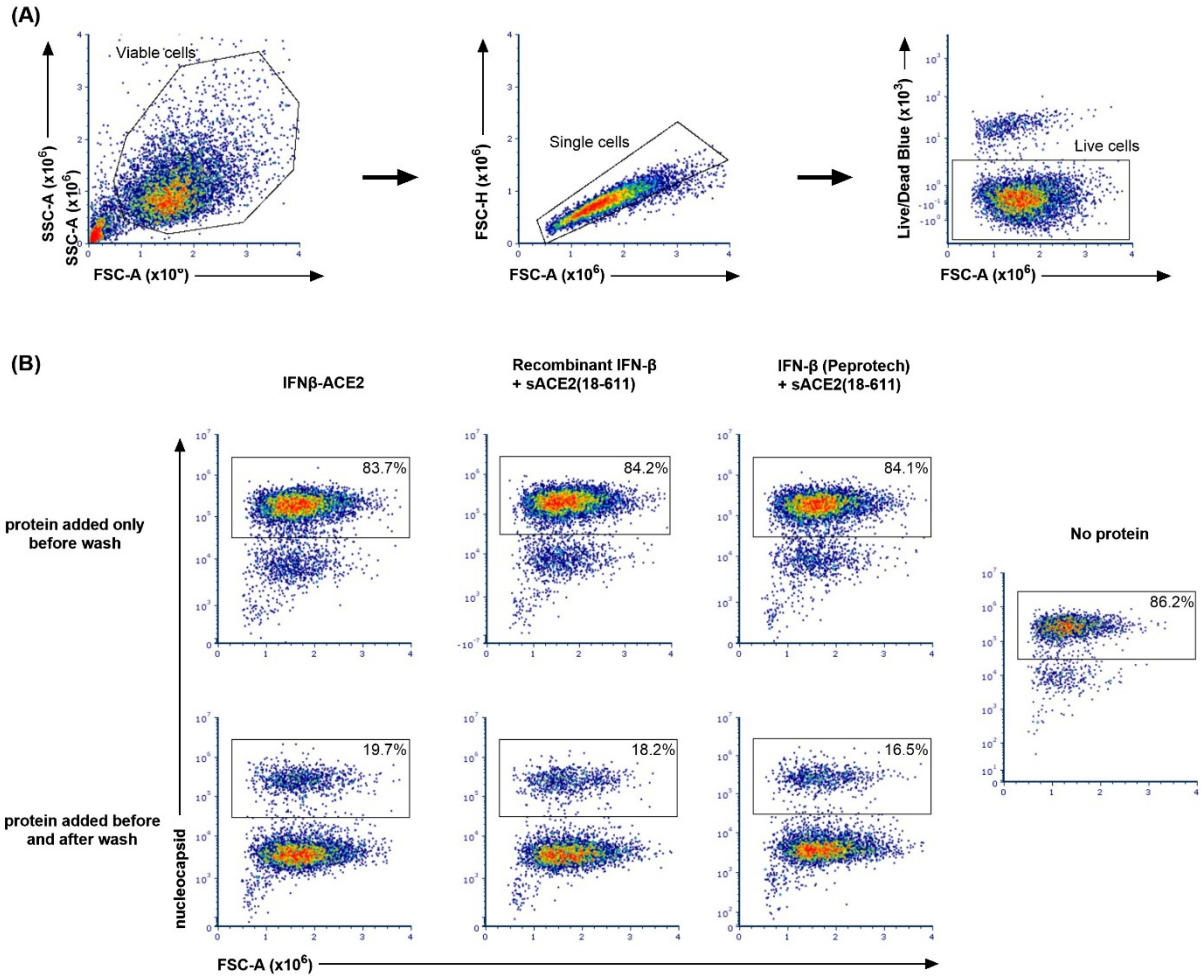
(A)
Viable cells
SSC-A (x10⁶)
FSC-A (x10⁶)
Single cells
FSC-H (x10⁶)
Live cells
Live/Dead Blue (x10³)
(B)
IFNβ-ACE2
Recombinant IFN-β + sACE2(18-611)
IFN-β (Peprotech) + sACE2(18-611)
No protein
protein added only before wash
protein added before and after wash
83.7%
84.2%
84.1%
86.2%
19.7%
18.2%
16.5%
nucleocapsid
FSC-A (x10⁶)
(C)
ns
****
% nucleocapsid⁺ cells (229E-infected)
100
50
0
1nM IFNβ-ACE2
1nM Recombinant IFN-β + sACE2(18-611)
1nM IFN-β (Peprotech) + sACE2(18-611)
No protein
– : protein added only before wash
+ : protein added before AND after wash

FIGURE 4.5. The sACE2 domain of IFNβ-ACE2 did not target IFN-β to the surface of 229E. 229E viruses was incubated at 4 °C with either IFNβ-ACE2 or the unlinked combination of IFN-β and sACE2(18-611). After a 1-hour incubation, the 229E + protein mixtures were washed, and IFNβ-ACE2 or the unlinked combination IFN-β and sACE2(18-611) were directly added to designated groups. The retentate containing virion-protein complexes were used for infection of A549 cells in a 96-well plate. The cells were harvested after a 2-day incubation and stained with LIVE/DEAD Fixable Blue Dead Cell Stain. After fixation and permeabilization, cells were stained with AF647-conjugated rabbit anti-229E nucleocapsid antibody. Cells were then analyzed for viral infection by flow cytometry. Cells were gated on viable, single, and live cells (A) before subgating on nucleocapsid$^+$ cells (B). Shown (B) are representative dot plots including percentages of nucleocapsid$^+$ 229E-infected cells (1 nM concentrations). (C) Bar graph shows mean percentages of nucleocapsid$^+$ 229E-infected cells when proteins were or were not added after the washing step (1 nM concentrations). Each data point represents the mean value (n=2), and error bars represent SD. Statistical significance was analyzed by use of two-way ANOVA with Tukey's multiple comparisons test (ns nonsignificant, **** $p < 0.0001$). Experiments shown are representative of three independent experiments.

CHAPTER 5: IFNβ-ACE2 SHOWED ENHANCED ANTIVIRAL ACTIVITY COMPARED TO THE INDIVIDUAL CONTROL PROTEINS AND THE UNLINKED COMBINATION OF THE CONTROL PROTEINS AGAINST NL63 BUT NOT 229E

This chapter is modified from Jabbour et al., A novel antiviral therapeutic platform: anchoring IFN-β to the surface of infectious virions equips interferon-evasive virions with potent antiviral activity. Viruses 2025, 17, 697. https://doi.org/10.3390/v17050697

5.1 ABSTRACT

IFN-β is a key modulator of antiviral defense during viral infection. However, a common viral immune evasion technique is the inhibition of IFN-β production and/or signaling. Viruses, including NL63, SARS-CoV, and SARS-CoV-2, encode multiple proteins that may inhibit IFN-I production. To reinstate the antiviral effects of IFN-I, researchers have tested IFN-I in clinical trials against different viruses, including SARS-CoV-2. However, as of May 2025, IFN-I are only approved for treatment of Hepatitis B and C infections. We hypothesize that targeting IFN-I to the exact site of infection will imitate the endogenous and local production of IFN-I and thereby will yield enhanced antiviral activity compared to the untargeted administration of IFN-I. To test this hypothesis, we compared the antiviral activity of IFNβ-ACE2 to sACE2(18-611), IFN-β, or the unlinked combination of sACE2(18-611) and IFN-β. IFNβ-ACE2 had enhanced antiviral activity against NL63, but not 229E, in comparison to the control proteins. These findings indicate that targeting IFN-β to the surface of virions using our fusion protein technology enables localized signaling at the precise site of impending infection, enhancing antiviral activity

compared to non-targeted IFN-β. This enhancement was not seen during 229E infection since ACE2 does not bind to 229E. Thus, IFN-β is not targeted to the surface of 229E in this system.

5.2 RESULTS

IFNβ-ACE2 had potentiated antiviral activity compared to IFN-β and/or sACE2 in a non-washed *in vitro* infection system against NL63 (Figure 5.1 and 5.2).

The rationale for a 'virus-washed' system (Figures 4.1 and 4.2) was to assess the antiviral action of virion surface-bound IFNβ-ACE2 and sACE2. However, this system did not assess soluble IFN-β action because soluble IFN-β did not independently bind the virus and therefore was not retained in the retentate. Thus, comparison of 'virus-washed' systems to 'non-washed' *in vitro* infection systems was needed to compare virus-targeted and virus-nontargeted IFN-β/ IFNAR interactions. That is, the 'virus-washed' system solely reveals the action of virion surface IFN-β whereas the non-washed system combines the activities of virus-targeted IFN-β and virus non-targeted IFN-β. The prediction is that virus-mediated targeting of IFN-β will be less apparent when all reagents are present within the confines of the 96-well 100 µl volume.

In non-washed infection systems, virus and reagents were incubated together for 1 hour then added directly to the well without a virus-washing step. That is, NL63 (MOI of 0.1) was incubated with IFNβ-ACE2, sACE2(18-611), sACE2(18-740), recombinant IFN-β, IFN-β (Peprotech) (Figure 5.1), or the unlinked combination of sACE2(18-611) and IFN-β (Figure 5.2). After a 1-hour incubation at 4 °C, the NL63 and protein mixtures were seeded (without washing virus) onto Vero E6-TMPRSS2-T2A-ACE2 cells. After a 48-hour incubation, cells were harvested, stained, and analyzed for infection by flow cytometry. Figures 5.1A and 5.2A show

the gating scheme. Cells were gated on viable, single, and live cells (Figures 5.1A and 5.2A) before gating on nucleocapsid^{+} and ACE2^{+} cells (Figures 5.1B and 5.2B,C). Figures 5.1B and 5.2B show representative dot plots of the percentage of nucleocapsid^{+} cells (infected cells) (1 nM). Figure 5.2C shows representative dot plots of the percentage of ACE2^{+} cells (non-infected cells) (1 nM). Several results were noted. (a) IFNβ-ACE2 exhibited biphasic mechanism of antiviral activity as shown by intracellular staining of nucleocapsid (Figure 5B,F) and surface staining of ACE2 (Figure 5G). The first phase of IFNβ-ACE2 inhibition was evident in the 100 fM – 100 pM concentration range. This highly potent antiviral mechanism represented the antiviral activity of the IFN-β domain, which coincided with the antiviral activity of the two free IFN-β preparations (Figure 5.1C,D). (b) The second phase of IFNβ-ACE2 antiviral inhibition was evident in the 10 nM – 1 μM concentration range. This inhibitory mechanism represented sACE2-mediated viral neutralization, which coincided with the antiviral sensitivity of sACE2 (Figure 5.1C). Thus, IFN-β-mediated antiviral activity was more potent by several orders of magnitude compared to the neutralizing activity of the monomeric sACE2(18-611) and the dimeric sACE2(18-740) (Figure 5.1C). (c) IFNβ-ACE2 exhibited antiviral activity that was 10-fold more potent than IFN-β alone (Figure 5.1C) or the unlinked combination of IFN-β and sACE2 (Figures 5.2C,D). This finding supported the possibility that targeting of IFNβ-ACE2 to the viral surface potentiated antiviral activity in non-washed *in vitro* infection systems. (d) IFNβ-ACE2 appeared to have neutralization activity that was more potent than the control sACE2(18-611) protein. This finding shows that physical coupling of sACE2 to IFN-β does not impair sACE2 neutralizing activity. (e) Dimeric sACE2(18-740) had potentiated neutralization activity compared to monomeric sACE2(18-611) by approximately 2-orders of magnitude (Figure 5.1C). These data provide evidence that multimeric sACE2 proteins exhibit more stable binding

interactions with NL63, which probably reflects increased binding avidity to spike trimers. (f) These data complement the 'virus-washed' experiments (Figures 4.1-4.2), which showed IFNβ-ACE2 had antiviral activity with 100 pM sensitivity which is four orders of magnitude lower than the 1 μM sensitivity of sACE2(18-611)-mediated neutralization. These data reveal the predominant mechanism wherein the sACE2 domain provides an anchoring function that decorates spike with protruding IFN-β molecules. Conversely, direct sACE2-mediated neutralization appears to be an inhibitory mechanism that was evident only at high concentrations.

IFNβ-ACE2 had similar antiviral activity against 229E compared to the unlinked combination of IFN-β and sACE2 in a non-washed *in vitro* infection system.

In a non-washed *in vitro* infection system, 1 μM sACE2(18-611) or IFNβ-ACE2 were incubated with NL63 (MOI of 0.1) or 229E (MOI of 0.1) and then added (without virus wash) to Vero E6-TMPRSS2-T2A-ACE2 or A549 cells, respectively. Figure 5.3A shows the gating scheme. Cells were gated on viable, single, live cells prior to gating on nucleocapsid^{+} cells (Figure 5.3A). The main finding was that sACE2(18-611) robustly inhibited NL63 infectivity but was without effect on 229E infectivity, which confirms thatsACE2 specifically binds NL63 but not 299E (Figure 5.3B). Also, IFNβ-ACE2 fully inhibited NL63 infectivity, which represented the covalently linked action of sACE2-mediated neutralization, IFN-β-anchoring, and IFN-β-mediated antiviral activity (Figure 5.3B). In contrast, IFNβ-ACE2 only partially inhibited 229E infectivity (Figure 5.3B), which reflected a unilateral IFN-β-mediated antiviral activity that plateaued at a nadir of approximately 40% infection in the 1-100 nM concentration range (Figure

5.4). Figure 5.4A shows the gating scheme. Cells were gated on viable, single, live cells (Figure 5.4A) prior to gating on nucleocapsid$^+$ cells (Figure 5.4B). Figure 5.4B shows representative plots of the percentages of nucleocapsid$^+$ cells. In Figure 5.4C, the overlapping infection curves indicate that IFNβ-ACE2 did not inherently have more antiviral activity compared to the 'IFN-β + sACE2' control proteins, such that the IFNβ-ACE2 covalent linkage was not important for 229E inhibition. Overall, these findings support the concept that highly specific interactions of the sACE2 domain with an ACE2-specific viral spike glycoprotein appears critical for the anchoring of IFNβ-ACE2 antiviral activity directly to the surfaces of pathogenic viruses in ACE2-viral tropism.

5.3 DISCUSSION

Demonstrating specific targeting in a 100 µL *in vitro* system presents significant challenges due to the inherently homogenous nature of small-volume cell culture environments. In such constrained settings, diffusion rapidly distributes both targeted and non-targeted IFN-β throughout the entire volume, effectively minimizing concentration gradients and spatial specificity due to targeting. As a result, distinguishing truly targeted from non-targeted IFN-β signaling becomes difficult. Moreover, the small volume limits the ability to mimic complex tissue architecture or localized delivery scenarios observed *in vivo*, further complicating the assessment of targeting precision and efficacy. Nonetheless, we conducted *in vitro* "no wash" experiments to assess whether an enhancement in IFN-β antiviral activity could be observed under these simplified conditions.

As seen in Figure 5.1, sACE2 inhibits infection only at high concentrations (1 nM – 1 µM). Specifically, sACE2(18-611) inhibits NL63 infection at 100 nM – 1 µM. On the other

hand, IFN-β control proteins inhibit NL63 infection more potently, showing antiviral activity at concentrations as low as 10 pM. Thus, the antiviral activity of IFN-β is about 10^4 – 10^5 times more potent than the neutralization activity of sACE2(18-611). Although sACE2(18-611) has no neutralization activity at 1 pM – 10 pM, IFNβ-ACE2 showed enhanced antiviral activity against NL63 in comparison to the IFN-β controls. This indicates that sACE2(18-611) neutralization is not necessary to enhance the antiviral activity of IFN-β. Instead, sACE2(18-611) serves as a targeting agent for IFN-β at low concentrations, regardless of neutralization.

The increase in antiviral activity of IFN-β in this system is due to the targeting effect of the sACE2 domain. However, unlike the "virus wash" system, the targeted and non-targeted proteins both produce an antiviral effect in this system, minimizing the effects seen with targeting. Nonetheless, we see a 10-fold increase in antiviral activity of IFNβ-ACE2 compared to the control IFN-β proteins.

Experiments comparing IFNβ-ACE2 to the unlinked combination of IFN-β and sACE2 confirmed our findings. To test whether the covalent linkage of IFN-β to sACE2 is necessary for the enhanced activity of IFN-β by targeting IFN-β to the surface of NL63, we repeated the above experiment with the unlinked combination of these proteins. These experiments showed that the covalent linkage between sACE2 and IFN-β is necessary for targeting IFN-β to the surface of NL63 and thus enhancing the antiviral activity of IFN-β (Figure 5.2). These experiments also confirmed that IFNβ-ACE2's antiviral activity was 10-fold more potent compared to IFN-β, despite the limited concentration gradients and spatial specificity of an *in vitro* system.

To confirm that IFNβ-ACE2 did not inherently have more antiviral activity in comparison to IFN-β and sACE2, we repeated the above experiment with HCoV 229E. These control experiments showed that sACE2(18-611) does not neutralize 229E and that the antiviral activity

of IFNβ-ACE2 on 229E is solely due to the IFN-β domain (Figure 5.3). Additionally, IFNβ-ACE2 had similar antiviral activity against 229E in comparison to the unlinked combination of IFN-β and sACE2 (Figure 5.4). Overall, these control experiments confirmed that sACE2(18-611) specifically targets IFN-β to the surface of NL63 through host receptor specificity and that this targeting enhances the antiviral activity of IFN-β by introducing IFN-β to the exact site of imminent viral infection.

Finally, as mentioned earlier, these "no wash" *in vitro* experiments do not mimic *in vivo* targeting conditions due to the small volumes and rapid distribution of the proteins within the confined system. Targeting IFN-β to the surface of a virion *in vivo* would require that the protein reach the lungs in sufficient concentrations before being cleared by the body through mechanisms such as mucus production and mucociliary clearance. Thus, future animal studies will provide us with a better understanding of the feasibility and benefit of targeting IFN-β to the surface of a virion *in vivo*.

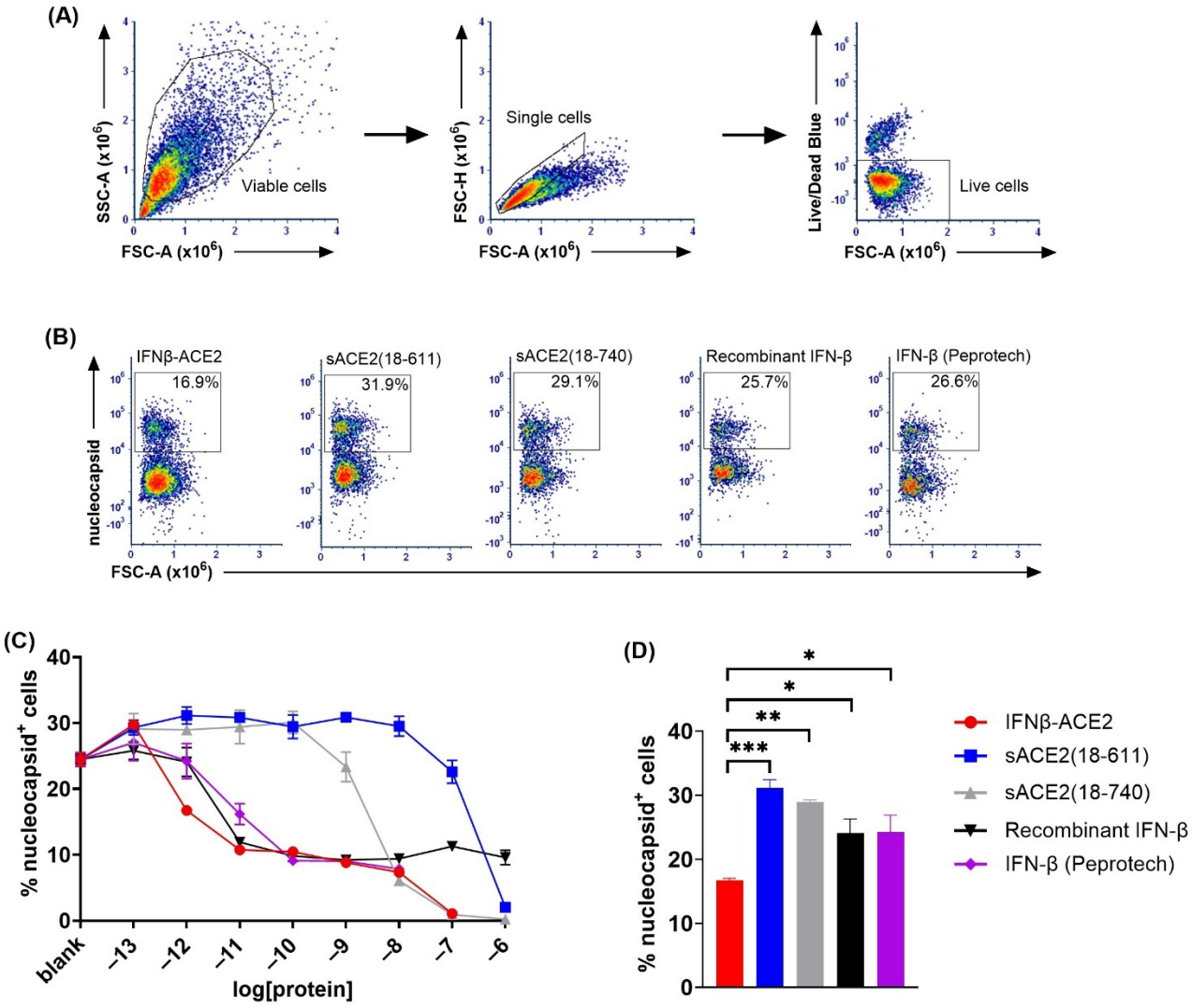

FIGURE 5.1. In a non-washed *in vitro* infection system, IFNβ-ACE2 exhibited enhanced antiviral activity compared to IFN-β, sACE2(18-611), and sACE2(18-740) control proteins. NL63 was incubated for 1 hour at 4 °C with either IFNβ-ACE2, sACE2(18-611), sACE2(18-740), recombinant IFN-β, or IFN-β (Peprotech). The NL63 + protein mixtures were then added directly to Vero E6-TMPRSS2-T2A-ACE2 cells in a 96-well plate. The cells were harvested after a 2-day incubation at 33°C and stained with LIVE/DEAD Fixable Blue Dead Cell Stain. Cells were fixed and permeabilized and then intracellularly stained with AF647-conjugated

rabbit anti-NL63 nucleocapsid antibody. Cells were then analyzed for viral infection by flow cytometry. Cells gated as viable, single, and live cells (parent gate) (A) were subgated to define the nucleocapsid^{+} subset (B). Shown (B) are representative dot plots showing percentages of the nucleocapsid^{+} subset at the 1 pM concentration. Shown (C) are the percentages of the nucleocapsid^{+} subset for each group over concentrations ranging from 100 fM to 1 μM. Bar graph (D) shows mean percentage values of nucleocapsid^{+} cells at the 1 pM concentration. Each data point represents the mean value (n=2), and error bars represent SD. Statistical significance was analyzed by one-way ANOVA with the Dunnett multiple comparisons test comparing the control IFN-β and sACE2 treatment groups to the IFNβ-ACE2 treatment group at each concentration (* $p < 0.05$, ** $p < 0.01$, *** $p < 0.001$). These data are representative of three independent experiments.

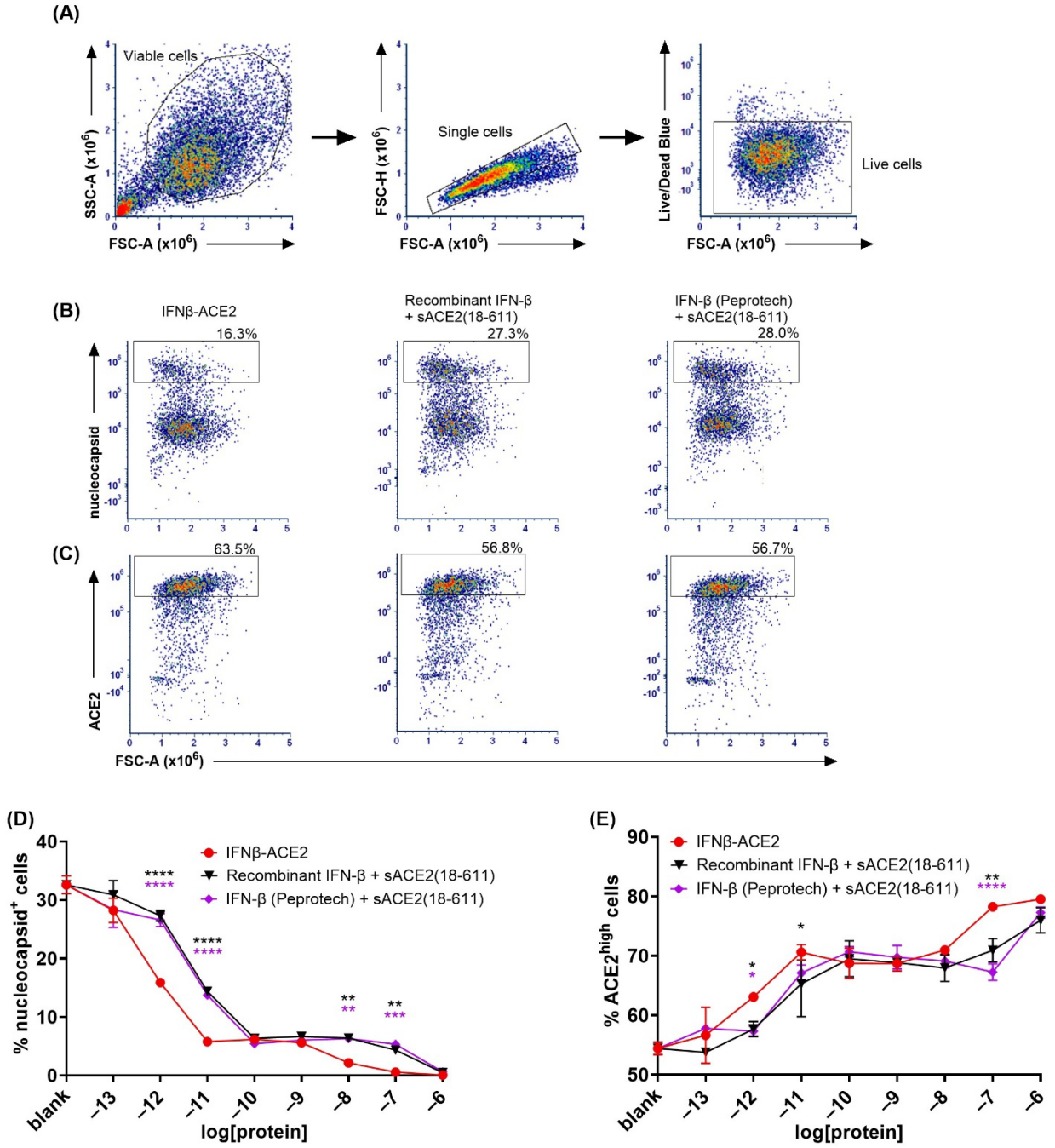

FIGURE 5.2. In a non-washed *in vitro* infection system, IFNβ-ACE2 exhibited enhanced antiviral activity compared to the unlinked combination of IFN-β and sACE2. NL63 was incubated for 1 hr at 4 °C with either IFNβ-ACE2 or the unlinked combination of sACE2(18-611) and IFN-β. The NL63 + protein mixtures were then added directly to Vero E6-TMPRSS2-T2A-ACE2 cells in

a 96-well plate. The cells were harvested after a 2-day incubation at 33 °C and stained with LIVE/DEAD Fixable Blue Dead Cell Stain. Cells were surface stained with FITC-conjugated mouse anti-human ACE2, were fixed and permeabilized, and then were intracellularly stained with AF647-conjugated rabbit anti-NL63 nucleocapsid antibody. Cells were then analyzed for viral infection by flow cytometry. Cells gated as viable, single, and live cells (parent gate) (A) were subgated to define nucleocapsid^{+} (B) and ACE2^{high} (C) subsets. Shown (B) are representative dot plots showing percentages of the nucleocapsid^{+} subset at the 1 pM concentration. Shown (C) are representative dot plots showing percentages of the ACE2^{high} subset at the 1 pM concentration. Shown (D) are the percentages of the nucleocapsid^{+} subset for each group over concentrations ranging from 100 fM to 1 μM. Shown (E) are the percentages of ACE2^{high} subset for each group over concentrations ranging from 100 fM to 1 μM. Each data point represents the mean value (n=2), and error bars represent SD. Statistical significance was analyzed by two-way ANOVA with Tukey's multiple comparisons test comparing the unlinked combination of IFN-β and sACE2 treatment groups to IFNβ-ACE2 treatment group at each concentration (* $p < 0.05$, ** $p < 0.01$, *** $p < 0.001$, **** $p < 0.0001$). These data are representative of three independent experiments.

(A)

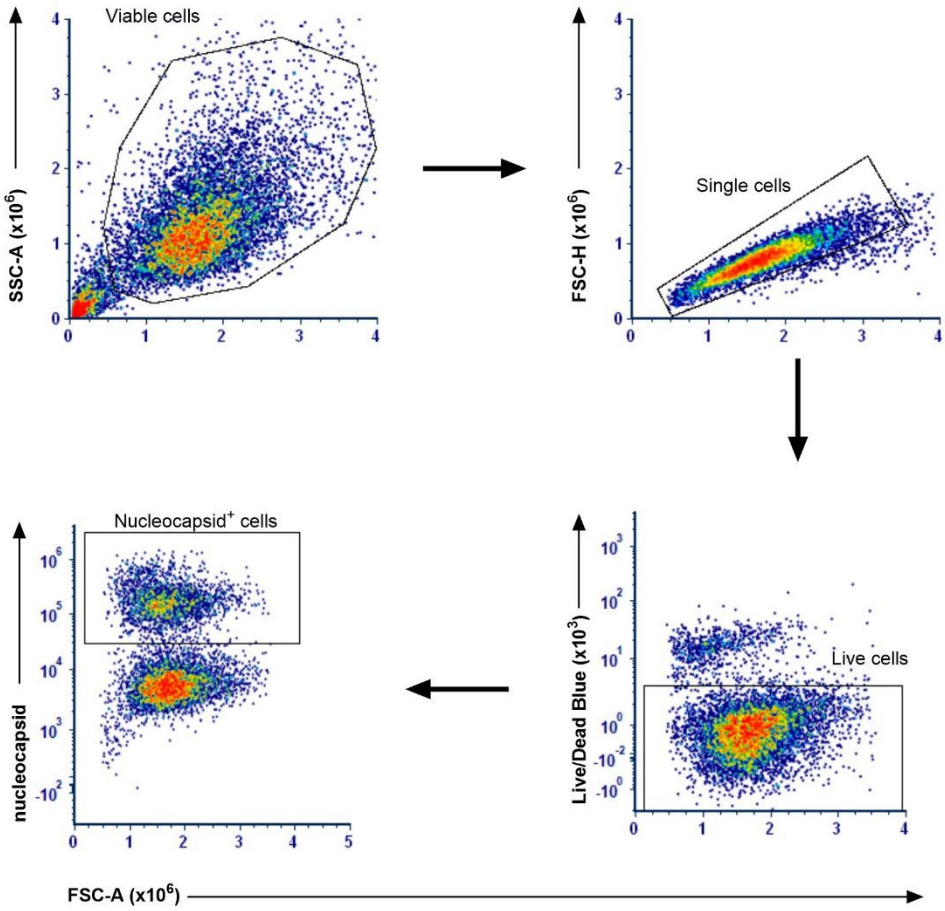
Viable cells
SSC-A (x10^6)
Single cells
FSC-H (x10^6)
Live cells
Live/Dead Blue (x10^3)
Nucleocapsid+ cells
nucleocapsid
FSC-A (x10^6)

(B)

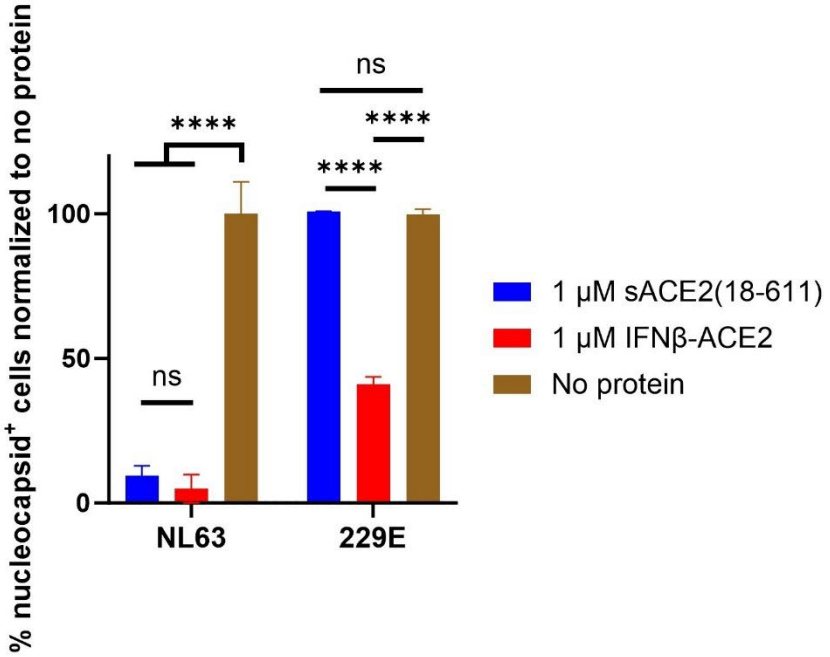
% nucleocapsid+ cells normalized to no protein
ns
****
****
****
ns
100
50
0
NL63
229E
1 μM sACE2(18-611)
1 μM IFNβ-ACE2
No protein

FIGURE 5.3. sACE2(18-611) inhibited NL63 but not 229E infection. The NL63 or 229E viruses were incubated at 4 °C with either IFNβ-ACE2 or sACE2(18-611). After a 1-hour incubation, the virus + protein mixtures were added directly to Vero E6-TMPRSS2-T2A-ACE2 (NL63) or A549 (229E) cells in a 96-well plate. The cells were harvested after a 2-day incubation and stained with LIVE/DEAD Fixable Blue Dead Cell Stain. After fixation and permeabilization, Vero E6-TMPRSS2-T2A-ACE2 cells were stained with AF647-conjugated rabbit anti-NL63 nucleocapsid antibody, and A549 cells were stained with AF647-conjugated rabbit anti-229E nucleocapsid antibody. Cells were then analyzed for viral infection by flow cytometry. (A) Cells were gated on viable, single, and live cells before subgating on nucleocapsid$^+$ cells. Shown (B) are the percentages of nucleocapsid$^+$ cells for each treatment group normalized to the 'no protein' group for each virus (1 μM concentrations). Each data point represents the mean value (n=2), and error bars represent SD. Statistical significance was analyzed by use of two-way ANOVA with Tukey's multiple comparisons test (ns nonsignificant, **** $p < 0.0001$). The experiments shown are representative of three independent experiments.

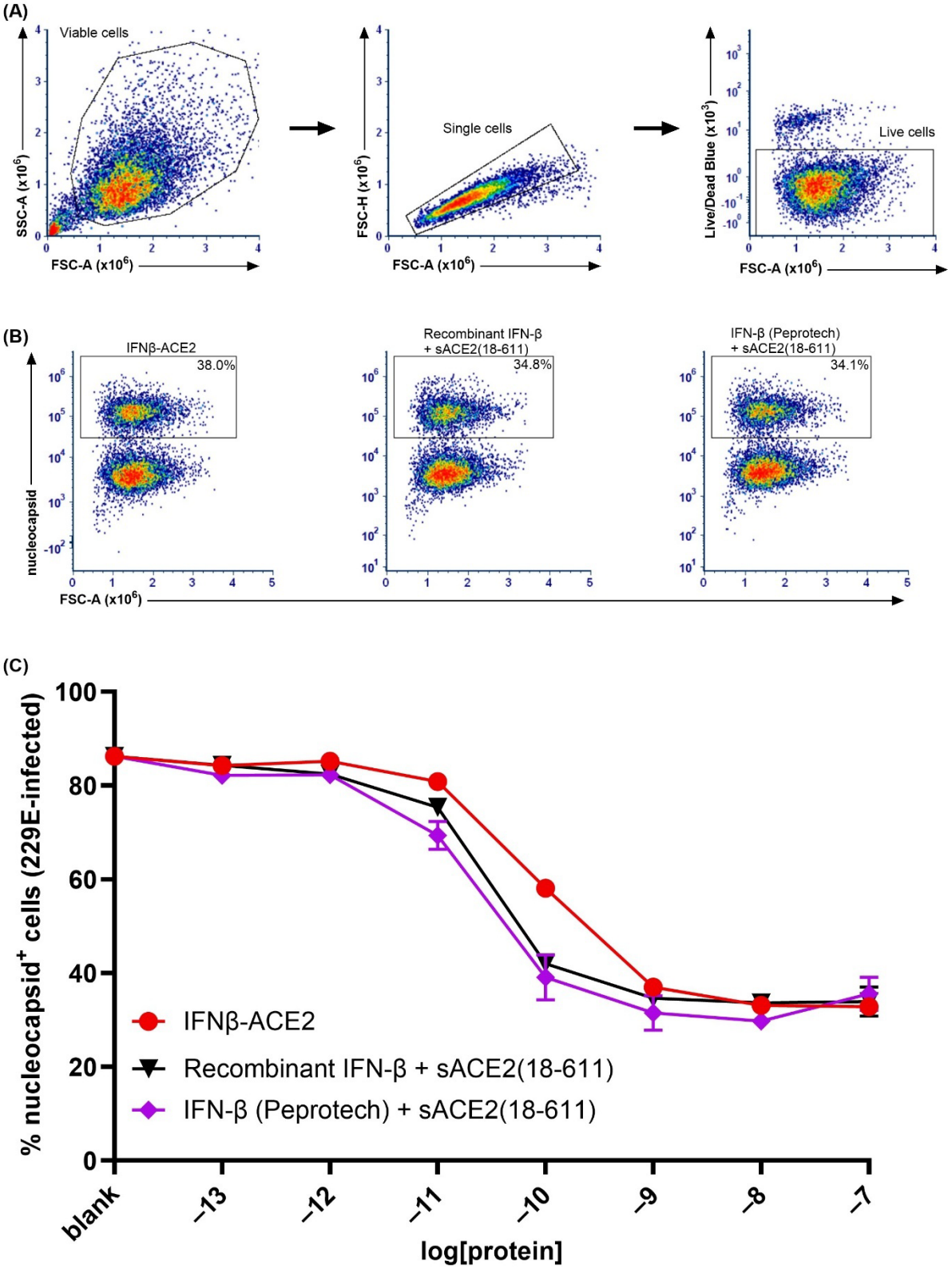
(A)
Viable cells
SSC-A (x10^6)
FSC-A (x10^6)
Single cells
FSC-H (x10^6)
FSC-A (x10^6)
Live cells
Live/Dead Blue (x10^3)
FSC-A (x10^6)
(B)
IFNβ-ACE2
38.0%
Recombinant IFN-β
+ sACE2(18-611)
34.8%
IFN-β (Peprotech)
+ sACE2(18-611)
34.1%
nucleocapsid
FSC-A (x10^6)
(C)
% nucleocapsid+ cells (229E-infected)
IFNβ-ACE2
Recombinant IFN-β + sACE2(18-611)
IFN-β (Peprotech) + sACE2(18-611)
blank
log[protein]

FIGURE 5.4. IFNβ-ACE2 had similar antiviral activity against 229E compared to the unlinked combination of IFN-β and sACE2(18-611). The 229E virus was incubated at 4 °C with either IFNβ-ACE2 or the unlinked combination of IFN-β and sACE2(18-611). After a 1-hour incubation, the virus + protein mixtures were directly added to A549 cells in a 96-well plate. The cells were harvested after a 2-day incubation and stained with LIVE/DEAD Fixable Blue Dead Cell Stain. After fixation and permeabilization, A549 cells were stained with AF647-conjugated rabbit anti-229E nucleocapsid antibody. Cells were then analyzed for viral infection by flow cytometry. Cells were gated on viable, single, and live cells (A) before subgating on nucleocapsid$^+$ cells (B). Shown (B) are representative dot plots including percentages of nucleocapsid$^+$ 229E-infected cells (1 nM concentrations). Shown (C) are the percentages of nucleocapsid$^+$ 229E-infected cells for each treatment group at designated concentrations (100 fM to 100 nM). Each data point represents the mean value (n=2), and error bars represent SD. The experiments shown are representative of three independent experiments.

CHAPTER 6: GENERAL DISCUSSION AND FUTURE DIRECTIONS

This chapter is modified from Jabbour et al., A novel antiviral therapeutic platform: anchoring IFN-β to the surface of infectious virions equips interferon-evasive virions with potent antiviral activity. Viruses 2025, 17, 697. https://doi.org/10.3390/v17050697

6.1. IFNβ-ACE2 is a prototype for a new modular class of antiviral therapeutics

The SARS-CoV-2 pandemic highlighted the need for modular antiviral platforms that can be repurposed to target emerging viral pathogens. The main advantage of the IFNβ-ACE2 fusion protein is that the physical linkage of sACE2 and IFN-β provides synergistic benefits because the virus/ IFNβ-ACE2 complex creates an IFN-β array at the viral surface such that robust IFN-β signaling and upregulation of antiviral innate defenses invariably precede cellular infection (Figure 3.1). This innovative concept has no parallel in the contemporary landscape of antiviral therapeutics. Based on the trimeric structure of the spike protein, each spike protein at the virion surface can 'present' as many as three IFN-β proteins to provide an outer shell of IFN-β that activate IFNAR signaling upon contact of the virus with a host cell. This targeted presentation of IFN-β at the viral surface is qualitatively different from subcutaneous or intravenous IFN-β administration, which leads to systemic distribution of IFN-β coupled with highly diffuse antiviral action, low IFN-β concentrations at the site of infection, and a primary impact on non-target cell types irrelevant to the viral infection. Importantly, this modular antiviral platform can be modified by replacement of the sACE2 domain with other viral host receptors to target alternative spectrums of viral pathogens. Likewise, the IFN-β effector domain can be replaced

with alternative effector domains to engage other antiviral defenses that may be more applicable to selected viral pathogens.

6.2. Rationale for use of sACE2 as an anti-inflammatory and antiviral mediator

The sACE2 domain has both anti-inflammatory and antiviral activity. The sACE2 domain is a major anti-inflammatory regulatory node of the renin-angiotensin system, in that ACE2 hydrolyzes the inflammatory angiotensin II hormone to the homeostatic angiotensin 1-7 modulator (113). ACE2-mediated anti-inflammatory activities may ameliorate diseases such as ARDS, ALI, and SARS (51, 55, 61, 126). Conversely, downregulation of transmembrane ACE2 in SARS-CoV- and SARS-CoV-2-infected cells is thought to exacerbate disease (55, 127-132). In addition to anti-inflammatory activity, the sACE2 domain also has antiviral applications, because sACE2 neutralizes the spike protein of HCoV NL63, SARS-CoV, and SARS-CoV-2 and thereby inhibits infection *in vitro* (54, 56, 59, 61).

Viruses may exhibit the evolutionary adaptation of reprogramming infected cells to shed host receptor and/or coreceptors to preclude superinfection. Virus-induced host receptor shedding causes release of the respective ectodomains into extracellular fluids and the circulation such that infection severity may correlate with circulating levels of receptor/ coreceptor ectodomains. This paradigm may apply to ACE2-tropic coronaviruses because the severity of infection appears to correlate with circulating levels of sACE2, which is used as a biomarker of infection. However, circulating sACE2 retains enzymatic activity and continues to produce anti-inflammatory angiotensin derivatives that may counteract virally-induced immunopathogenesis. Circulating sACE2 may also mediate viral neutralization. Although circulating levels of sACE2 may

correlate with COVID-19 pathogenesis, circulating sACE2 may be compensatory and serve to alleviate immunopathogenesis and facilitate disease remission. Thus, the transmembrane ACE2 host receptor which is required for pathogenesis may diametrically differ from the shed sACE2 ectodomain, which may act to reverse pathogenesis. In support, a double-blinded, randomized, placebo-controlled, phase 2 trial for COVID-19 showed that intravenous sACE2 significantly improved mechanical ventilator-free days and reduced viral RNA load compared to placebo (ClinicalTrials.gov ID NCT04335136). Additionally, intravenous sACE2 led to a decrease in pro-inflammatory angiotensin II and an increase in anti-inflammatory angiotensin 1-7 and angiotensin 1-5 (ClinicalTrials.gov ID NCT04335136). In a phase I, double-blind, placebo-controlled, dose-escalation study, aerosolized sACE2 was found to be safe and well-tolerated, with no dose-limiting toxicities and no detection of anti-ACE2 antibodies (ClinicalTrials.gov ID NCT05065645) (62). Thus, in addition to the sACE2-mediated targeting of IFNβ-ACE2 to the virion surface, the sACE2 domain may provide anti-inflammatory activity to improve overall therapeutic efficacy.

6.3 Rationale for use of sACE2 rather than an anti-Spike antibody as a targeting moiety

As an alternative to the IFNβ-ACE2 platform, fusion proteins that couple IFN-β to high affinity anti-spike antibodies/ nanobodies may more efficiently target IFN-β to surfaces of selected pathogenic viruses, simply because anti-spike modalities may have higher affinity than sACE2 for spike glycoproteins. Nonetheless, the choice of ACE2 as the targeting vehicle has several major advantages over anti-spike antibodies. Namely, the IFNβ-ACE2 platform targets diverse viral species, including NL63, SARS-CoV, and SARS-CoV-2 and all variants of these viral species. Thus, the IFNβ-ACE2 platform is impervious to immune evasion via immune-

selected variant evolution. The IFNβ-ACE2 platform may also target future pandemic viral pathogens that use ACE2 as the primary host receptor by a cross-reactive mechanism that would preclude continual emergence of new pathogenic variants. Conversely, an IFNβ-anti-spike platform would likely target a limited number of variants of one viral species and would have to be reinvented and gain new regulatory approvals seasonally for each new emergent viral variant. Given that the IFNβ-ACE2 affinity for spike is adequate to achieve robust antiviral activity (Figures 4.1 and 4.2), the IFNβ-ACE2 platform appears to have compelling advantages over an IFNβ-anti-spike platform.

6.3 Rationale for use of type I interferons as the effector moiety

Over the past several decades, IFN-Is have proven to be safe and effective as FDA-approved biologics for a broad spectrum of disease classes, including cancer, infectious diseases (e.g. Hepatitis B and C), and autoimmune diseases (e.g. Multiple Sclerosis) (133-136). IFN-Is were extensively tested in COVID-19 and were uniformly found to be safe without adverse consequences, and multiple studies provided suggestive evidence of clinical efficacy (83-85, 88, 90, 137-139). For example, a randomized, double-blind, placebo-controlled, phase 2 trial showed that inhaled pulmonary administration of IFN-β was efficacious in treating SARS-CoV-2-infected patients, as shown by accelerated recovery and a 79% decrease in progression to severe disease or death (ClinicalTrials.gov ID NCT04385095) (84). A randomized, double-blind, placebo-controlled, phase 3 trial showed that nebulized IFN-β trended towards reducing relative risk of progression to severe disease or death within 35 days compared to patients who received placebo, especially in high-risk patient subgroups. However there was no significant difference in the time to recovery and time to hospital discharge (primary endpoints) (isrctn.com ID

ISRCTN85436698) (85). Additionally, subcutaneous administration of IFN-β in the World Health Organization Solidarity Trial did not show clinical efficacy (83), which raised the question of whether subcutaneous IFN-I is an optimal administration route. From a safety standpoint, these clinical studies showed that administration of IFN-Is was well-tolerated, lacked pro-inflammatory action, and did not exacerbate disease. Given that IFN-I administration via parenteral or mucosal routes is associated with inconsistent or modest efficacy, new strategies are needed for dose-sparing, targeted delivery of interferon-based drugs to improve efficacy. It is informative to compare clinical application of IFN-Is to the endogenous innate production of IFN-Is in that the innate immune system locally produces IFN-Is at sites of viral infection. Thus, an important clinical goal is to administer IFN-Is via strategies in line with the specificity and locality of the innate immune response. As SARS-CoV-2 inhibits IFN-I production, the IFNβ-ACE2 targeting strategy may fulfill these criteria by introducing IFN-β directly to the site of infection by binding to ACE2-tropic viruses, including emergent coronaviruses that represent a clear global threat for future pandemics.

6.4 Interpretation of the 'virus-washing' methodology

The main question of this study is whether anchoring IFN-β to the virion surface enables strong antiviral activity. Although the 'virus-wash' experiments are unconventional, the 'virus-washing' approach represented a direct means to test our hypothesis. Importantly, the 'virus-washing' methodology provided the key experimental data for the conclusion that IFNβ-ACE2 mechanistically targeted IFN-β to confer high anti-viral efficacy to the exact physical interface of infection. The comparison of 'virus-washed' (Figures 4.1 and 4.2) and 'non-washed' (Figures 5.1 and 5.2) systems also enabled comparison of virus-anchored IFN-β (targeted) versus virus-

anchored IFN-β mixed with free IFN-β (non-targeted) systems, respectively. In comparison to IFN-β, IFNβ-ACE2 had superlative antiviral activity in targeted systems and had advantageous antiviral activity in non-targeted systems. That is, in a non-targeted system, IFNβ-ACE2 had a 10-fold enhanced potency compared to the unlinked combination of IFN-β and sACE2 (Figures 5.1 and 5.2). The EC_{50} of IFNβ-ACE2 was ~1 pM, whereas the EC_{50} of IFN-β or the unlinked combination of IFN-β and sACE2(18-611) was ~10 pM. In conclusion, IFNβ-ACE2 had major advantages over IFN-β in targeted systems but also had significant advantages compared to IFN-β in non-targeted systems.

6.5 The physiological significance represented by the 'virus-washing' methodology

In this study, we compared two environments based via the 'virus-washed' versus 'non-washed' virus systems. The 'virus-washed' system uses centrifugal fluid flow to remove free unbound proteins while retaining proteins that are directly bound to the virion surface. In non-washed conditions, all protein reagents, virions, and cells were confined to a 100 µl volume without any directional fluid flow. A central question pivots on which system best reflects the *in vivo* environment, given that all physiological environments are subject to constant dynamic fluid flow. Fluid flow in the lung parenchyma is driven by rhythmic ciliary beating that constantly moves fluid and mucus from the lung. Major fluidic drivers in all tissues include circulatory and/or lymphatic flow, together with many complementary drivers (osmotic, hydrostatic, oncotic, etc.). The virus-washed system was devised to address a technical question: does virion-anchored IFN-β exhibit antiviral efficacy? We also maintain that virus-washed systems have physiological significance, because the system features fluid flow dynamics which are central to all physiological environments. That is, IFNβ-ACE2/ virus complexes will retain

targeted antiviral activity regardless of *in vivo* fluid flow dynamics that would otherwise separate an antiviral reagent from infectious virions. Unlike IFNβ-ACE2, for example, free IFN-β will readily diffuse from infectious virus by any differential/ diffusional flow kinetics. In a physiological context, fluid-flow tissue transit of virions versus soluble IFN-β differs fundamentally. Virions are more massive, are precipitable rather than soluble, are readily trapped in a web of extracellular matrix, and form extracellular long-lived infectious reservoirs upon binding cell appendages or tissue matrix components. IFN-β, in contrast, is freely diffusible and swiftly achieves broad systemic biodistribution coupled with rapid degradation. Thus, the principle of this platform is defined by the anchoring of IFNβ-ACE2 to virion surfaces coupled with pinpoint targeting of antiviral activity to the site of infection by a mechanism impervious to differential fluid flow. The tight physical association of IFNβ-ACE2 and virions and the lack of differential diffusion (Figures 4.1 and 4.2) are unique features of this platform with important physiological significance.

6.6 Is antiviral efficacy of IFNβ-ACE2 contingent upon ACE2-mediated targeting or ACE2-mediated neutralization?

This study shows that the sACE2 domain of IFNβ-ACE2 effectively targets IFN-β to the surface of NL63 at sub-neutralizing concentrations. Indeed, IFNβ-ACE2 exhibited biphasic inhibition curves (Figures 5.1 and 5.2) in that IFN-β-mediated antiviral activity was several orders of magnitude more potent than the neutralizing activity of sACE2. These findings support the concept that the low-zone picomolar concentration range mediates the dominant antiviral activity of IFNβ-ACE2 without the need for viral neutralization, which is only observed at much higher concentrations (Figure 4.1B). Based on this vantage point, the dominant mechanism of

antiviral efficacy may be ACE2-mediated targeting of IFN-β to the viral surface rather than ACE2-mediated viral neutralization. Future experimentation in preclinical infection models will reveal the dose-dependent antiviral activity of IFNβ-ACE2 versus control proteins, and these experiments will reveal whether ACE2-mediated targeting alone or in combination with ACE2-mediated neutralization represents the dominant therapeutic mechanism *in vivo*.

6.7 NL63 viral infection causes transmembrane ACE2 and TMPRSS2 downregulation together with intracellular nucleocapsid production

Transmembrane TMPRSS2 plays an important role in NL63, SARS-CoV, and SARS-CoV-2 spike protein priming and viral entry by cleaving spike protein at the S1/S2 and the S2′ sites (53, 57, 58, 115, 140-142). Figure 4.3 shows the negative correlation between nucleocapsid expression and ACE2/TMPRSS2 expression. As shown in Figures 4.1, 4.2, 4.3, and 5.2, NL63 infection of Vero E6-TMPRSS2-T2A-ACE2 cells caused downregulation of ACE2 and TMPRSS2. Because IFNβ-ACE2 blocks NL63 infection, IFNβ-ACE2 also preserved normal surface levels of ACE2 and TMPRSS2. As SARS-CoV and SARS-CoV-2 infection is postulated to cause pulmonary inflammation in part by causing ACE2 downregulation, IFNβ-ACE2 may prevent inflammatory lung diseases in infected patients by blocking ACE2 downregulation and augmenting anti-inflammatory sACE2 concentrations (51, 126, 128, 129, 143). A previous report, however, noted that NL63 infection did not decrease ACE2 expression on VeroE6 cells despite the increase of viral RNA and protein levels (129) in contrast to our study showing that NL63 infection drives decreased ACE2 expression on Vero E6-TMPRSS2-T2A-ACE2 cells. This inconsistency could be due to multiple reasons. First, we compared NL63 infection in VeroE6 and Vero E6-TMPRSS2-T2A-ACE2 cells and found that Vero E6-TMPRSS2-T2A-ACE2 cells

are more susceptible to NL63 infection. As the decrease of ACE2 expression is dependent on the efficiency of NL63 infection and replication (144), this increase in infection may lead to the downregulation and/or shedding of ACE2. Second, flow cytometry is an inherently more sensitive technique than Western blots. Overall, transmembrane ACE2 and TMPRSS2 downregulation closely correlated with nucleocapsid production in infected cells and thus served as a valid marker for viral infection.

6.8 The potency of virion-targeted IFN-β

The virological potency of virus-absorbed IFNβ-ACE2 is difficult to measure, but nonetheless one can estimate upper bounds of these values based on theoretical considerations. As shown in Figures 4.1 and 4.2, NL63 exhibited stable capture of IFNβ-ACE2 when incubated with 100 pM – 1 nM IFNβ-ACE2. Binding appeared stable in that virion/ IFNβ-ACE2 complexes did not dissociate during extensive washing of the virus. Because one does not know the actual number of IFNβ-ACE2 molecules bound per virion, we instead calculated upper limits based on the assumption of 100% binding efficiencies, which provided an upper limit of the IFNβ-ACE2 concentration that was stably absorbed by the virus and carried into the host cell infection assay. We estimate upper limits of 3 IFNβ-ACE2 molecules per spike glycoprotein x 300 spike glycoproteins per virion x 3000 infectious virions per 100 µl culture (MOI of 0.1 in a 30,000-cell culture), which equals an upper limit of 2.7 x 10^6 IFNβ-ACE2 molecules per 100 µl culture or an equivalent molarity of 45 femtomolar. IFNβ-ACE2 exhibited half-maximal inhibitory values in the 10 pM – 1 nM concentration range in a 229E infection system, representing IFNβ-ACE2 anti-virological potency of the IFN-β domain when IFNβ-ACE2 lacks binding to the virion (Figure 5.4). Based on these considerations, virus absorbed IFNβ-ACE2

was several orders of magnitude more potent than soluble (i.e., virus non-absorbed) IFNβ-ACE2 for antiviral activity. The caveat is that virion-arrayed IFN-β is surface-bound and not in solution per se, but nonetheless this consideration points to a limited array of IFN-β having unexpectedly high bioactivity. It is currently unknown whether immobilized IFN-β may have activities that supersede soluble IFN-β on a per molecule basis, perhaps reflecting fixed surface immobilization and increased avidity for IFNAR, thereby providing superior IFNAR crosslinking. In addition, an immobilized IFN-β array may affect IFNAR trafficking to enhance receptor signaling (145-150).

6.10 Future Directions

Animal studies are crucial to properly assess the feasibility and therapeutic benefit of targeting IFN-β to the surface of virions within a host. *In vivo* experiments would allow for a more comprehensive evaluation of our platform's effectiveness in the context of a complex immune environment, viral dissemination, protein diffusion, and tissue-specific responses. These studies can also help identify any unforeseen side effects or off-target effects that may not be apparent *in vitro*.

Multiple animal models exist for testing therapies for COVID-19. A commonly used animal model is the K18-hACE2 mice. These transgenic mice express human ACE2 (hACE2) under the control of the human keratin 18 (K18) promoter. The expression of hACE2 in K18-hACE2 mice is observed in epithelial cells, including epithelial cells of the airway where SARS-CoV and SARS-CoV-2 infection typically begin. K18-hACE2 mice have been used extensively to study NL63 and SARS-CoV-2 pathogenesis as well as therapeutic options.

Syrian hamsters are commonly used to study NL63 and SARS-CoV-2 *in vivo*, particularly to test the effects of IFN on infection. As observed in humans, SARS-CoV-2 causes dysregulation of IFN-I in both respiratory and non-respiratory tissues in the Syrian hamster model (151). This disease model offers insights into the pathogenesis of COVID-19 and allows us to evaluate potential therapeutic strategies to counter IFN dysregulation.

To test our therapeutic *in vivo*, we first need to generate a mouse IFNβ-ACE2 construct. This construct would consist of a mouse IFN-β covalently linked to a human ACE2 domain. The development of such construct would enable us to study the targeted delivery of IFN-β in a physiologically relevant setting.

Before transitioning to animal studies, the newly developed construct must then be validated *in vitro*. This step ensures that the construct behaves as expected – demonstrating proper virion binding and biological activity of IFN-β. These *in vitro* assays serve as a crucial quality control measure for the fusion protein before committing to more complex and resource-intensive animal experiments.

Once the *in vitro* results are validated, the final step involves testing the construct in an appropriate animal model of viral infection. These studies would evaluate key outcomes such as viral clearance, immune activation, and overall disease progression. The results will be instrumental in determining whether targeting IFN-β to the surface of virions *in vivo* is feasible and can provide a meaningful therapeutic advantage.

Figure 6.1 offers a schematic overview of the testing strategy in a K18-hACE2 mouse model. Briefly, nebulized IFNβ-ACE2 or the unlinked combination of IFN-β and ACE2 will be administered either 1 hour pre-infection, at time of infection, or 24 hours post-infection with SARS-CoV-2. Mice will be weighed daily to monitor progression of disease. Lung tissue will be

harvested either 4 days post-infection or at humane endpoint to measure viral titer via quantitative reverse transcription polymerase chain reaction (qRT-PCR) and immune cell infiltration and activation markers via flow cytometry. In comparison to mice receiving the unlinked combination of IFN-β and ACE2, we expect to find decreased viral titers in groups receiving the therapeutic as well as an improved disease score as measured by weight loss. We also expect to find an increased virus-specific immune response indicated by increased levels of virus-specific T cells and B cells as well as an increased state of activation in these cells. These results will help us highlight the potential therapeutic and vaccination role of this platform and give more insight into the ability of the fusion protein to function in a complex, immune-replete environment.

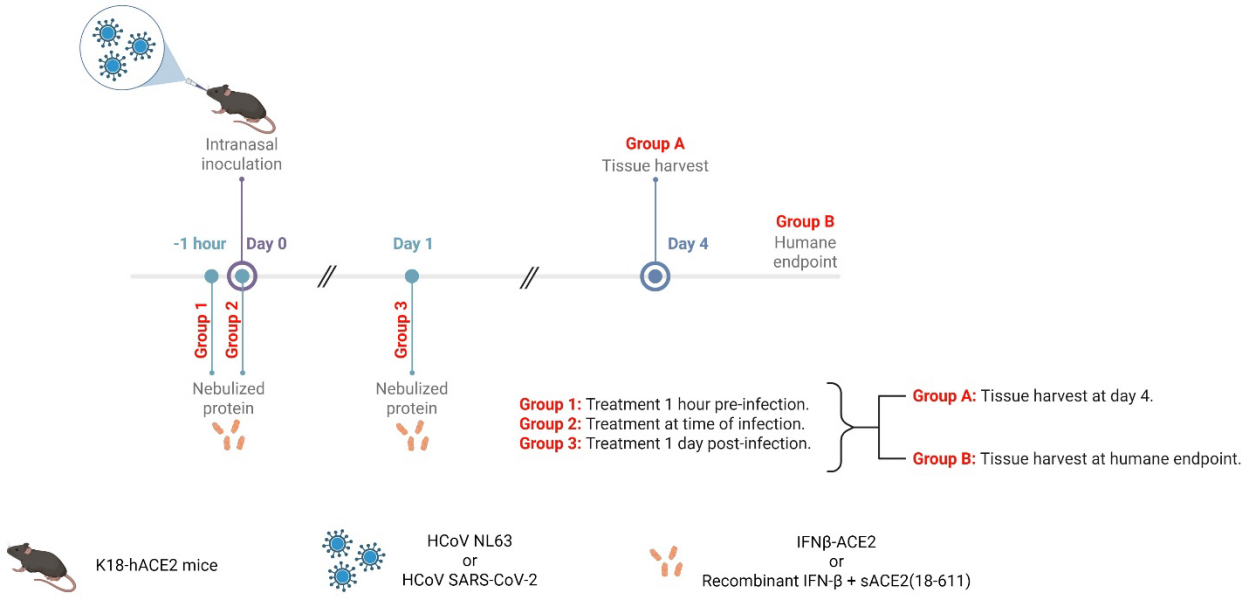

Figure 6.1. Schematic overview of *in vivo* testing strategy (152).

6.10 Conclusion

The likelihood of future viral epidemics and pandemics requires advancement of new antiviral therapies. This study provides a new antiviral platform that synergistically combines the virus-anchoring activity of a specific soluble host receptor (sACE2) and an immune modulator (IFN-β) by targeting the immune modulator to the surface of infectious virions, thereby engendering highly-specific antiviral activity. Overall, this study advanced the concept of an antiviral fusion protein that assembles an IFN-β shield at the virion surface to constitute a potent antiviral therapy.

CHAPTER 7: REFERENCES

1. M. Marani, G. G. Katul, W. K. Pan, A. J. Parolari, Intensity and frequency of extreme novel epidemics. *Proc Nat Acad Sci USA* **118**, e2105482118 (2021).

2. Anonymous (David J. Sencer CDC Museum: In Association with the Smithsonian Institution. CDC Museum COVID-19 Timeline. (https://www.cdc.gov/museum/timeline/covid19.html).

3. Anonymous (World Health Organization 2023 data.who.int, WHO Coronavirus (COVID-19) dashboard > Cases [Dashboard]. (https://data.who.int/dashboards/covid19/cases).

4. J. Poorolajal, The global pandemics are getting more frequent and severe. *Journal of Research in Health Sciences* **21**, e00502-e00502 (2021).

5. C. B. Jackson, M. Farzan, B. Chen, H. Choe, Mechanisms of SARS-CoV-2 entry into cells. *Nat Rev Mol Cell Biol* **23**, 3-20 (2022).

6. J. B. Zawilska, A. Lagodzinski, M. Berezinska, COVID-19: from the structure and replication cycle of SARS-CoV-2 to its disease symptoms and treatment. *J Physiol Pharmacol* **72** (2021).

7. S. M. Haque, O. Ashwaq, A. Sarief, A. K. Azad John Mohamed, A comprehensive review about SARS-CoV-2. *Future Virol* **15**, 625-648 (2020).

8. M. Tahir, Coronavirus genomic nsp14-ExoN, structure, role, mechanism, and potential application as a drug target. *J Med Virol* **93**, 4258-4264 (2021).

9. Y. Chen *et al.*, Functional screen reveals SARS coronavirus nonstructural protein nsp14 as a novel cap N7 methyltransferase. *Proc Natl Acad Sci USA* **106**, 3484-3489 (2009).

10. M. Becares *et al.*, Mutagenesis of Coronavirus nsp14 Reveals Its Potential Role in Modulation of the Innate Immune Response. *J Virol* **90**, 5399-5414 (2016).

11. V. E. Hillary, S. A. Ceasar, An update on COVID-19: SARS-CoV-2 variants, antiviral drugs, and vaccines. *Heliyon* **9**, e13952 (2023).

12. F. Mambelli *et al.*, An Update on Anti-COVID-19 Vaccines and the Challenges to Protect Against New SARS-CoV-2 Variants. *Pathogens* **14** (2025).

13. A. Ahmad, M. A. M. Fawaz, A. Aisha, A comparative overview of SARS-CoV-2 and its variants of concern. *Infez Med* **30**, 328-343 (2022).

14. E. Volz *et al.*, Assessing transmissibility of SARS-CoV-2 lineage B.1.1.7 in England. *Nature* **593**, 266-269 (2021).

15. J. Y. Choi, D. M. Smith, SARS-CoV-2 Variants of Concern. *Yonsei Med J* **62**, 961-968 (2021).

16. D. Duong, Alpha, Beta, Delta, Gamma: What's important to know about SARS-CoV-2 variants of concern? *Cmaj* **193**, E1059-e1060 (2021).

17. R. E. Chen *et al.*, Resistance of SARS-CoV-2 variants to neutralization by monoclonal and serum-derived polyclonal antibodies. *Nat Med* **27**, 717-726 (2021).

18. C. K. Wibmer *et al.*, SARS-CoV-2 501Y.V2 escapes neutralization by South African COVID-19 donor plasma. *Nat Med* **27**, 622-625 (2021).

19. N. R. Faria *et al.*, Genomics and epidemiology of the P.1 SARS-CoV-2 lineage in Manaus, Brazil. *Science* **372**, 815-821 (2021).

20. A. Saito *et al.*, Enhanced fusogenicity and pathogenicity of SARS-CoV-2 Delta P681R mutation. *Nature* **602**, 300-306 (2022).

21. J. Zhang *et al.*, Structural impact on SARS-CoV-2 spike protein by D614G substitution. *Science* **372**, 525-530 (2021).

22. C. Huang *et al.*, Clinical features of patients infected with 2019 novel coronavirus in Wuhan, China. *The Lancet* **395**, 497-506 (2020).

23. K. C. Xin Zou, Jiawei Zou, Peiyi Han, Jie Hao, Zeguang Han, Single-cell RNA-seq data analysis on the receptor ACE2 expression reveals the potential risk of different human organs vulnerable to 2019-nCoV infection. *Front. Med.* **14**, 185-192 (2020).

24. Y. Zhao *et al.*, Single-Cell RNA Expression Profiling of ACE2, the Receptor of SARS-CoV-2. *Am J Respir Crit Care Med* **202**, 756-759 (2020).

25. C. Phetsouphanh *et al.*, Immunological dysfunction persists for 8 months following initial mild-to-moderate SARS-CoV-2 infection. *Nature Immunology* **23**, 210-216 (2022).

26. J. Seeßle *et al.*, Persistent Symptoms in Adult Patients 1 Year After Coronavirus Disease 2019 (COVID-19): A Prospective Cohort Study. *Clinical Infectious Diseases* **74**, 1191-1198 (2021).

27. E. Pretorius *et al.*, Persistent clotting protein pathology in Long COVID/Post-Acute Sequelae of COVID-19 (PASC) is accompanied by increased levels of antiplasmin. *Cardiovascular Diabetology* **20**, 172 (2021).

28. M. J. Peluso, S. G. Deeks, Early clues regarding the pathogenesis of long-COVID. *Trends in Immunology* **43**, 268-270 (2022).

29. A. Iwasaki, D. Putrino, Why we need a deeper understanding of the pathophysiology of long COVID. *The Lancet Infectious Diseases* **23**, 393-395 (2023).

30. Q. Liu *et al.*, Gut microbiota dynamics in a prospective cohort of patients with post-acute COVID-19 syndrome. *Gut* **71**, 544-552 (2022).

31. Y. Su *et al.*, Multiple early factors anticipate post-acute COVID-19 sequelae. *Cell* **185**, 881-895.e820 (2022).

32. C. Cervia *et al.*, Immunoglobulin signature predicts risk of post-acute COVID-19 syndrome. *Nat Commun* **13**, 446 (2022).

33. S. R. Stein *et al.*, SARS-CoV-2 infection and persistence in the human body and brain at autopsy. *Nature* **612**, 758-763 (2022).

34. M. J. Peluso *et al.*, Markers of Immune Activation and Inflammation in Individuals With Postacute Sequelae of Severe Acute Respiratory Syndrome Coronavirus 2 Infection. *The Journal of Infectious Diseases* **224**, 1839-1848 (2021).

35. Y. Zhang *et al.*, Viral afterlife: SARS-CoV-2 as a reservoir of immunomimetic peptides that reassemble into proinflammatory supramolecular complexes. *Proc Natl Acad Sci USA* **121**, e2300644120 (2024).

36. B. M. Scott, V. Lacasse, D. G. Blom, P. D. Tonner, N. S. Blom, Predicted coronavirus Nsp5 protease cleavage sites in the human proteome. *BMC Genom Data* **23**, 25 (2022).

37. Y. Liu *et al.*, SARS-CoV-2 Nsp5 Demonstrates Two Distinct Mechanisms Targeting RIG-I and MAVS To Evade the Innate Immune Response. *mBio* **12**, e0233521 (2021).

38. J. Hammond *et al.*, Oral Nirmatrelvir for High-Risk, Nonhospitalized Adults with Covid-19. *New England Journal of Medicine* **386**, 1397-1408 (2022).

39. J. Hammond *et al.*, Alleviation of COVID-19 Symptoms and Reduction in Healthcare Utilization Among High-risk Patients Treated With Nirmatrelvir/Ritonavir (NMV/R): A Phase 3 Randomized Trial. *Clin Infect Dis* **80**, 323-330 (2025).

40. J. H. Beigel *et al.*, Remdesivir for the Treatment of Covid-19 — Final Report. *New England Journal of Medicine* **383**, 1813-1826 (2020).

41. S. A. Olender *et al.*, Remdesivir for Severe Coronavirus Disease 2019 (COVID-19) Versus a Cohort Receiving Standard of Care. *Clin Infect Dis* **73**, e4166-e4174 (2021).

42. B. M. Maas *et al.*, Molnupiravir: Mechanism of action, clinical, and translational science. *Clin Transl Sci* **17**, e13732 (2024).

43. A. Jayk Bernal *et al.*, Molnupiravir for Oral Treatment of Covid-19 in Nonhospitalized Patients. *N Engl J Med* **386**, 509-520 (2022).

44. O. Abani *et al.*, Tocilizumab in patients admitted to hospital with COVID-19 (RECOVERY): a randomised, controlled, open-label, platform trial. *The Lancet* **397**, 1637-1645 (2021).

45. C. Salama *et al.*, Tocilizumab in Patients Hospitalized with Covid-19 Pneumonia. *New England Journal of Medicine* **384**, 20-30 (2021).

46. A. C. Kalil *et al.*, Baricitinib plus Remdesivir for Hospitalized Adults with Covid-19. *New England Journal of Medicine* **384**, 795-807 (2021).

47. K. Akinosoglou *et al.*, Efficacy and safety of early soluble urokinase plasminogen receptor plasma-guided anakinra treatment of COVID-19 pneumonia: A subgroup analysis of the SAVE-MORE randomised trial. *EClinicalMedicine* **56**, 101785 (2023).

48. E. Kyriazopoulou *et al.*, Early treatment of COVID-19 with anakinra guided by soluble urokinase plasminogen receptor plasma levels: a double-blind, randomized controlled phase 3 trial. *Nat Med* **27**, 1752-1760 (2021).

49. A. P. J. Vlaar *et al.*, Anti-C5a antibody (vilobelimab) therapy for critically ill, invasively mechanically ventilated patients with COVID-19 (PANAMO): a multicentre, double-blind, randomised, placebo-controlled, phase 3 trial. *Lancet Respir Med* **10**, 1137-1146 (2022).

50. J. Kuriakose, A. C. Montezano, R. M. Touyz, ACE2/Ang-(1-7)/Mas1 axis and the vascular system: vasoprotection to COVID-19-associated vascular disease. *Clin Sci (Lond)* **135**, 387-407 (2021).

51. A. Khan *et al.*, A pilot clinical trial of recombinant human angiotensin-converting enzyme 2 in acute respiratory distress syndrome. *Crit Care* **21**, 234 (2017).

52. A. R. Hemnes *et al.*, A potential therapeutic role for angiotensin-converting enzyme 2 in human pulmonary arterial hypertension. *Eur Respir J* **51** (2018).

53. M. Hoffmann *et al.*, SARS-CoV-2 cell entry depends on ACE2 and TMPRSS2 and Is blocked by a clinically proven protease inhibitor. *Cell* 10.1016/j.cell.2020.02.052 (2020).

54. H. Hofmann *et al.*, Human coronavirus NL63 employs the severe acute respiratory syndrome coronavirus receptor for cellular entry. *Proc Nat Acad Sci USA* **102**, 7988-7993 (2005).

55. K. Kuba *et al.*, A crucial role of angiotensin converting enzyme 2 (ACE2) in SARS coronavirus-induced lung injury. *Nat Med* **11**, 875-879 (2005).

56. W. Li *et al.*, Angiotensin-converting enzyme 2 is a functional receptor for the SARS coronavirus. *Nature* **426**, 450-454 (2003).

57. A. Milewska *et al.*, Entry of human Coronavirus NL63 into the cell. *J Virol* **92**, 10.1128/jvi.01933-01917 (2018).

58. I. Glowacka *et al.*, Evidence that TMPRSS2 activates the severe acute respiratory syndrome coronavirus spike protein for membrane fusion and reduces viral control by the humoral immune response. *J Virol* **85**, 4122-4134 (2011).

59. V. Monteil *et al.*, Inhibition of SARS-CoV-2 infections in engineered human tissues using clinical-grade soluble human ACE2. *Cell* **181**, 905-913.e907 (2020).

60. L. Hassler *et al.*, Intranasal soluble ACE2 improves survival and prevents brain SARS-CoV-2 infection. *Life Sci Alliance* **6** (2023).

61. A. Zoufaly *et al.*, Human recombinant soluble ACE2 in severe COVID-19. *Lancet Respir Med* **8**, 1154-1158 (2020).

62. M. Bauer *et al.*, Phase I dose-escalation study to assess the safety, tolerability, pharmacokinetics and pharmacodynamics of an inhaled recombinant human ACE2. *ERJ Open Research* **10**, 00567-02023 (2024).

63. D. Bencze, T. Fekete, K. Pázmándi, Type I Interferon Production of Plasmacytoid Dendritic Cells under Control. *International Journal of Molecular Sciences* **22**, 4190 (2021).

64. Y. Q. Min *et al.*, Immune evasion of SARS-CoV-2 from interferon antiviral system. *Comput Struct Biotechnol J* **19**, 4217-4225 (2021).

65. D. Blanco-Melo *et al.*, Imbalanced host response to SARS-CoV-2 drives development of COVID-19. *Cell* **181**, 1036-1045.e1039 (2020).

66. J. H. Lee, L. Koepke, F. Kirchhoff, K. M. J. Sparrer, Interferon antagonists encoded by SARS-CoV-2 at a glance. *Med Microbiol Immunol* **212**, 125-131 (2023).

67. J. Hadjadj *et al.*, Impaired type I interferon activity and inflammatory responses in severe COVID-19 patients. *Science* **369**, 718-724 (2020).

68. Q. Zhang *et al.*, Inborn errors of type I IFN immunity in patients with life-threatening COVID-19. *Science* **370** (2020).

69. E. Meffre, A. Iwasaki, Interferon deficiency can lead to severe COVID. *Nature* **587**, 374-376 (2020).

70. C. Zanza *et al.*, Cytokine Storm in COVID-19: Immunopathogenesis and Therapy. *Medicina (Kaunas)* **58** (2022).

71. G. Bucciol, I. Meyts, Inherited and acquired errors of type I interferon immunity govern susceptibility to COVID-19 and multisystem inflammatory syndrome in children. *J Allergy Clin Immunol* **151**, 832-840 (2023).

72. T. M. Campbell *et al.*, Respiratory viral infections in otherwise healthy humans with inherited IRF7 deficiency. *J Exp Med* **219** (2022).

73. H. Abolhassani *et al.*, Inherited IFNAR1 Deficiency in a Child with Both Critical COVID-19 Pneumonia and Multisystem Inflammatory Syndrome. *J Clin Immunol* **42**, 471-483 (2022).

74. S. Khanmohammadi, N. Rezaei, M. Khazaei, A. Shirkani, A Case of Autosomal Recessive Interferon Alpha/Beta Receptor Alpha Chain (IFNAR1) Deficiency with Severe COVID-19. *J Clin Immunol* **42**, 19-24 (2022).

75. T. Asano *et al.*, X-linked recessive TLR7 deficiency in ~1% of men under 60 years old with life-threatening COVID-19. *Sci Immunol* **6** (2021).

76. X. Solanich *et al.*, Genetic Screening for TLR7 Variants in Young and Previously Healthy Men With Severe COVID-19. *Front Immunol* **12**, 719115 (2021).

77. P. Bastard *et al.*, Autoantibodies neutralizing type I IFNs are present in ~4% of uninfected individuals over 70 years old and account for ~20% of COVID-19 deaths. *Sci Immunol* **6** (2021).

78. M. G. P. van der Wijst *et al.*, Type I interferon autoantibodies are associated with systemic immune alterations in patients with COVID-19. *Sci Transl Med* **13**, eabh2624 (2021).

79. E. R. Simula *et al.*, Increased Presence of Antibodies against Type I Interferons and Human Endogenous Retrovirus W in Intensive Care Unit COVID-19 Patients. *Microbiol Spectr* **10**, e0128022 (2022).

80. W. C. Chen *et al.*, Clinical efficacy and safety of interferon-β-containing regimens in the treatment of patients with COVID-19: a systematic review and meta-analysis of randomized controlled trials. *Expert Rev Anti Infect Ther* **20**, 741-747 (2022).

81. F. Sodeifian, M. Nikfarjam, N. Kian, K. Mohamed, N. Rezaei, The role of type I interferon in the treatment of COVID-19. *J Med Virol* **94**, 63-81 (2022).

82. S. Ryoo *et al.*, Clinical efficacy and safety of interferon (Type I and Type III) therapy in patients with COVID-19: A systematic review and meta-analysis of randomized controlled trials. *PLoS One* **18**, e0272826 (2023).

83. H. Pan *et al.*, Repurposed antiviral drugs for Covid-19 - Interim WHO Solidarity Trial results. *N Engl J Med* 10.1056/NEJMoa2023184 (2020).

84. P. D. Monk *et al.*, Safety and efficacy of inhaled nebulised interferon beta-1a (SNG001) for treatment of SARS-CoV-2 infection: a randomised, double-blind, placebo-controlled, phase 2 trial. *Lancet Respir Med* 10.1016/s2213-2600(20)30511-7 (2020).

85. P. D. Monk *et al.*, Nebulised interferon-β1a (SNG001) in hospitalised COVID-19: SPRINTER phase III study. *ERJ Open Research* **9**, 00605-02022 (2023).

86. M. Wadman, Can interferons stop COVID-19 before it takes hold? *Science* **369**, 125-126 (2020).

87. A. Park, A. Iwasaki, Type I and Type III Interferons - Induction, Signaling, Evasion, and Application to Combat COVID-19. *Cell Host Microbe* **27**, 870-878 (2020).

88. I. F. Hung *et al.*, Triple combination of interferon beta-1b, lopinavir-ritonavir, and ribavirin in the treatment of patients admitted to hospital with COVID-19: an open-label, randomised, phase 2 trial. *Lancet* **395**, 1695-1704 (2020).

89. M. Estébanez *et al.*, Clinical evaluation of IFN beta1b in COVID-19 pneumonia: a retrospective study. *medRxiv* 10.1101/2020.05.15.20084293, 2020.2005.2015.20084293 (2020).

90. E. Davoudi-Monfared *et al.*, A randomized clinical trial of the efficacy and safety of Interferon β-1a in treatment of severe COVID-19. *Antimicrob Agents Chemother* **64** (2020).

91. H. Rahmani *et al.*, Interferon β-1b in treatment of severe COVID-19: A randomized clinical trial. *Int Immunopharmacol* **88**, 106903 (2020).

92. F. Khamis *et al.*, Randomized controlled open label trial on the use of favipiravir combined with inhaled interferon beta-1b in hospitalized patients with moderate to severe COVID-19 pneumonia. *Int J Infect Dis* **102**, 538-543 (2021).

93. P. Baghaei *et al.*, Combination therapy of IFNβ1 with lopinavir-ritonavir, increases oxygenation, survival and discharging of sever COVID-19 infected inpatients. *Int Immunopharmacol* **92**, 107329 (2021).

94. C. K. H. Wong *et al.*, Clinical outcomes of different therapeutic options for COVID-19 in two Chinese case cohorts: A propensity-score analysis. *EClinicalMedicine* **32**, 100743 (2021).

95. I. Alavi Darazam *et al.*, Role of interferon therapy in severe COVID-19: the COVIFERON randomized controlled trial. *Sci Rep* **11**, 8059 (2021).

96. F. Ader *et al.*, An open-label randomized controlled trial of the effect of lopinavir/ritonavir, lopinavir/ritonavir plus IFN-β-1a and hydroxychloroquine in hospitalized patients with COVID-19. *Clin Microbiol Infect* **27**, 1826-1837 (2021).

97. A. C. Kalil *et al.*, Efficacy of interferon beta-1a plus remdesivir compared with remdesivir alone in hospitalised adults with COVID-19: a double-bind, randomised, placebo-controlled, phase 3 trial. *Lancet Respir Med* **9**, 1365-1376 (2021).

98. S. Jangra *et al.*, SARS-CoV-2 spike E484K mutation reduces antibody neutralisation. *Lancet Microbe* **2**, e283-e284 (2021).

99. S. A. Kemp *et al.*, SARS-CoV-2 evolution during treatment of chronic infection. *Nature* 10.1038/s41586-021-03291-y (2021).

100. K. Kupferschmidt, New mutations raise specter of 'immune escape'. *Science* **371**, 329-330 (2021).

101. K. A. Lythgoe *et al.*, SARS-CoV-2 within-host diversity and transmission. *Science* 10.1126/science.abg0821 (2021).

102. K. R. McCarthy *et al.*, Recurrent deletions in the SARS-CoV-2 spike glycoprotein drive antibody escape. *Science* **371**, 1139-1142 (2021).

103. I. M. Rouzine, G. Rozhnova, Evolutionary implications of SARS-CoV-2 vaccination for the future design of vaccination strategies. *Commun. Med.* **3** (2023).

104. C. R. Triggle *et al.*, A comprehensive review of viral characteristics, transmission, pathophysiology, immune response, and management of SARS-CoV-2 and COVID-19 as a basis for controlling the pandemic. *Front Immunol* **12**, 631139 (2021).

105. T. T. Truong *et al.*, Increased viral variants in children and young adults with impaired humoral immunity and persistent SARS-CoV-2 infection: A consecutive case series. *EBioMedicine* **67**, 103355 (2021).

106. D. Van Egeren *et al.*, Vaccines alone cannot slow the evolution of SARS-CoV-2. *Vaccines* **11**, 853 (2023).

107. B. Jackson *et al.*, Generation and transmission of interlineage recombinants in the SARS-CoV-2 pandemic. *Cell* **184**, 5179-5188.e5178 (2021).

108. P. V. Markov *et al.*, The evolution of SARS-CoV-2. *Nat. Rev. Micro.* **21**, 361-379 (2023).

109. T. Sekizuka *et al.*, Genome recombination between the delta and alpha variants of Severe Acute Respiratory Syndrome Coronavirus 2 (SARS-CoV-2). *Jap. J. Infect. Disease* **75**, 415-418 (2022).

110. J. H. Kuhn, W. Li, H. Choe, M. Farzan, What's new in the renin-angiotensin system? *Cell Mol Life Sci* **61**, 2738-2743 (2004).

111. W. Song, M. Gui, X. Wang, Y. Xiang, Cryo-EM structure of the SARS coronavirus spike glycoprotein in complex with its host cell receptor ACE2. *PLoS Pathog* **14**, e1007236 (2018).

112. W. Tai *et al.*, Characterization of the receptor-binding domain (RBD) of 2019 novel coronavirus: implication for development of RBD protein as a viral attachment inhibitor and vaccine. *Cell Mol Immunol* 10.1038/s41423-020-0400-4 (2020).

113. T. Verano-Braga, A. L. V. Martins, D. Motta-Santos, M. J. Campagnole-Santos, R. A. S. Santos, ACE2 in the renin-angiotensin system. *Clin Sci (Lond)* **134**, 3063-3078 (2020).

114. D. Acharya, G. Liu, M. U. Gack, Dysregulation of type I interferon responses in COVID-19. *Nat Rev Immunol* **20**, 397-398 (2020).

115. G. Castillo *et al.*, Molecular mechanisms of human coronavirus NL63 infection and replication. *Virus Res* **327**, 199078 (2023).

116. M. A. Clementz *et al.*, Deubiquitinating and interferon antagonism activities of coronavirus papain-like proteases. *J Virol* **84**, 4619-4629 (2010).

117. I. E. Galani *et al.*, Untuned antiviral immunity in COVID-19 revealed by temporal type I/III interferon patterns and flu comparison. *Nat Immunol* 10.1038/s41590-020-00840-x (2020).

118. Y. Konno *et al.*, SARS-CoV-2 ORF3b is a potent interferon antagonist whose activity is increased by a naturally occurring elongation variant. *Cell Rep* **32**, 108185 (2020).

119. L. Sun *et al.*, Coronavirus papain-like proteases negatively regulate antiviral innate immune response through disruption of STING-mediated signaling. *PLoS One* **7**, e30802 (2012).

120. A. Vanderheiden *et al.*, Type I and Type III Interferons restrict SARS-CoV-2 infection of human airway epithelial cultures. *J Virol* **94** (2020).

121. C. K. Yuen *et al.*, SARS-CoV-2 nsp13, nsp14, nsp15 and orf6 function as potent interferon antagonists. *Emerg Microbes Infect* **9**, 1418-1428 (2020).

122. R. A. Nickle, K. B. DeOca, B. L. Garcia, M. D. Mannie, Soluble CD25 imposes a low-zone IL-2 signaling environment that favors competitive outgrowth of antigen-experienced CD25(high) regulatory and memory T cells. *Cell Immunol* **384**, 104664 (2023).

123. L. J. Reed, H. Muench, A simple method of estimating fifty per cent endpoints. *Am J Epidemiol* **27**, 493-497 (1938).

124. M. D. Mannie, J. L. Devine, B. A. Clayson, L. T. Lewis, D. J. Abbott, Cytokine–neuroantigen fusion proteins: New tools for modulation of myelin basic protein (MBP)-specific T cell responses in experimental autoimmune encephalomyelitis. *Journal of Immunological Methods* **319**, 118-132 (2007).

125. Created in BioRender. Bastian, A. (2025). https://BioRender.com/88iulrr.

126. Y. Imai *et al.*, Angiotensin-converting enzyme 2 protects from severe acute lung failure. *Nature* **436**, 112-116 (2005).

127. N. Banu, S. S. Panikar, L. R. Leal, A. R. Leal, Protective role of ACE2 and its downregulation in SARS-CoV-2 infection leading to Macrophage Activation Syndrome: Therapeutic implications. *Life Sci* **256**, 117905 (2020).

128. I. Glowacka *et al.*, Differential downregulation of ACE2 by the spike proteins of severe acute respiratory syndrome coronavirus and human coronavirus NL63. *J Virol* **84**, 1198-1205 (2010).

129. S. Haga *et al.*, Modulation of TNF-alpha-converting enzyme by the spike protein of SARS-CoV and ACE2 induces TNF-alpha production and facilitates viral entry. *Proc Natl Acad Sci USA* **105**, 7809-7814 (2008).

130. Y. Lu *et al.*, SARS-CoV-2 down-regulates ACE2 through lysosomal degradation. *Mol Biol Cell* **33**, ar147 (2022).

131. M. E. Mehrabadi *et al.*, Induced dysregulation of ACE2 by SARS-CoV-2 plays a key role in COVID-19 severity. *Biomedicine & Pharmacotherapy* **137**, 111363 (2021).

132. G. Y. Oudit *et al.*, SARS-coronavirus modulation of myocardial ACE2 expression and inflammation in patients with SARS. *Eur J Clin Invest* **39**, 618-625 (2009).

133. J. J. Kiladjian, R. A. Mesa, R. Hoffman, The renaissance of interferon therapy for the treatment of myeloid malignancies. *Blood* **117**, 4706-4715 (2011).

134. M. Farhangian, F. Azarafrouz, N. Valian, L. Dargahi, The role of interferon beta in neurological diseases and its potential therapeutic relevance. *Eur J Pharmacol* **981**, 176882 (2024).

135. M. S. Freedman *et al.*, Twenty Years of Subcutaneous Interferon-Beta-1a for Multiple Sclerosis: Contemporary Perspectives. *Neurol Ther* **13**, 283-322 (2024).

136. R. M. Friedman, S. Contente, Treatment of hepatitis C infections with interferon: a historical perspective. *Hepat Res Treat* **2010**, 323926 (2010).

137. N. Peiffer-Smadja, Y. Yazdanpanah, Nebulised interferon beta-1a for patients with COVID-19. *Lancet Respir Med* 10.1016/s2213-2600(20)30523-3 (2020).

138. R. Pereda *et al.*, Therapeutic effectiveness of Interferon-α2b against COVID-19: The Cuban experience. *J Interferon Cytokine Res* **40**, 438-442 (2020).

139. B. Wang *et al.*, Subcutaneous injection of IFN alpha-2b for COVID-19: an observational study. *BMC Infect Dis* **20**, 723 (2020).

140. N. Iwata-Yoshikawa *et al.*, Essential role of TMPRSS2 in SARS-CoV-2 infection in murine airways. *Nat Commun* **13**, 6100 (2022).

141. S. Matsuyama *et al.*, Efficient activation of the severe acute respiratory syndrome coronavirus spike protein by the transmembrane protease TMPRSS2. *J Virol* **84**, 12658-12664 (2010).

142. A. Shulla *et al.*, A transmembrane serine protease is linked to the severe acute respiratory syndrome coronavirus receptor and activates virus entry. *J Virol* **85**, 873-882 (2011).

143. J. Wang, H. Zhao, Y. An, ACE2 Shedding and the Role in COVID-19. *Front Cell Infect Microbiol* **11**, 789180 (2021).

144. R. Dijkman *et al.*, Replication-dependent downregulation of cellular angiotensin-converting enzyme 2 protein expression by human coronavirus NL63. *J Gen Virol* **93**, 1924-1929 (2012).

145. D. Chmiest *et al.*, Spatiotemporal control of interferon-induced JAK/STAT signalling and gene transcription by the retromer complex. *Nat Commun* **7**, 13476 (2016).

146. G. Schreiber, The molecular basis for differential type I interferon signaling. *J Biol Chem* **292**, 7285-7294 (2017).

147. N. Zanin, C. Viaris de Lesegno, C. Lamaze, C. M. Blouin, Interferon Receptor Trafficking and Signaling: Journey to the Cross Roads. *Front Immunol* **11**, 615603 (2020).

148. N. Zanin *et al.*, STAM and Hrs interact sequentially with IFN-α Receptor to control spatiotemporal JAK-STAT endosomal activation. *Nat Cell Biol* **25**, 425-438 (2023).

149. C. Schindler, C. Plumlee, Inteferons pen the JAK-STAT pathway. *Semin Cell Dev Biol* **19**, 311-318 (2008).

150. C. Thomas *et al.*, Structural linkage between ligand discrimination and receptor activation by type I interferons. *Cell* **146**, 621-632 (2011).

151. M. E. Francis *et al.*, SARS-CoV-2 infection in the Syrian hamster model causes inflammation as well as type I interferon dysregulation in both respiratory and non-respiratory tissues including the heart and kidney. *PLoS Pathog* **17**, e1009705 (2021).

152. Created in BioRender. Bastian, A. (2025). https://BioRender.com/dbli22k.